Untargeted lipidomics of propionic acidemia patients vs Targeted lipidomics of sphingolipids

Masterproject

Author:	L.M Steringa (S2678101)
Institutions:	University of Groningen Laboratory of Metabolic Diseases, Department of Laboratory Medicine University Medical Center Groningen
Daily supervisor:	J.C. van der Weerd
First examiner:	dr. M.R. Heiner-Fokkema
Second examiner:	dr. D.A.J. Dijck Brouwer
Start date:	11-10-2021
End date:	22-07-2022

Table of content

List of abbreviations

Abbreviation	
BUME	Butanol-methanol
CE	Collision energy
CID	Collision induced dissociation
CXP	Collision cell exit potential
DP	Declustering potential
EP	Entrance potential
FA	Fatty acyls
FT-ICR	Fourier transform ion cyclotron resonance
GL	Glycerolipids
GP	Glycerophospholipids
HPLC	High-performance liquid chromatography
HRMS	High-resolution Mass spectrometry
LRMS	Low resolution mass spectrometry
MBTE	Methyl-tert-butyl ether
MMC	Methanol/MBTE/chloroform
MRM	Multiple reaction monitoring
MS	Mass spectrometry
NMR	Nuclear magnetic resonance
OT	Orbitrap
PK	Polyketides
PR	Prenol lipids
QTOF	Quadrupole-time-of-flight
RT	Retention time
SL	Saccharolipids
SP	Sphingolipids
ST	Sterols
TOF	Time-of-flight
UHPLC	Ultra-high performance liquid chromatography

Abstract

Biological systems, such as cells, consist of thousands of individual molecular lipid species, called the lipidome. Lipids have multiple and crucial roles in cellular functions, such as the composition of the membrane bilayer, creating an appropriate hydrophobic environment for membrane proteins and their interactions, cell growth, multiplication, and death. Lipidomics is a branch of metabolomics, where the aim is to analyze the lipidome, in a cell or organism to study their biological roles concerning health and diseases. This study is focused on the two main branches of lipidomics: untargeted and targeted lipidomics. The purpose of the first part of this study is based on untargeted lipidomics using an ultra-high liquid chromatography system coupled to a quadrupole time-of-flight mass spectrometer. The aim is to explore the difference in lipid profiles of patients with propionic acidemia and healthy controls. The purpose of the second part of this study is based on targeted lipidomics using separation by high-performance liquid chromatography system coupled to a triple quadrupole mass spectrometer. The aim is the development and validates a specific and sensitive liquid chromatography triple quadrupole mass spectrometry method for quantification of sphingolipids. Results showed there was no natural grouping and differentiation between the groups regarding the lipid metabolism of PA patients and control samples. Three lipids were significantly downregulated in PA patients compared to the controls that were identified as TG(56:8), TG(44:2), and PC(20:3). The lipids were identified by the number of carbon atoms and double bonds present since it is not possible to distinguish between isomers. To check if the identification of the significantly downregulated lipids were valid the m/z values of the measured TG and PC were plotted against their retention times. All lipids fit into the curves plotted, thus concluding that the identification of the lipids was valid. The sphingolipid standard showed a large number of common product ions with the m/z values of 252, 264, and 282. The ceramides had common product ions with the m/z values of 520, 538, and 682. Using the determined optimal mass spectrometry parameters for the declustering potential, entrance potential, collision cell exit potential, and collision energy an optimal method was developed to measure the 5 selected sphingolipid standards. An isocratic elution of 70% mobile phase B is used to elute the sphingolipid standards in the following order: lactosyl sphingosine (RT: 2.5 min) galactosyl sphingosine (RT: 2.5 min), glucosyl sphingosine (RT: 2.5 min), D-sphingosine (RT: 2.7 min) and C16 galactosylceramide (RT: 7 min).
To conclude, further research needs to be performed using a bigger sample pool to validate the downregulated lipids in PA patients compared to healthy controls. The development of the liquid chromatography triple quadrupole mass spectrometry method was successful but needs more validation. To do this the experiment needs to be repeated to check the reproducibility of the method. The next steps include measuring the sphingolipid concentration using plasma serum.

Keywords: *Lipidomics, untargeted, targeted, propionacidemia, lipids, triple quadrupole mass spectrometry, quadrupole-time-of-flight mass spectrometry.*

1. Introduction

1.1. Lipids

The human body contains thousands of individual molecular lipid species, also known as the lipidome. Lipids have multiple and crucial roles in cellular functions, such as the composition of the membrane bilayer, creating an appropriate hydrophobic environment for membrane proteins and their interactions, cell growth, multiplication, and death. Because their biological properties depend on their chemical structure, each type of lipid has its role in a living system. When an imbalance occurs in this system, this can lead to different pathophysiological conditions.[1] Cellular processes such as growth division and response to environmental stimuli require lipid metabolism to maintain homeostatic balance. Lipids and their metabolites have a significant effect on the regulation and control of cellular function and disease. To completely understand the role of lipids in disease and to develop compounds of therapeutic interest, it is not only important to identify and characterize lipids but to also quantify the changes in their metabolites. This way biochemical pathways and interaction network maps can be developed.[2]

1.1.2. Lipids and food consumption

Lipids, such as edible oils and fats, play an important role in the human diet and health. They provide essential nutrients, metabolic energy, and cellular regulators and their excessive intake has been linked to various diseases. Dietary intake patterns and quality have changed due to increases in edible oil and fat consumption globally. [1] Morbidity rates of lipid-related chronic diseases, such as obesity, type 2 diabetes, hypertension, liver disease, and cardiovascular disease, have increased significantly over the years. These diseases are now becoming the leading causes of death and affect people of all ages and incomes throughout the world.[1,2]

1.1.3. Lipid classification

The classification system is based on the concept of 2 fundamental ''building blocks'': ketoacyl groups and isoprene groups. (Figure 1) Therefore, lipids are defined as hydrophobic or amphiphilic molecules that originate entirely or partly by carbanion-based condensations of ketoacyl thioesters and/ or by carbocation based condensations of isoprene units.[3] Because of the lack of a consistent classification and nomenclature methodology for lipids, the LIPID MAPS consortium has developed a classification system for lipids. They divided the lipidome into eight major lipid classes: fatty acyls (FA), glycerolipids (GL), glycerophospholipids (GP), sphingolipids (SP), sterol lipids (ST), prenol lipids (PR), saccharolipids (SL) and polyketides (PK).[6] (Table 1) Each category is divided into classes, and subclasses and is assigned a unique 12- or 14-character identifier (LIPID MAPS ID or "LM ID"). The fatty acyls (FA) are a group of molecules synthesized by chain elongation of an acetyl-CoA primer with malonyl-CoA (or methylmalonyl-CoA) groups that may contain a cyclic functionality and/or are substituted with heteroatoms. They contain not only fatty acids but several other functional variants such as alcohols, aldehydes, amides and esters. [3]Lipids containing structures with a glycerol group are the glycerolipids (GL), which include acylglycerols but also encompass alkyl and 1*Z*-alkenyl variants, and the glycerophospholipids (GP), which are defined by the presence of a phosphate (or phosphonate) group esterified to one of the glycerol hydroxyl groups.[3] The sterol lipids (ST) and prenol lipids (PR) share a common biosynthetic pathway via the polymerization of dimethylallyl pyrophosphate/isopentenyl pyrophosphate but differ in terms of their eventual structure and function.[3] The sphingolipids (SP) contain a long-chain nitrogenous base as their core structure. The saccharolipid (SL) category is characterized by fatty acyl groups that are linked directly to a sugar backbone. Glycosylated derivatives of the other 7 lipid categories are classified as members (classes/subclasses) of these categories and have a major effect on the structural diversity of lipids in general. Lastly, polyketides (PK) are a diverse group of metabolites from animal, plant and microbial

sources.[3] In this study we mainly focus on the glycerolipids (triglycerides) and the sphingolipids (sphingomyelins).

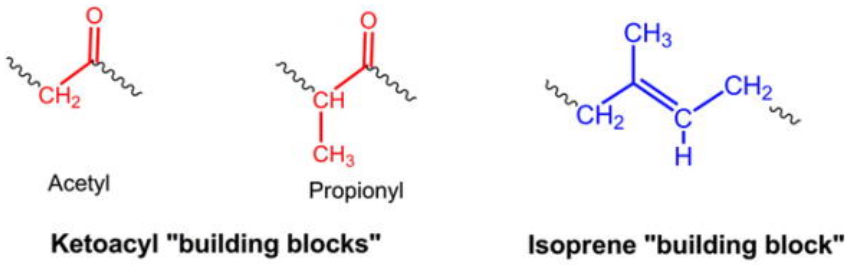

Figure 1. The ''building blocks'' of the LIPID MAPS classification system are: ketoacyl groups and isoprene groups. Figure adapted from [3]

Table 1. Examples of the eight categories of lipids with their structures and typical classes and subclasses are presented. Figure adapted from [7]

Categories	Structures Examples	Typical Classes: Subclasses
Fatty acyls, FA	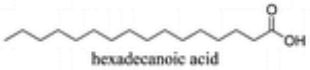 hexadecanoic acid	Fatty acids: straight-chain fatty acids Eicosanoids Fatty alcohols Fatty esters Fatty amides
Glycerolipids, GL	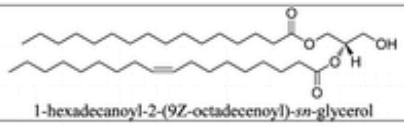 1-hexadecanoyl-2-(9Z-octadecenoyl)-*sn*-glycerol	Monoradylglycerols: monoacylglycerols Diradylglycerols: diacylglycerols Triradylglycerols: triacylglycerols
Glycerophospholipids, GP	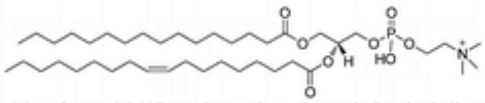 1-hexadecanoyl-2-(9Z-octadecenoyl)-*sn*-glycero-3-phosphocholine	Glycerophosphocholines Glycerophosphoethanolamines Glycerophosphoserines Glycerophosphoglycerols Glycerophosphoglycerophosphates Glycerophosphoinositols Glycerophosphoglycerophosphoglycerols
Sphingolipids, SP	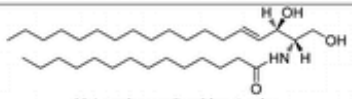 N-(tetradecanoyl)-sphing-4-enine	Sphingoid bases Ceramides Phosphosphingolipids Neutral glycosphingolipids Acidic glycosphingolipids
Sterol lipids, ST	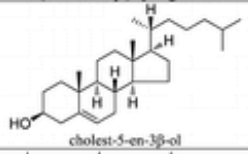 cholest-5-en-3β-ol	Sterols Cholesterol and derivatives Steroids Bile acids and derivatives
Prenol lipids, PR	 2E,6E-farnesol	Isoprenoids Quinones and hydroquinones Polyprenols
Saccharolipids, SL	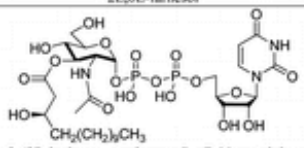 UDP-3-O-(3R-hydroxy-tetradecanoyl)-αD-N-acetylglucosamine	Acylaminosugars Acylaminosugar glycans Acyltrehaloses Acyltrehalose glycans
Polyketides, PK	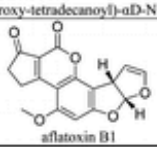 aflatoxin B1	Macrolide polyketides Aromatic polyketides Nonribosomal peptide/polyketide hybrids

1.1.4. Triglycerides

Glycerolipids play key structural and functional roles in bacterial, plant, and animal membranes. They have at least one hydrophobic chain linked to a glycerol backbone in an ester or ether linkage. They consist of mainly mono-, di- and trisubstituted glycerols, the most well-known is the fatty acid ester of glycerol (triacylglycerols), also known as triglycerides, and are present in the bulk of storage fat in mammalian tissues.[4] Triglycerides are composed of three fatty acids individually esterified to each carbon of a glycerol molecule as shown in Figure 2.

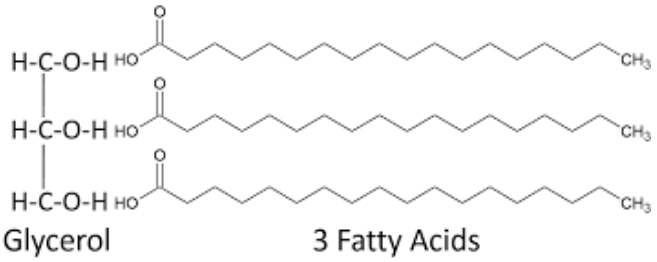

Figure 2. Molecular structure of Triglycerides. The figure is adapted from [5]

1.1.5. Sphingolipids

The name ''sphingosine'' backbone of sphingolipids was named by J.L.W. Thudichum in 1884 because of its enigmatic (sphinx-like) properties. The sphinx is portrayed in Greek mythology as a monster that posed riddles and destroyed those who could not answer the riddle. Although it is still an elusive class of lipids, research on the involvement of cell growth, differentiation, cell functions and cell death has been rapidly expanding our knowledge of these compounds.[6] Sphingolipids are found in all animals, fungi, plants and some prokaryotic organisms and viruses. The sphingolipids are known to act as first and second messengers in various signaling pathways and have vital roles in membrane microdomains, also known as ''lipid rafts''. As in the case of all membrane lipids, they are amphiphilic molecules with both hydrophobic and hydrophilic properties. The hydrophobic part consists of a sphingoid long chain base (often sphingosine, sphinganine or phytosphingosine) to which a fatty acid is attached by an amide bond to carbon 2.[6,7]

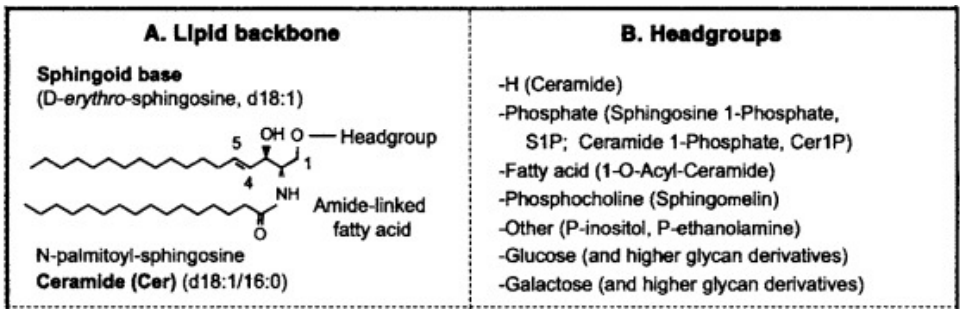

Figure 3. Basic structures of sphingolipid backbones and their head groups. A) shows an example of a ceramide backbone with the commonly used names and abbreviations of the components. (B) the common headgroups attached to ceramide in mammalian sphingolipids. Figure adapted from [7]

Sphingomyelin

Sphingomyelin (SM) is an important component present in many animal cell membranes. Although, the biological importance of SM is not established, it is known that SM, along with cholesterol, are key components of nanodomains in membranes called functional rafts.[8]

SM makes up for the majority of sphingophospholipids in mammals, accounting for 2% to 15% of total organ phospholipids. SM consists of a ceramide and phosphocholine head group. Unlike triglycerides, they don't contain a glycerol backbone, but a sphingosine backbone.[9] (Figure 4) Sphingomyelin can accumulate in a rare hereditary disease called Niemann-Pick disease, types A and B. Type A occurs in infants and is characterized by jaundice, enlarged liver and profound brain damage. Type B usually occurs in the pre-teen years and is characterized by an enlarged liver and spleen, but the brain is not affected.[10]

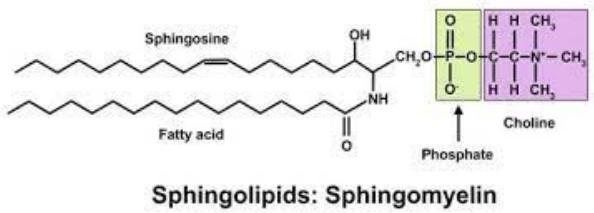

Figure 4. Molecular structure of sphingomyelin. The figure is adapted from [11].

1.1.6. Shorthand notation

There is a need for a standardized, practical annotation for structures of lipid species derived from mass spectrometric approaches. This adds defined levels of the information below the LIPID MAPS nomenclature, because detailed chemical structures, including stereochemistry, are usually not automatically provided by mass spectrometric analysis (Figure 5).
The following general rules are used for the shorthand notation of lipid species:

- Lipid class abbreviation heads each species description.[12]
- Variable components (constituents), such as fatty acids, are assigned based on their mass as the number of C-atoms and number of double bonds (C-atoms: double bonds).[12]
- Only experimentally proven structural details of constituent fatty acids are assigned according to the rules defined for fatty acyls.[12]
- When structural ambiguities are present (e.g., bond type, hydroxyl groups, branched chains, species are assigned by one of the following rules:
    - Lipid class and the (uncharged) molecular mass (Da) are in parentheses (preferred for reporting in databases lipid class level mass).[12]
    - Annotation based on assumptions must be visible (preferred for publications lipid species level).[12]

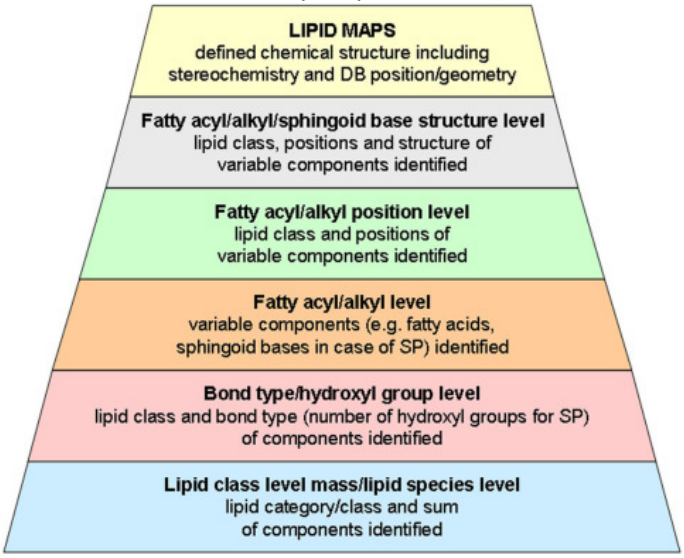

Figure 5. MS shorthand notation for lipid species. The levels cover a correct presentation of the structural information provided by MS analysis. Figure adapted from [12].

1.2. Lipidomics

Lipidomics is a branch of metabolomics, where the aim is to analyze the complete set of lipids, also called the lipidome, in a cell or organism to study their biological roles concerning health and diseases. Lipidomics has advanced recently due to the development of analytical tools such as mass spectrometry (MS), nuclear magnetic resonance (NMR) and high-performance liquid chromatography (HPLC) and the LIPID MAPS classification. A typical workflow for the lipidomic analysis of biological samples includes sample preparation, mass spectrometry-based analysis and data processing. Before the analysis, proper sampling and sample storage is important to avoid error and variability in the analytical samples.[17] It is clear that the lipidome is altered during disease development, similar to other metabolomic parameters. Lipidomics has therefore been applied for not only gaining insight into lipid metabolism but also the potential discovery of new lipid metabolites associated with both normal and disease states in humans.[18]

1.2.1. Untargeted vs targeted lipidomics

MS is the preferred analytical tool to perform lipidomics studies as it provides selectivity, sensitivity, resolution and throughput.[19] MS-based lipidomics can be performed by using either targeted or untargeted approaches, each with its own advantages and disadvantages.

Untargeted lipidomics is unbiased and has broad coverage, as they measure potentially all lipids in a sample.[14,15] A high-resolution MS (HRMS) platform is used to determine the exact mass and thus discriminate each lipid species. Quadrupole-time-of-flight (QTOF), Orbitrap, and Fourier transform ion cyclotron resonance (FT-ICR) mass spectrometers are used for untargeted lipidomics. Often the MS is coupled with ultra-high-performance liquid chromatography (UHPLC) to separate isomeric and isobaric lipids present in a biological matrix.[16] Untargeted platforms are often used to provide relative quantification and aspects of the workflow, such as data normalization and lipid identification, are very challenging, not standardized and time-consuming.[17]

Untargeted lipidomics is a promising strategy for discovering lipid biomarkers present in biological samples and revealing novel lipid metabolic pathways by annotating previously uncharacterized lipid-metabolizing enzymes. However, the appropriate polarity for the analysis differs according to the physicochemical properties of the lipid classes. Although polarity switching acquires data in both modes in a single run, it decreases the sensitivity and can't be performed by all mass spectrometers.[18] Furthermore, the favorable solvent conditions, such as pH and composition, are different between the different lipid classes.[18]

In contrast, targeted lipidomics focuses on the absolute quantification of a small number of predefined lipids using isotopically labeled internal standards. The number of lipids is often limited due to the lack of commercially available standards. Targeted platforms are high-throughput because analysis and data generation is fast and straightforward, quantitative, but have a limited coverage of lipids.[17] Targeted lipidomics is implemented when the goal is to study specific target lipids or lipid classes. Multiple reaction monitoring (MRM) using a triple-quadrupole mass spectrometer is one of the most used platforms for targeted analysis, due to the wide dynamic range and the high sensitivity and selectivity.[16] It measures specific lipids of interest by selecting predefined pairs of precursor and product ions. Lipid classes with characteristic fragmentation patterns are suitable for targeted analysis, such as sphingomyelins yielding phosphocholine ions with an m/z 184 as a product ion measured in positive ion mode.[16] Another motivation for using targeted lipidomics is the detection and quantification of low abundance lipids, due to the requirement of high sensitivity. Quantification of low abundance lipids often requires the removal of abundant lipids using solid-phase extraction to avoid ion suppression.[16]

1.3. Lipid analysis

1.3.1 Lipid extraction

LC-MS systems are able to detect most of the known lipid classes in a biological matrix, but no technique can extract all of the known lipid classes simultaneously from a biological matrix. The most commonly used methods for lipid extraction are the so called two-phase extractions that were described by Folch et al.[24] and Bligh and Dyer.[25] The basis of these lipid extractions remains using chloroform/methanol mixtures that separate into a methanol-rich upper layer, containing the hydrophilic compounds and a chloroform-rich lower layer containing mainly lipids.[26]
A disadvantage of the two-phase extraction is the high chance of contamination of the samples, due to the retrieval of lipids from the chloroform-rich lower layer. A way to avoid this issue is to use the methyl-tert-butyl ether (MTBE) extraction method or the butanol-methanol (BUME) method that were described by Matyash et al.[27] and Löfgren et al.[28] Even though both of these methods have the advantage that the lipid-rich organic phase is the upper layer, dissatisfying recovery of the more polar lipid classes have been observed.
The main objectives of the lipidomics studies are to increase the number of extracted and detected lipids and to do this in an uncomplicated and reproducible manner to avoid bias due to technical variability. To achieve these objectives, while avoiding the problems of the two-phase extraction methods, one-phase lipid extraction methods have been developed. These one-phase extractions have an ''all-in-one-tube'' approach and eliminates the phase separation steps by denaturation of the proteins and removing them after by centrifugation. The MMC one-phase extraction method is a more recently described method by Gil et al.[29] Research shows that the one-phase MMC (methanol/MBTE/chloroform) extraction method shows comparable results with the two-phase extraction methods, and performed even better in case of polar lipids when applied to plasma samples or cultured cells.[30]

1.3.2 Ultra-Performance Liquid Chromatography

In the past, lipids have been analyzed by diverse chromatography-based separation methods. Commonly used technologies comprised methods like one or two dimensional thin layer chromatography in combination with different visualization strategies, but also high performance liquid chromatography (HPLC) methods combined with various detection systems.[31]
There have been two main strategies for the analysis op lipids described. The first one is shotgun lipidomics, which relies on a direct infusion analysis of a crude lipid extract on triple quadrupole or quadrupole time-of-flight (qTOF) mass spectrometers. The second one is chromatography-based separation prior to mass spectrometric measurement for the lipid analysis (LC-based lipidomics). Shotgun lipidomics is biased towards the more abundant and easily ionized lipids, while LC-based lipidomics increases the number of detectable lipids because of its reduced ion suppression and is the preferred method.[32] HPLC is based on the distribution of the analyte (sample) between a mobile phase (eluent) and a stationary phase (column). Depending on the chemical structure of the analyte, the molecules are slowed down while passing the stationary phase. This causes different constituents of a sample to elute at a different time from the column. Chromatography with 1.5 – 2.0 µm-diameter particles at high pressure is commonly called Ultra-Performance Liquid Chromatography (UPLC).[33] Reversed-phase HPLC is based on the selective interactions of analytes with a nonpolar stationary phase and a polar mobile phase.

1.3.3. Mass spectrometry

Mass spectrometry (MS) is an analytical technique commonly used for qualitative and quantitative chemical analysis by which analytes are identified by the sorting of gaseous ions in electric and magnetic fields. A mass spectrometer consists of an ion source, a mass analyzer and a detector which are operated under high vacuum conditions (Figure 6). In the ion source ions are created from gas-phase neutral sample molecules and sent into the mass analyzer.MS measures the mass to charge ratio (m/z) of an analyte, which has previously been ionized. Only the ions are registered in MS, but the particles with zero net electric charge (molecules or radicals) are not detected. Therefore, MS does not directly measure mass, but it determines the m/z, being m the relative mass of an ion on the unified atomic scale divided by the charge number, z, of the ion.[34]

Mass measurements in mass spectrometry can be carried out using low resolution (LRMS) or high resolution (HRMS). An LRMS measurement provides information about the nominal mass (number of protons and neutrons) of the analyte[35], where the m/z for each ion is measured to single-digit mass units (integer mass). However, exact mass is measured by HRMS, where the m/z for each ion is measured to four to six decimal points.[36] HRMS is very useful to structure elucidation of unknown compounds having the same nominal mass, but with very small differences in their exact masses.[34] The performance of a high-resolution analyzer is usually expressed in instrument resolution. HRMS instruments include time-of-flight (TOF), FT-ICR and orbitrap (OT) mass analyzers.[37]

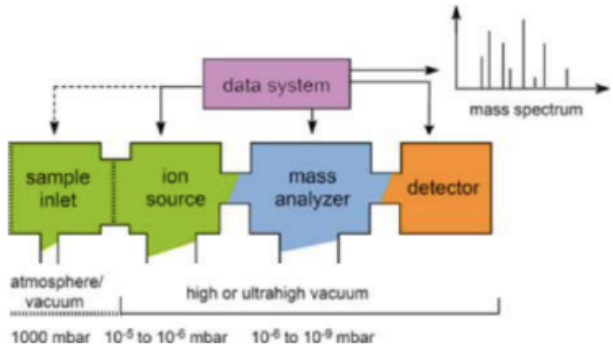

Figure 6. General scheme of a mass spectrometer. The figure is adapted from [38]

Quadrupole analyzers

The quadrupole mass spectrometer is a type of mass analyzer that is commonly used in mass spectrometry. It consists of four parallel cylindrical rods (Figure 7). The quadrupole is in this type of mass spectrometer the mass analyzer, which is responsible for selecting sample ions based on their m/z. The separation of the ions is based on the stability of their trajectories in the oscillating electric fields that are applied in the rods.[38] A particularly useful mass spectrometer configuration is the triple quadrupole mass spectrometer, a type of tandem MS, where a collision cell is placed between two quadrupole mass analyzers and two or more stages of the mass analysis are independently applied. [39]

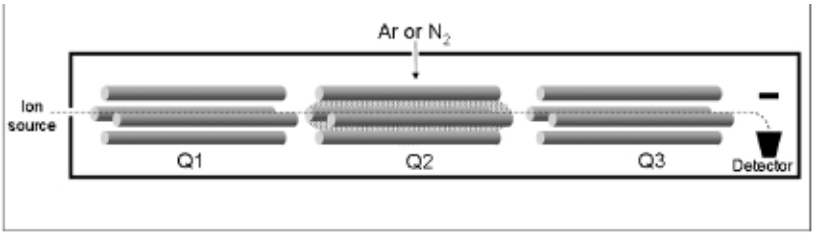

Figure 7. Schematic representation of a triple quadrupole mass spectrometer. Q1 and Q3 act as mass filters and Q2 is a collision cell. The figure is adapted from [39]

The Q-TOF mass spectrometer is an instrument that combines quadrupole technologies with a TOF analyzer. It closely resembles a triple-quadrupole mass spectrometer, where the third quadrupole has been replaced by a TOF tube. The first quadrupole (Q1) operates as a mass filter for selecting specific ions based on their m/z. The second quadrupole (Q2) is a collision cell where ions are bombarded by neutral gas molecules, causing the fragmentation of ions by a process called collision-induced dissociation (CID). After the ions leave the quadrupole, they are reaccelerated into the ion modulator region of the TOF analyzer, pulsed by an electric field and accelerated to their original direction. The ions enter the flight tube which is a field-free drift region where mass separation occurs, based on the time that it takes to traverse the flight path to the detector.[37] (Figure 8)

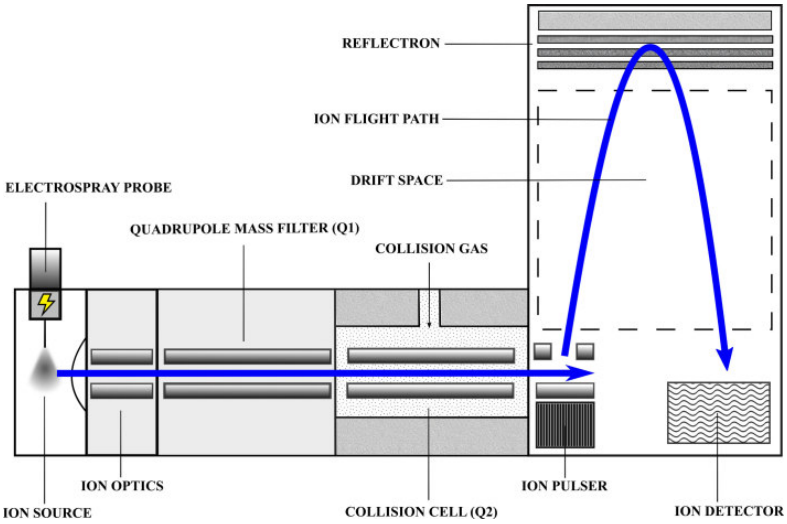

Figure 8. Schematic representation of a quadrupole time-of-flight mass spectrometer. The figure is adapted from [37]

1.3.4. Statistical analysis

Univariate and multivariate statistical analysis represent two approaches to statistical analysis. Univariate analysis, such as volcano plots, involve the analysis of a single variable while multivariate analysis such as PCA plots examine two or more variables. Most multivariate analysis involves a dependent variable and multiple independent variables. Most univariate analysis emphasizes description while multivariate methods emphasize hypothesis testing and explanation.[40]

1.4 Propionic Acidemia

Propionic academia is an autosomal recessive inherited, metabolic disorder affecting from 1/20.000 to 1/250.000 individuals caused by a defective form of the enzyme propionyl-coenzyme A (CoA) carboxylase, which results in the accumulation of propionic acid.[41]

1.4.1. Signs and symptoms

In most cases, the features of propionic acidemia become apparent within a few days after birth. The initial symptoms include poor feeding, loss of appetite, vomiting, weak muscle tone (hypotonia), failure to grow and gain weight at the expected rate (failure to thrive), dehydration, and a lack of energy (lethargy). These symptoms sometimes progress to more serious medical problems such as heart abnormalities, seizures, coma and death. The recurrence or worsening of symptoms may be associated with an infection, constipation or consumption of high amounts of protein. In some affected patients, episodes of symptoms may alternate with periods of apparently normal health and development. As patients age, they can develop various symptoms affecting nearly all organ systems: brain damage (encephalopathy), hypotonia, intellectual disability, pancreatitis, recurrent vomiting, severe vision problems, heart failure (cardiomyopathy), prolonged QTc interval, chronic renal failure

and osteoporosis. Patients may also develop a reduced number of cells in their blood which can cause anemia, leukopenia, thrombocytopenia and pancytopenia. These blood abnormalities can cause a variety of symptoms such as bleeding problems and immune deficiency.[41]

1.4.2. Cause

Propionic acidemia is caused by mutations in the PCCA (Propionyl-CoA Carboxylase Subunit Alpha) and PCCB (Propionyl-CoA Carboxylase Subunit Beta) genes and results in a deficiency of propionyl-CoA carboxylase. This enzyme plays a role in the normal breakdown of proteins and certain types of lipids and cholesterol in the body.[42] Propionyl-CoA is produced by the catabolism of cholesterol, valine, odd chain fatty acids, methionine, isoleucine, and threonine. Propionyl-CoA carboxylase catalyzes the carboxylation of propionyl-CoA with bicarbonate and produces methylmalonyl-CoA. This is converted to succinyl-CoA, which is an intermediate in the tricarboxylic acid cycle (citric acid cycle).[43] Figure 1 shows the difference in the metabolic pathway of a healthy individual vs a patient with propionic acidemia.

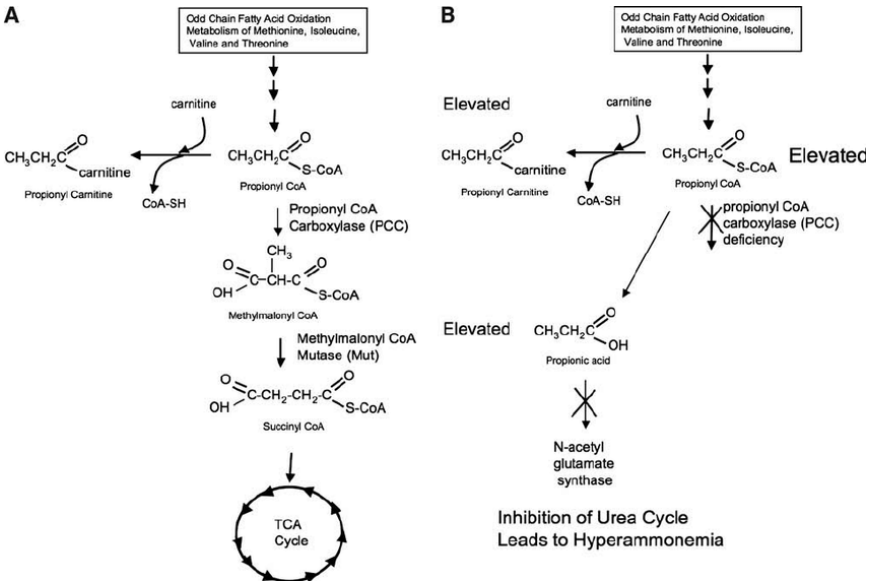

Figure 9. Metabolic Pathway for propionyl-CoA carboxylase (PCC). A shows the pathway of a normal patient and B of a patient with propionic acidemia. Fig Adapted from. [44]

1.4.3. Treatment

During severe episodes, the treatment of infants affected with propionic acidemia may need fluid therapy measures to provide for the nutritional intake administration of medication to prevent/treat bacterial infections. In severe cases of acidosis or hyperammonemia hemodialysis is used to remove excess waste from the blood. Long-term treatment of propionic patients includes maintaining a low-protein diet, possibly in combination with medical formula with low content of specific amino acids (isoleucine, valine, threonine and methionine). Infants can develop a secondary deficiency of carnitine, where administration of L-carnitine (carnitine or levocarnitine) may be needed. Metronidazole as antibiotic therapy can reduce the burden of propionyl-CoA in the body by reducing the production of short chain fatty acids, including propionic acid.[45]
Liver transplantation is a potential surgical option for patients with severe symptoms and frequent recurrent acute episodes (decompensation). Liver recipients generally have a lower risk of hospitalization and decompensation, but have to use lifelong immunosuppressive therapy to prevent the rejection of the liver. All patients will need to be followed by dieticians with experience in metabolic diseases. Some children may find the need to take special education classes, because intellectual disability is very common for patients with propionic acidemia.[41]

1.6. Aim of this study

The purpose of the first part of this study is based on untargeted lipidomics. The aim is to explore the difference in lipid profile of patients with propionic acidemia and controls. The purpose of the second part of this study is based on targeted lipidomics. The aim is the development of a specific and sensitive liquid chromatography triple quadrupole mass spectrometry method for quantification of sphingolipids.

2. Materials

UPLC-grade methanol absolute (MeOH), 2-propanol (IPA), acetonitrile (ACN), methyl-ethyl-butyl ether (MTBE) were purchased from Biosolve BV (Valkenswaard, The Netherlands). Chloroform ($CHCl_3$), Formic acid (98-100%) and ammonium acetate were purchased from Merck KGaA (Darmstadt, Germany). Ultra-pure Milli-Q water was obtained from a Milli-Q system (Millipore, MA, USA). All the lipid standards were acquired from Avanti Polar Lipids Inc. (Alabama, USA).

3. Methods

3.1 Untargeted Lipidomics

3.1.1 Preparation of Lipid internal standard solutions

An internal standard working solution mix (IS mix) was prepared by dilution of PG(17:0/17:0), PS(14:0/14:0), CA(14:0/14:0), Lyso PC (14:0/14:0), PE(15:0/15:0) and C16 glucosyl (beta) Ceramide (d18:1/16:0) in $CHCl_3$/MeOH/H_2O (60:30:4.5, v/v/v), yielding a concentration of 20 µmol/L. A list of the lipid standards can be found in Appendix 7.1. The IS mix was prepared by taking 500 µL of each lipid standard solution. All lipid standard solutions were stored at -20 °C.

3.1.2 Lipids extraction

Lipid extraction was performed with the one-phase MMC extraction method based on a protocol described by Gil et al. A volume of 40 µL of an internal standard mix containing 6 non-physiologic or stable isotope-labelled lipid standards was added to an Eppendorf tube and vacuum dried at 40 °C. 10 µL plasma and 200 µL MMC extraction solution containing MeOH/MTBE/$CHCl_3$ (1.33:1:1, v/v/v) was added and vortexed (~10s). The samples were incubated in the Eppendorf Thermomixer (Eppendorf, Hamburg, Germany) on the Eppendorf ThermoMixer with a rate of 800 rpm for 1h at room temperature. The samples were vortexed again and centrifuged with a speed of 1000g (rcf) for 10 minutes at 21 °C. Subsequently, the supernatant was collected and transferred into a clean Eppendorf tube with a spin filter. The samples were centrifugated for 5 minutes at 1020 RCF and vacuum dried at 40°C. The lipids were dissolved in a final volume of 100 µL composed of 25 µL CHCl3/MeOH/MQ (60:30:4.5, v/v/v) and 75 µL ACN/IPA/MQ (2:1:1, v/v/v). All samples were transferred into a vial with insert shortly before analysis.

3.1.3 Study design

A total 6 serum samples of 5 different patients with propionic acidemia were used for the analysis. The ages of the patients range from 5 days to 8 years old at the time the samples were collected. In total 13 control serum samples were selected of people with no known propionic acidemia diagnosis or any other diagnosis that might interfere with the lipid metabolism. The controls were selected based on their age and ranged from 7 days to 9 years old. All five patients were female and the control group consisted of 3 females and 10 males. The MMC extractions were performed on 19 samples in Duplo.

3.1.5 UPLC conditions

The extracted lipids samples were separated by reverse phase chromatography using an Acquity UPLC® CSH™ C_{18} column (Waters, Manchester, UK) on an Acquity UPLC system (Waters, Manchester, UK). The column was pre-heated to 80°C and the autosampler was set to 17°C. 2 µL of the samples were injected and separated under gradient conditions with a flow rate of 0.5 mL/min. The mobile phases consisted 20% Methanol in MilliQ water (A) and 80% Methanol in MilliQ water (B). Linear gradient elution proceeded as follows: 0 min. 40% mobile phase A and 100% mobile phase B, 7.5-15 min from 40% to 10% mobile phase A, followed by an isocratic elution of 0% mobile phase A and 100% mobile phase B for 17.6 min.

3.1.6 MS conditions

The Lockspray solution was prepared by dilution of 1 ng/µL leucine encephalin + ACN/MilliQ-water (50:50, v/v) + 0.1% formic acid, resulting a concentration of 0.2 ng/µL leucine encephalin. A wash solution was prepared of ACN/IPA/MeOH/MilliQ water (1:1:1:1, v/v/v/v) + 0,2% Formic Acid. All solutions were sonicated for 5 min. The high resolution accurate mass measurements were collected on a Synapt G2-Si high-resolution QTof mass spectrometer with a Jetstream ESI source (Waters, Manchester, UK). Lipids were detected by electrospray ionization in positive (ESI^+) and negative (ESI^-) mode. Nitrogen and argon were used desolvation and collision gas. The desolvation temperature was 500 °C and the source temperature was 150 °C. Data was acquired over the m/z range 50 to 2000 m/z. The injection volume for the resolution positive and negative mode was 2 µl. Fragmentation experiments were performed by MS^E analysis at low energy level of 1 kV and a high-energy range of 30 – 100 kV. An infusion flow rate of the Lockspray solution and the calibration solution were both 10 µL/min. MMC extractions were performed on two pool samples from unknown identities as described in chapter 3.1.2. for quality control. 10 µL was taken from every sample to prepare the pooled lipid extracts. Two blank measurement samples were prepared with and without the internal standard mix following the MMC extraction steps, with exception of the addition of the serum samples. A system blank measurement was prepared using only mobile phase A and mobile phase B. A total of 58 injections were subjected to lipidomics analysis.

3.1.7 Data analysis

The MassLynx software version 4.1 (Waters) was used for data acquisition. Waters raw files were analyzed using Progenesis QI software (Waters Corporation, Milford, MA) for peak alignment, peak picking, normalization of the LC-MS data and feature annotation. Peak alignment was performed to correct for drift in retention times, by selecting a reference LC-MS run that was the best representative of the entire data. The following adducts were used for peak picking and feature selection: [M+H], [M+NH4], [M+K], [M+2Na-H], [2M+H], [2M+NH4] and [2M+K] in positive mode; and [M-H], [M+FA-H], [M+Cl], [2M-H], [2M+FA-H], [M-2H] and [M+Na-2H] in negative mode. The peak picking was set at a range of 3 – 40 min and was set at default sensitivity mode. The feature annotation was performed using an in-house database that contains the retention times and exact masses of about 800 lipid species, as well as online databases LipidBlast, LIPID MAPS and Human Metabolome Database (HMDB). All lipids were identified within a precursor mass error < 8 ppm and a fragment ion error < 20 ppm. In Metabo analyst (version 5.0, Wishart Research Group) the statistical data is analyzed by uploading the data. The missing values were estimated using KNN (feasure-wise). Normalization is performed by normalization by a reference sample (QC 10). In the data editor the group controls and PA patients are selected. Normalization is performed by normalization by median and the data is log transformed. The results are displayed using volcano plots to show the statistical significance (*p* value) versus the magnitude of change (fold change). A volcano-plot is used to assess the statistical data with a Fold change (FC) threshold of 2.0 and a *p* value threshold of 0.05 with the non-parametric tests. Volcano plots is a univariate statistical analysis commonly used to display lipidomic experiments. PCA plots were used as multivariate statistical analysis. The normalization was performed by log transformation and autoscaling of the data.

3.2 Targeted lipidomics

3.2.1 Preparation of sphingolipid internal standard solutions

The internal standard solutions were prepared by dilution of Galactosyl Ceramide, Galactosyl Sph d18:1, D-sphingosine, Glucosyl sphingosine, Lactosyl sphingosine, Lactosyl ceramide, C16 Ceramide and C16 glucosyl ceramide using $CHCl_3$/MeOH (2:1, v/v), yielding a concentration of 1 and 100 µmol/L. A list of the lipid standards can be found in Appendix 7.1. The IS mix was prepared by taking 200 µL of the 100 µM lipid standard solutions of Galactosyl Cer, Galactosyl Sph d18:1, D-sphingosine, glucosyl sphingosine and lactosyl sphingosine. All lipid standard solutions were stored at -20 °C.

3.2.2 preparation of solutions

For the HPLC separation of the sphingolipid internal standards the mobile phases were prepared by taking (A) 600 mL MeOH + 400 mL MilliQ water + 1.33 mL 7.5 M ammonium acetate solution and (B) using 600 mL MeOH + 400 mL 2-propanol + 1.33 mL 7.5 M ammonium acetate solution.

3.2.3 MS tuning of internal standard solutions

For the development and optimization of measuring the sphingolipid standards the optimal MS parameters were determined for every internal standard on the triple quadrupole mass spectrometer (SCIEX API 3200 LC-MS/MS) using the program Analyst (version 1.7, SCIEX). A syringe was filled with one of the sphingolipid internal standard solutions with a concentration of 100 µM. The used MS parameters used for lipid analysis are presented in Table 2. In Analyst Q1 MS (Q1), a range which includes the exact mass of the standard is selected. In analyst Product ion (MS2) the [M+H] adduct is used as the precursor ion and the daughter ions are used for MRM mode. In MRM mode, the Ramp parameter settings are used to determine the optimal values of the Declustering Potential (DP), Entrance Potential (EP), Collision Cell Exit Potential (CXP) and Collision Energy (CE) of the daughter ions. DP is a voltage applied to the orifice that helps to prevent the ions from clustering together. EP is the potential difference between the voltage of Q0 and ground. It is applied to guide and focus ions to go through the Q0 region. CXP focuses, accelerates and transmits all of the fragmentation ions out of Q2 into Q3. CE refers to the rate of acceleration as the ions enter the collision cell. The higher the collision energy, the more fragmentation it will induce.

Table 2. MS parameters for standard lipid analysis used on the SCIEX API 3500 LC-MS/MS.

Parameter	Value
Curtain Gas (CUR)	35.0
IonSpray Voltage (IS)	5500.0
Temperature (TEM)	550.0
Ion Source Gas 1 (GS1)	50.0
Ion Source Gas 2 (GS2)	60.0
Declustering Potential (DP)	60.0
Entrance Potential (EP)	10.0
Collision Cell Exit Potential (CXP)	15

3.2.4 HPLC conditions

The development and optimization of the separation of the sphingolipid standards was performed using an Acquity UPLC® CSH™ C_{18} column (Waters, Manchester, UK) on an Acquity HPLC system (Waters, Manchester, UK). The standards were separated by reverse phase chromatography using the mobile phases A and B described in chapter 3.2.2. Elution was carried out using different multistep gradients as well as isocratic elution to determine the best method for separation. The exact conditions used are described in the results section. For every standard the qualitative and quantitative daughter ions were selected with their corresponding Collision Energies. The average of

the optimal values of the Declustering Potential, Entrance Potential, Collision Cell Exit Potential were used for mass measurement. The flow-rate was 0.3 ml/min and the column temperature was set at 60°C. The rinsing volume was 200 µL. The needle stroke was 52 mm. The Rinsing speed was 35 µL/sec. The sampling speed was 15.0 µL/sec.

4. Results

4.1. Untargeted lipidomics

4.1.1. Lipid identification

Lipid identification was performed based on their retention time (RT), adducts and qualitative fragments. A total of 10.007 compound ions were found, of which 788 lipids were annotated. 352 lipids were annotated as Glycerolipids (GL), including the subclasses triacylglycerols (TG), diacylglycerols (DG) and monoacylglycerols (MG). 369 lipids were annotated as Glycerophospholipids (GP), including the subclasses glycerophosphoethanolamines (PE), glycerophosphates (PA), glycerophosphoserines (PS) and glycerophosphocholines (PC). 67 lipids were annotated as Sphingolipids (SP), including the subclasses ceramides (Cer) and sphingomyelines (SM). Figure 10 shows the number of lipids annotated of the subclasses. The raw data of each scan mode is available in 311221batch1PApos folder on the drive: Z:\mass_spectrometry\QTof_Synapt\Lipidomics\Experimenten\Jorien\20211207\Intra-assay.PRO\Data

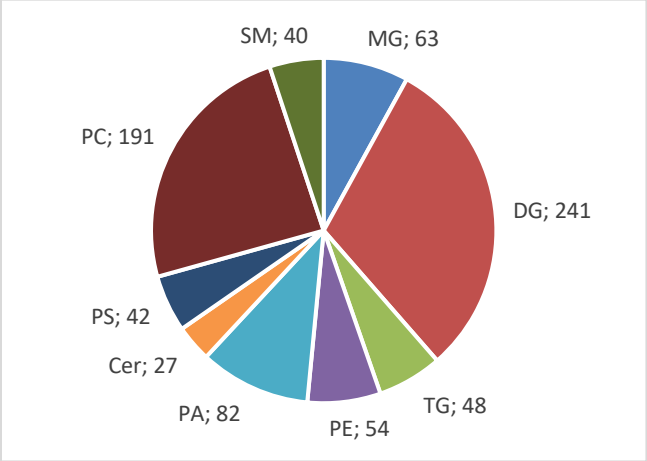

Figure 10. Pie chart showing the number of lipids identified of their corresponding subclasses. Three types of mainclasses are presented: Glycerolipids (GL) including the subclasses MG, DG and TG, Glycerophospholipids (GP) including the subclasses PE, PA, PS and PC and Sphingolipids (SP) including the subclasses Cer and SM.

4.1.2. Differential lipid profiles between PA and controls

A PCA model was constructed to evaluate the differences between groups regarding lipid metabolism of PA patients and controls presented in Figure 11. The differences in normalization are presented in appendix 7.2. The two-dimensional PCA score plots performed on the TG's revealed that PC1 explained 18.5% of the variance and PC2 explained 15% of the variance (Figure 11). There was no natural grouping and differentiation of the individual samples due to the variation in lipid metabolism based on the first two principal components. The two-dimensional PCA score plots performed on the TG's showing the first and third principal component, and the second and third principal components are presented in Appendix 7.3, showing no natural grouping of TG of the individual samples. The two-dimensional PCA score plots performed on the PC revealed that PC1 explained 9.4% of the variance and PC2 explained 7.5% of the variance (Figure 12). There was no

natural grouping and differentiation of the individual samples due to the variation in lipid metabolism based on the first two principal components. The two-dimensional PCA score plots performed on the TG's showing the first and third principal component, and the second and third principal components are presented in Appendix 7.3, showed no natural grouping of PC of the individual samples. The two-dimensional PCA score plots performed on all annotated lipids revealed that PC1 explained 7.5% of the variance and PC2 explained 6% of the variance (Figure 13). There was no natural grouping and differentiation of the individual samples due to the variation in lipid metabolism based on the first two principal components. The two-dimensional PCA score plots performed on the all annotated lipids showing the first and third principal component, and the second and third principal components are presented in Appendix 7.3, showed no natural grouping of the individual samples.

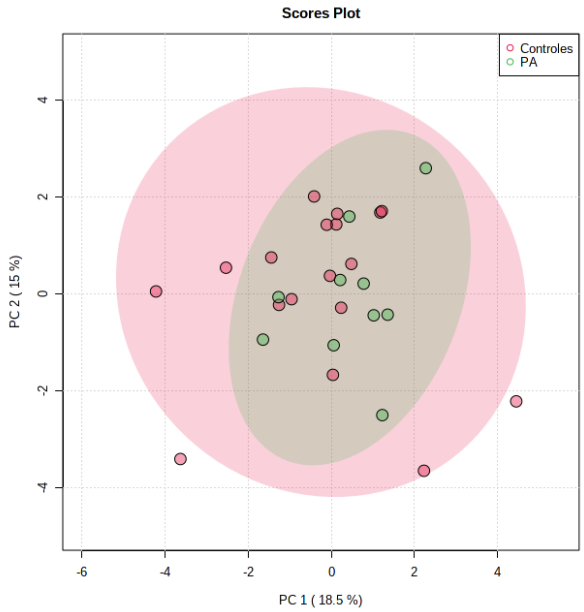

Figure 11. 2-dimensional PCA score plot generated of TG using MetaboAnalyst based on plasma serum samples of propionic aciduria patients and control samples.

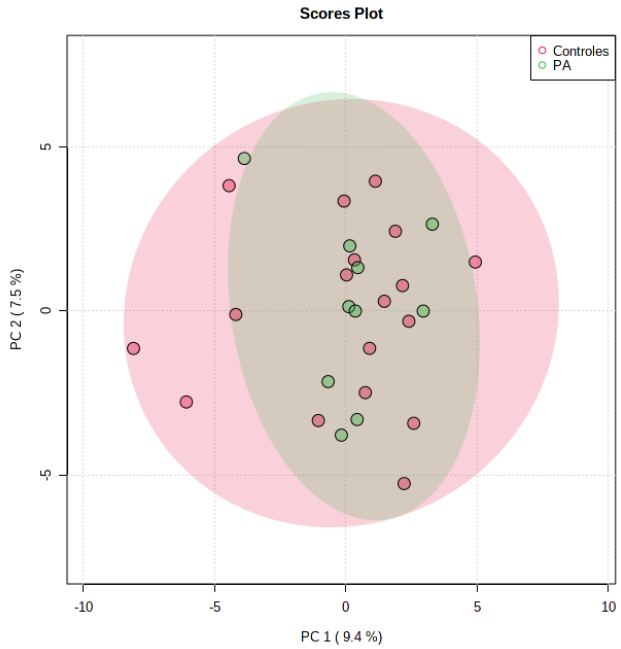

Figure 12. 2-dimensional PCA score plot generated of PC using MetaboAnalyst based on plasma serum samples of propionic aciduria patients and control samples.

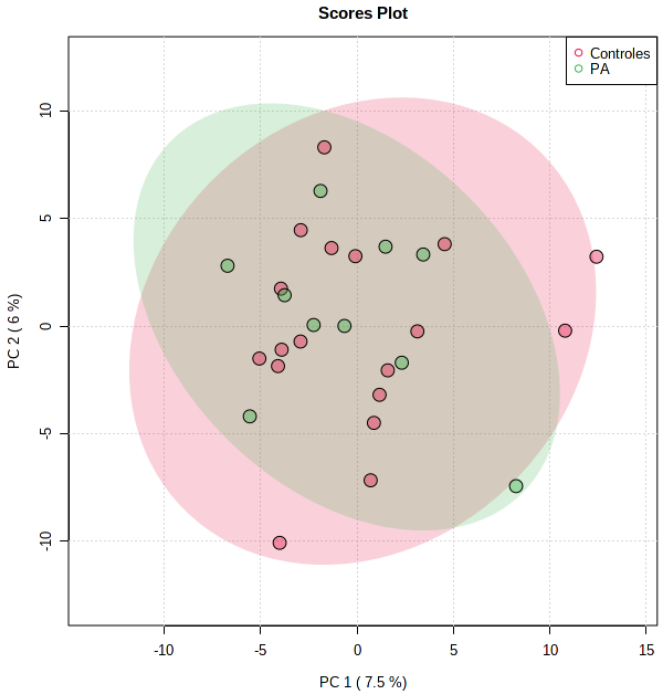

Figure 13. 2-dimensional PCA score plot generated using MetaboAnalyst based on all annotated lipids of plasma serum samples of propionic aciduria patients and control samples.

Volcano plots are used to assess the statistical data with a Fold change (FC) threshold of 2.0 and a P-value threshold of 0.05 with the non-parametric tests of the different lipid subclasses. In Figure 14 is shown that two TG lipids were significantly downregulated in PA patients compared to controls; compound 18,93_902,7365n (p=0.010) and 16,64_746,6428n (0.026). Compound 18,93_902,7365n was identified as TG(56:8) with an average intensity of 10214.7 for healthy controls and 7280.7 for PA patients. Compound 16,64_746,6428n was identified as TG(44:2) with an average intensity of 2807.1 for healthy controls and 2214.1 for PA patients. The normalization of the two downregulated TG are presented in appendix 7.2. The subclasses DG, MG, PE, PA, PS, SM and Cer showed no significant difference between the PA patients compared to controls (Appendix 7.4). In Figure 15 is shown that one PC lipid was significantly downregulated in PA patients compared to controls; compound 5,74_545,3491n (p=0.006), which was identified as PC(20:3) with an average intensity of 15321.5 for controls and 19789.7 for PA patients. The normalization of the downregulated PC is presented in appendix 7.2. The three downregulated lipids didn't fit within the 2.0 FC value threshold. The loading plot of the TG is presented in Figure 16 shows that TG(56:8) is present in the top left quadrant and TG(44:2) is present in the bottom left quadrant, indicating that the two lipids are inversely correlated. The loading plot of the PC is presented in Figure 17.

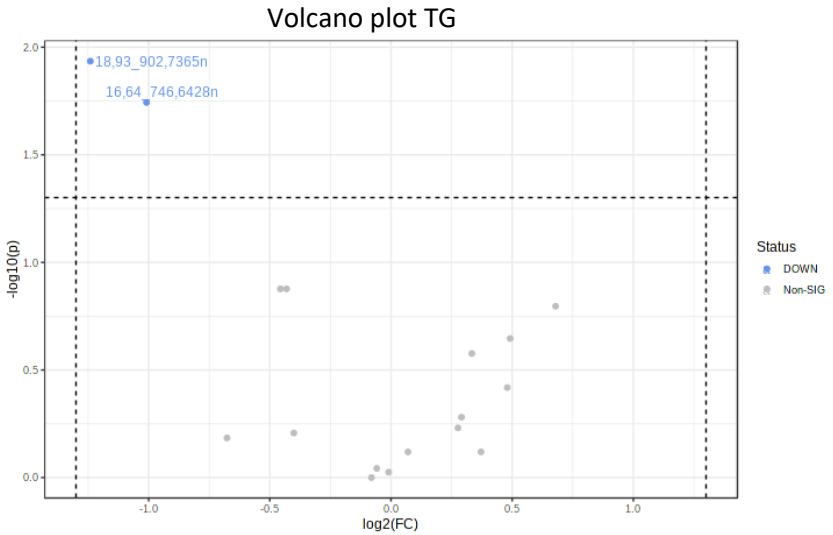

Figure 14. Volcano plot of the lipid subclass TG altered in propionic aciduria patients vs controls. The Log_2 fold change (FC) was plotted against the $-log_{10}$ p-value. Statistical significance was evaluated by t-test (p-value <0.05) and the FC threshold was set to 2.0

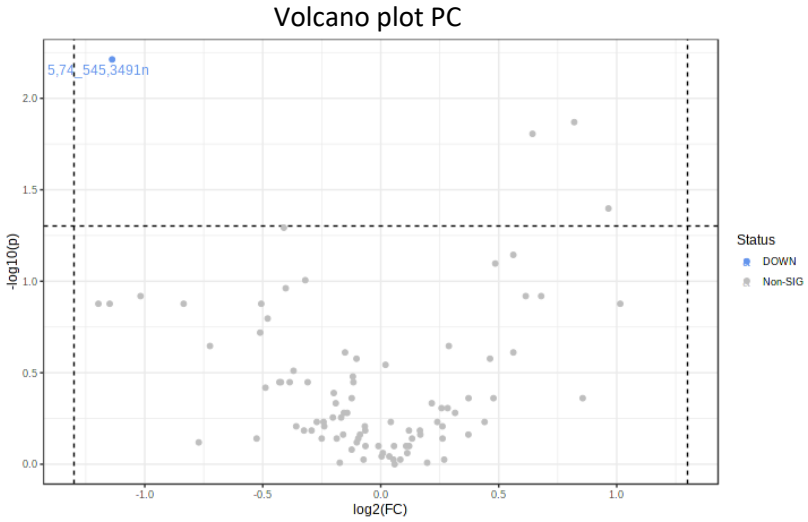

Figure 15. Volcano plot of the lipid subclass PC altered in propionic aciduria patients vs controls. The Log_2 fold change (FC) was plotted against the $-log_{10}$ p-value. Statistical significance was evaluated by t-test (p-value <0.05) and the FC threshold was set to 2.0

Figure 16. Loading plot generated using MetaboAnalyst of TG based of plasma serum samples of propionic aciduria and healthy control samples. The two compound indicated by the red circles are: TG(56:8) (top) and TG(44:2) (bottom).

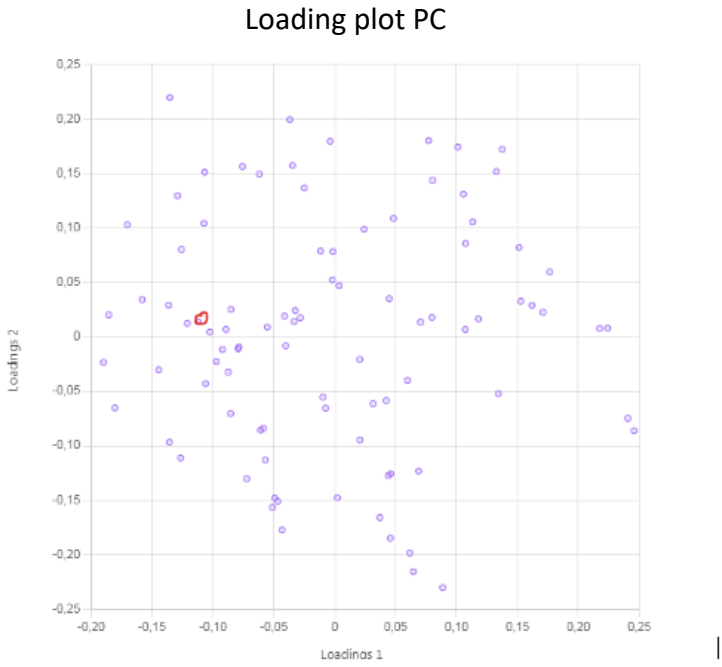

Figure 17. Loading plot generated using MetaboAnalyst of PC based of plasma serum samples of propionic aciduria and healthy control samples.

4.1.2. Confirmation of lipid identity

To confirm the identity of the three downregulated lipids in patients with propionic acidemia the m/z values were plotted against the Retention times of the TG and PC subclasses with different numbers of carbon atoms and double bonds. The raw data that was used is presented in appendix 7.5. In Figure 18 are m/z values plotted against the retention time of the TG along with their number of carbon atoms and double bonds. The average increase in retention time is 0.493 min per carbon atom when the number of double bonds remain the same. The average decrease in retention time is 0.805 min per double bond when the number of carbon atoms remain the same.
In Figure 19-21 are m/z values plotted against the retention time of the PC along with their number of carbon atoms and double bonds. The average increase in retention time is 0.504 min per carbon atom when the number of double bonds remain the same. The average decrease in retention time is 0.539 min per double bond when the number of carbon atoms remain the same.

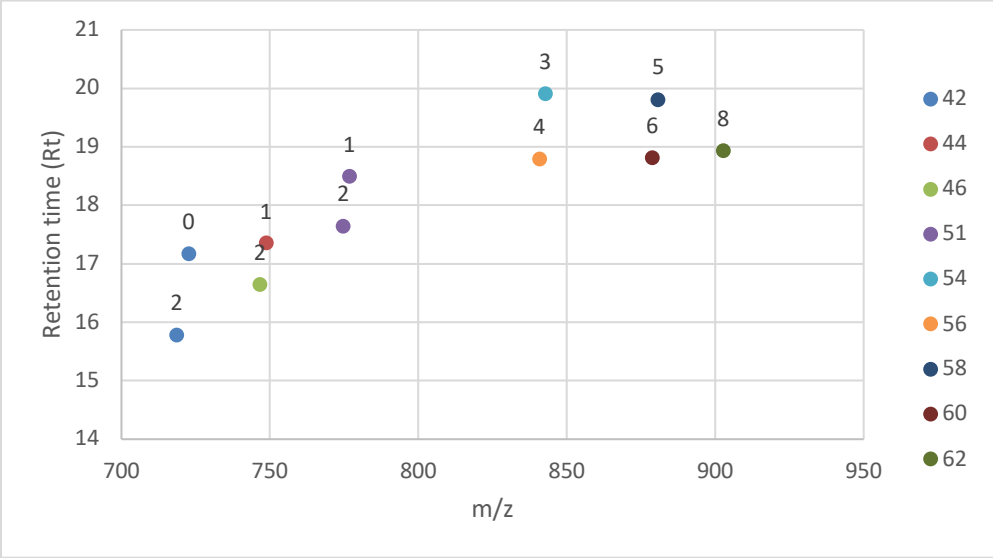

Figure 18. m/z values plotted against the retention time of the TG along with their number of carbon atoms (expressed as different colors presented in the legend) and double bonds (presented as a number in the chart).

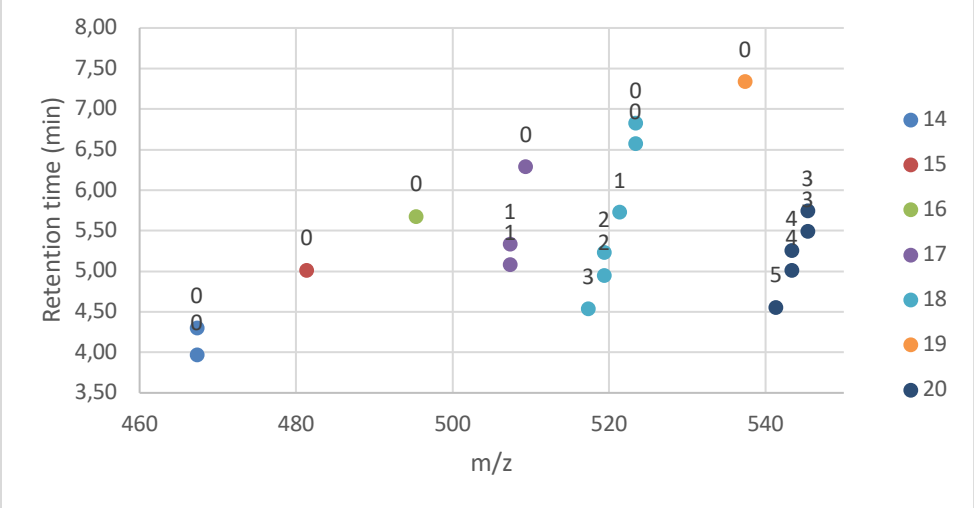

Figure 19. m/z values plotted against the retention time of the TG along with their number of carbon atoms (expressed as different colors presented in the legend) and double bonds (presented as a number in the chart).

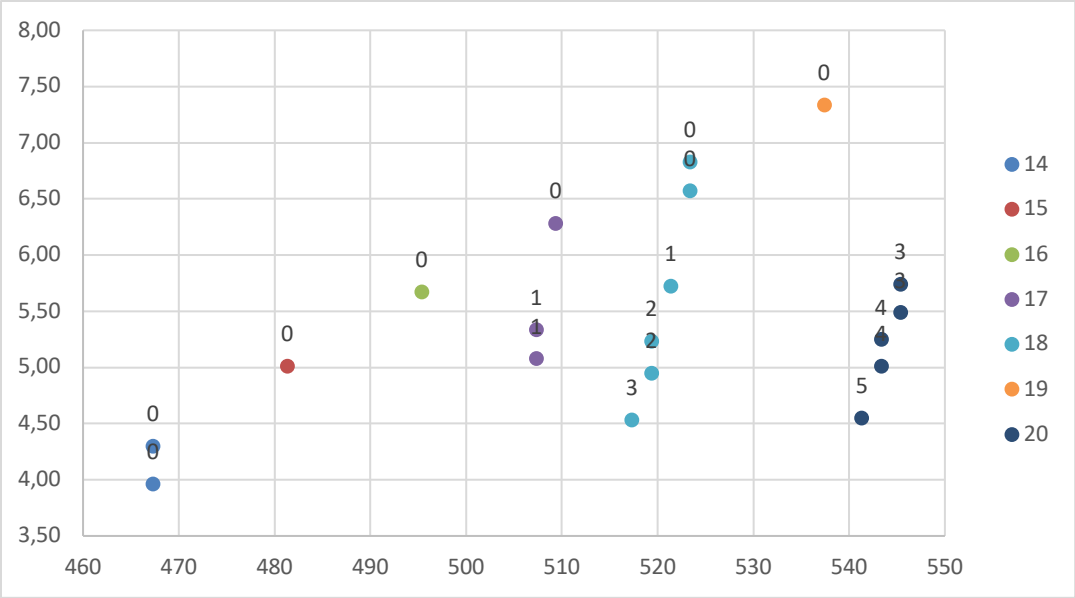

Figure 20. m/z values plotted against the retention time of the TG along with their number of carbon atoms (expressed as different colors presented in the legend) and double bonds (presented as a number in the chart).

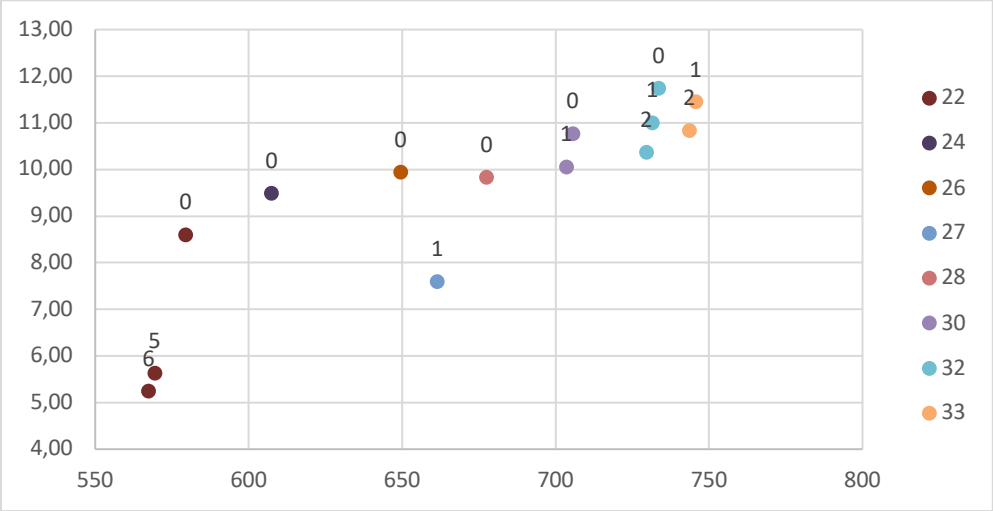

Figure 21. m/z values plotted against the retention time of the TG along with their number of carbon atoms (expressed as different colors presented in the legend) and double bonds (presented as a number in the chart).

4.2 Targeted lipidomics

4.2.1 Optimization of triple quadrupole mass spectrometry parameters

In appendix 7.6 are the mass spectra presented determining the [M+H] adduct in Q1 and its product ions of the sphingolipid standards in MS2 mode using direct infusion of the sphingolipid standards. In Table 3 is presented the optimal parameters of the declustering potential, entrance potential and the collision cell exit potential for all the sphingolipid standards measured in MRM mode. The determined optimal value of the collision energy of the product ions of the [M+H] adducts of the sphingolipid standards are presented in Table 4. The spectra used to determine the optimal parameters are presented in appendix 7.6.

Table 3. The determined optimal values for the declustering potential, entrance potential and collision cell exit potential of the 8 different sphingolipid standards.

Nr.	Lipid standard	Declustering potential (V)	Entrance potential (V)	Collision cell exit potential
1	C16- galactosyl ceramide	50	5	15
2	Galactosyl sphingosine	60	7	15
3	glucosyl sphingosine	50	7	15
4	lactosyl sphingosine	70	8	15
5	D-sphingosine	35	8	15
6	Lactosyl ceramide	65	7	25
7	C16 Ceramide	35	5,5	15
8	glucosyl ceramide	20	5	15
	Average	50	7	15

Table 4. The determined optimal value of the collision energy of the product ions of the [M+H] adducts of the 8 different sphingolipid standards.

C16 galactosyl Ceramide		Galactosyl sphingosine		Glycosyl sphingosine		Lactosyl sphingosine		D-sphingosine		Lactosyl ceramide		C16 Ceramide		Glucosyl ceramide	
m/z	CE (V)	m/z	CE (V)	m/z	CE (V)	m/z	CE (V)	m/z	CE (V)	m/z	CE (V)	m/z	CE (V)	m/z	CE (V)
252,5	52	252,4	40	282,4	35	264,2	32	282,2	20	862,7	73	520,6	24	252,4	50
264,5	47	264,2	32	264,2	30	282,4	40	264,3	28	844,5	70	502,6	28	264,2	50
282,4	55	282,5	33	444,3	26	300,3	30	252,2	28	700,4	70	490,5	32	282,4	50
490,5	40	300,5	25	462,4	16	606,5	30	55,3	50	682,1	70	282,4	38	444,4	30
502,5	40	444,5	26	252,4	43	624,3	23	68,5	35	563,3	70	264,3	36	490,6	30
520,7	30	462,4	20	-	-	324,3	40	82,4	35	538,4	72	256,2	32	502,5	28
538,7	30	-	-	-	-	426,2	40	94,6	35	520,5	70	252,4	38	520,3	25
682,7	30	-	-	-	-	444,3	40	108,6	35	502,4	69	-	-	538,1	25
700,7	23	-	-	-	-	-	-	120,7	35	490,6	70	-	-	682,5	28
-	-	-	-	-	-	-	-	-	-	282,3	68	-	-	-	-
-	-	-	-	-	-	-	-	-	-	264,3	70	-	-	-	-
-	-	-	-	-	-	-	-	-	-	252,2	70	-	-	-	-

4.2.2. Optimization of the liquid chromatography method

Mass measurement settings

Qualitative and quantitative product ions were selected with their optimal collision energy for every sphingolipid standard for the mass measurement of the sphingolipid standards (Table 5). The average of the optimal value of the declustering potential, entrance potential and collision cell exit potential of the standards were used for mass measurement (Table 3).

Table 5. The m/z value of the qualitative product ions and quantitative product ions of the [M+H] adducts with their optimal Collision energies of C16 galactosyl ceramide, galactosyl sphingosine, glucosyl sphingosine, lactosyl sphingosine and D-sphingosine.

	Qualitative product ion (m/z)	Collision energy (CE)	Quantitative product ion (m/z)	Collision energy (CE)
C16 galactosyl Ceramide	682.7	30	264.5	47
	-	-	538.7	30
Galactosyl sphingosine	300.5	25	264.2	32
	-	-	282.5	33
	-	-	444.5	26
Glucosyl sphingosine	444.3	26	282.4	35
	-	-	264.2	30
Lactosyl sphingosine	606.5	30	264.2	32
	624.3	23	282.4	40
	-	-	300.3	30
D-sphingosine	55.3	50	282.2	20
	94.6	35	264.3	28

LC settings

The initial gradient profile for the liquid chromatography analysis used for separation of sphingolipid standards is presented in figure 22 with the settings presented in Table 6. Standards with a concentration of 25 µM and 10 µM were used showing no visibility of the standards present in the chromatogram. Using a concentration of 1 µM resulted in the measurement of only lactosyl sphingosine with a retention time of 21.8 min. Changing the gradient profile by decreasing the mobile phase B concentration in the first 5 minutes resulted in the measurement of lactosyl sphingosine (RT: 8 min), galactosyl sphingosine (RT: 19 min) and glucosyl sphingosine (RT: 19 min). Changing the gradient profile by keeping the mobile phase B concentration at the end of the run high for longer, resulted in no measurement of any of the standards.

Table 6. Gradient profile settings of LC analysis used for separation of sphingolipid standards.

Time (min)	Module	Event	Parameter (%)
2.00	Pumps	Pump B conc.	40
10.00	Pumps	Pump B conc.	70
20.00	Pumps	Pump B conc.	90
22.00	Pumps	Pump B conc.	10
25.00	Controller	Stop	-

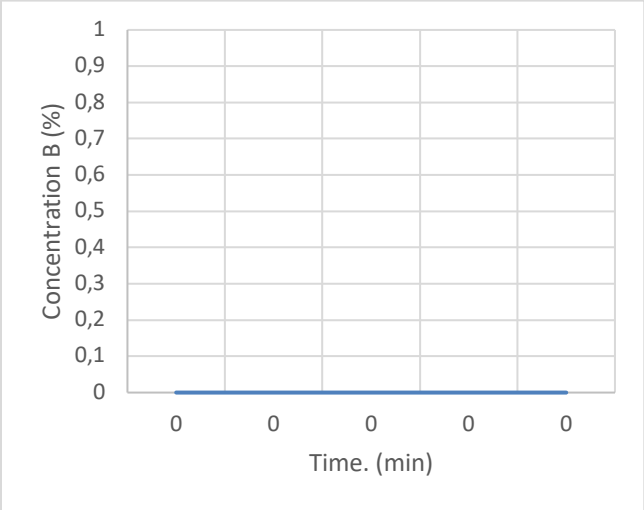

figure 22. Gradient profile of LC analysis used for separation of sphingolipid standards. The concentration (%) of mobile phase B is plotted against the time in minutes.

Using a 40 min isocratic elution with 60% mobile phase B resulted in the measurement of D-sphingosine (RT: 15 min) and lactosyl sphingosine (RT: 37 min).
Using a 40 min isocratic elution with 50% mobile phase B resulted in the measurement of galactosyl sphingosine (RT: 31 min) , glucosyl sphingosine (RT: 31 min) and lactosyl sphingosine (RT: 35 min).
Using a 60 min isocratic elution with 55% mobile phase B resulted in the measurement of lactosyl sphingosine (RT: 34 min) galactosyl sphingosine (RT: 38 min) , glucosyl sphingosine (RT: 38 min) and D-sphingosine (RT: 53 min). The isocratic elution of 55% mobile phase B was repeated following a blank measurement resulting in the elution of D-sphingosine in the blank measurement (appendix 7.7). Lastly a 60 min isocratic elution with 70% mobile phase B resulted in the measurement of all 5 sphingolipid standards: lactosyl sphingosine (RT: 2.5 min) galactosyl sphingosine (RT: 2.5 min), glucosyl sphingosine (RT: 2.5 min), D-sphingosine (RT: 2.7 min) and C16 galactosyl ceramide (RT: 7 min) presented in Figure 23. Followment of a blank measurement showed no elution of any lipid standards. The theoretical column void time is calculated to be 0.76 min (Appendix 7.8).

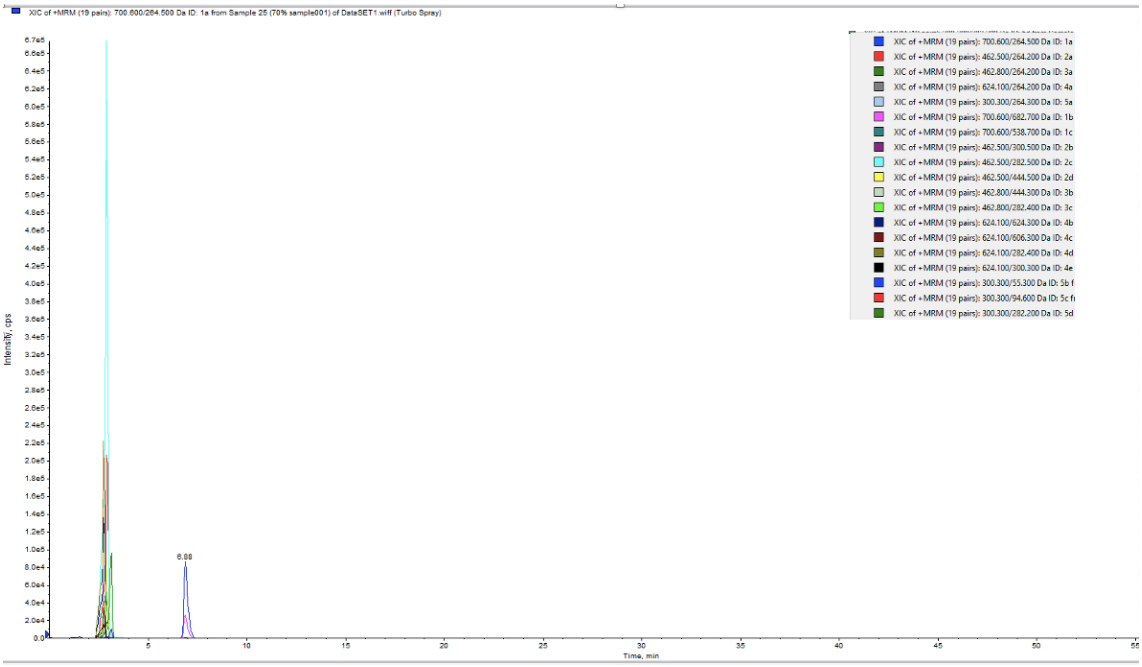

Figure 23. LC-MS/MS chromatogram using an isocratic elution of 70% mobile phase B showing the intensity (cps) plotted against the time (min) eluting the sphingolipid standards: lactosyl sphingosine, galactosyl sphingosine , glucosyl sphingosine, D-sphingosine and C16 galactosyl ceramide. The legend at the top right shows the colors of the product ions of the sphingolipid standards.

5. Discussion

5.1 Untargeted vs targeted lipidomics

Untargeted lipidomics is used when you have a suspicion, but no specific research question. In this case the suspicion of a different lipid profile of PA patients vs healthy controls. However, targeted lipidomics is used when you have a hypothesis. In this study the hypothesis can be based on the chemical and physical properties of the sphingolipid standards used. For untargeted is high-resolution MS necessary, because it can provide m/z values of 4 decimals, providing more sensitivity to identify lipids.

5.2. Untargeted lipidomics

5.2.1. Differential lipid profiles between PA and controls

The first objective of this study was to investigate the differential lipid profiles between PA patients and controls. Until date, there is no information available on the effect of PA on the lipid profile of patients. Surprisingly, the PCA model in Figure 11 showed that there was no natural grouping and differentiation between the groups regarding the lipid metabolism of PA patients and control samples. Even though the PA group seems to have a smaller deviation within the group itself, compared to the control group, there is no grouping present in the PCA plot. The PCA plot shows a difference between groups, but it is not based on the disease itself. These results do not match the initial expectation, since the PA causes the body to not be able to properly process certain proteins and lipids. The volcano plots in Figure 14 and Figure 15 show that three lipids were significantly downregulated in PA patients compared to the controls that were identified as TG(56:8), TG(44:2) and PC(20:3). Literature shows that lipid intake in diets can increase inflammatory pathways and oxidative stress.[46] An explanation for the downregulation of the three lipids in PA patients, could be due to the fact that the healthy control group consumed a ‘normal’ diet which is higher in fat compared to the specific diet that PA patients follow for treatment.

5.2.2. Validation of lipid identification

The lipids were identified by the amount of carbon atoms and double bonds present, since it is not possible to distinguish between isomers. To check if the identification of the lipids is valid the m/z values of the measured TG and PC were plotted against their retention times. In Figure 18 is shown that the increase in the number of carbon atoms causes an increase in retention time and an increase in double bonds causes a decrease in retention time of the TG. TG with 42-51 carbon atoms show a linear correlation. TG with 54 carbon atoms or higher show no linear relation, probably due to the increase of sterical hindrance. The downregulated lipids in PA patients TG(56:8) and TG(44:2) fit into the curve, proving that the identification of the lipids is most probably valid. In Figure 19 is shown that the increase in the number of carbon atoms causes an increase in retention time and the increase in double bonds causes a decrease in retention time of the PC. The PC's show a linear relation with 14-20 number of carbon atoms. In Figure 20 and 21 is shown that the increase of carbon atoms also shows a linear relation, with the exception of a few fluctuations, probably due to the increase of sterical hinder. The downregulated lipid in PA patients PC(20:3) fits into the curve, proving that the identification of the lipids is most probably valid.

5.2. Targeted lipidomics

5.2.1.Optimization of triple quadrupole mass spectrometry parameters

The [M+H] adducts were easily detected for all sphingolipid standards in Q1 mode. The product ions of the [M+H] ions were detected in MS2 mode presented in Table 4. The sphingolipid standard showed a large amount of common product ions with the m/z values of: 252, 264 (triple dehydration of 4-Hydroxysphinganine[47]) and 282 (double dehydration of 4-Hydroxysphinganine[47]).
The ceramides had common product ions with the m/z values of: 520 (loss of inositol monophosphate residue[48]), 538 (loss of inositol monophosphate[47]) and 682. Based on the measured product ions, qualitative ions were selected that were unique to the standard (as much as possible since they were a lot of common ions) and quantitative ions used to determine the concentration of the standard (Table 5).

The mass spectrometry parameters were optimized for the sphingolipid standards using the ramp edit of the parameters: declustering potential, entrance potential, collision cell exit potential and collision energy. The intensity dips shown in Appendix 7.6 were ignored to read the optimal value, since this is due to lack of constant infusion with the syringe. The optimal values for the sphingolipid standards are presented in Table 3 and 4. The measured optimal value DP, EP and CXP were close to the initial starting values for standard lipid measurement presented in the method section. The optimal CE values ranged from 20-70 V between the different sphingolipid standards and product ions.

5.2.2. Optimization of the liquid chromatography method

The optimal collision energy for the different selected qualitative and quantitative product ions of the sphingolipid standards were selected as well as the average of the optimal values for the DP, EP and CXP for the mass measurements. To start a gradient profile was used for analysis for separation of the sphingolipid standards. Using a concentration of 25 µM and 10 µM of the standards resulted in no signal, probably due to saturation of the detector. A concentration of 1 µM resulted in the best signal. Changing the gradient profile showed an inconsequent elution of 3 out of 5 lipid standards. When an isocratic elution was used 4 out of 5 lipid standard were measured using 55% mobile phase B. When the measurement was repeated following a blank measurement it showed that 1 lipid standard eluted during the blank measurement. The best method was during the elution using a 70% mobile phase B resulting in the elution of all sphingolipid standards: lactosyl sphingosine (RT: 2.5 min) galactosyl sphingosine (RT: 2.5 min) , glucosyl sphingosine (RT: 2.5 min), D-sphingosine (RT: 2.7

min) and C16 galactosyl ceramide (RT: 7 min) (Figure 23). In the following blank measurement, no elution took place. This method uses a more practical timeframe, compared to the 60 min measurement using an elution gradient. In the following blank measurement, no elution took place. The order in which the standards eluted from the column is according to the expectation, based on the logP value of the standards. The higher the logP value the more hydrophobic the compound is and the longer it retains on the column. Lactosyl sphingosine, galactosyl sphingosine and glucosyl sphingosine all have a logP value of 4 and eluted simultaneously first. The second one to elute is D-sphingosine which has a logP value of 5. Lastly C16 galactosyl ceramide elutes which has a log P value of 11. To minimize the ion suppression of the compounds, the theoretical void time was calculated to see if any of the standards eluted during this time. The theoretical void time was 0.76 min and showed that none of the compounds eluted during the void time. To make sure the liquid chromatography triple quadrupole mass spectrometry method for quantification of sphingolipid standards is valid, the measurement needs to be repeated at least 10 times in a row to check the reproducibility of the method. Next steps would be to perform a lipid extraction on plasma to measure the concentration of the sphingolipids using the standards.

5.3. Limitations

For the untargeted part of this study the limitations include the small sample size, since only 5 PA patient samples were used. Selecting healthy control samples by gender was not possible, because of the small selection provided. The limitations for the targeted part of this study includes time. By lack of time optimization of the LC-MS/MS was not possible.

6. Conclusion

The objective of the first part of this study was to investigate the differential lipid profiles between PA patients and controls using untargeted lipidomics methods. Results showed there was no natural grouping and differentiation between the groups regarding the lipid metabolism of PA patients and control samples. Three lipids were significantly downregulated in PA patients compared to the controls that were identified as TG(56:8), TG(44:2) and PC(20:3). The lipids were identified by the number of carbon atoms and double bonds present, since it is not possible to distinguish between isomers. To check if the identification of the significantly downregulated lipids were valid the m/z values of the measured TG and PC were plotted against their retention times. All lipids fit into the curves plotted, thus concluding that the identification of the lipids was valid.
The second part of this study was focused on the development and validation of a specific and sensitive liquid chromatography triple quadrupole mass spectrometry method for the quantification of sphingolipids. The sphingolipid standard showed a large amount of common product ions with the m/z values of: 252, 264 and 282. The ceramides had common product ions with the m/z values of: 520, 538 and 682. Using the determined optimal mass spectrometry parameters for the declustering potential, entrance potential, collision cell exit potential and collision energy an optimal method was developed measuring the 5 selected sphingolipid standards. An isocratic elution of 70% mobile phase B is used to elute the sphingolipid standards in the following order: lactosyl sphingosine (RT: 2.5 min) galactosyl sphingosine (RT: 2.5 min) , glucosyl sphingosine (RT: 2.5 min), D-sphingosine (RT: 2.7 min) and C16 galactosyl ceramide (RT: 7 min). To conclude, further more research needs to be performed using a bigger sample pool to validate the downregulated lipids in PA patients compared to healthy controls. The development of the liquid chromatography triple quadrupole mass spectrometry method was successful, but needs more validation. To do this the experiment needs to be repeated to check the reproducibility of the method. Next steps include measuring the sphingolipid concentration using plasma serum.

References

1. Mensink RP, Sanders TA, Baer DJ, Hayes KC, Howles PN, Marangoni A. The Increasing Use of Interesterified Lipids in the Food Supply and Their Effects on Health Parameters. *Adv Nutr*. 2016;7(4):719-729. doi:10.3945/AN.115.009662
2. Chen H, Wei F, Dong X yan, Xiang J qian, Quek S young, Wang X. Lipidomics in food science. *Curr Opin Food Sci*. 2017;16:80-87. doi:10.1016/J.COFS.2017.08.003
3. Fahy E, Cotter D, Sud M, Subramaniam S. Lipid classification, structures and tools. *Biochim Biophys Acta*. 2011;1811(11):637. doi:10.1016/J.BBALIP.2011.06.009
4. LIPID MAPS. https://www.lipidmaps.org/resources/tutorials/lipid_tutorial. Accessed July 11, 2022.
5. 2.35 Triglycerides | Nutrition Flexbook. https://courses.lumenlearning.com/suny-nutrition/chapter/2-35-triglycerides/. Accessed July 11, 2022.
6. Merrill AH, Schmelz E-M, Dillehay DL, et al. SYMPOSIUM Sphingolipids-The Enigmatic Lipid Class: Biochemistry, Physiology, and Pathophysiology 1. *Toxicol Appl Pharmacol*. 1997;142:208-225.
7. Merrill AH. Sphingolipids. *Biochem Lipids, Lipoproteins Membr*. January 2008:363-397. doi:10.1016/B978-044453219-0.50015-5
8. Simons K, Ikonen E. Functional rafts in cell membranes. *Nat 1997 3876633*. 1997;387(6633):569-572. doi:10.1038/42408
9. Ramstedt B, Slotte JP. Membrane properties of sphingomyelins. *FEBS Lett*. 2002;531(1):33-37. doi:10.1016/S0014-5793(02)03406-3
10. Bruhn H, Winkelmann J, Andersen C, Andrä J, Leippe M. Dissection of the mechanisms of cytolytic and antibacterial activity of lysenin, a defence protein of the annelid Eisenia fetida. *Dev Comp Immunol*. 2006;30(7):597-606. doi:10.1016/J.DCI.2005.09.002
11. IVD Antibody Development Services for Sphingomyelin Marker - Creative Biolabs. https://www.creative-biolabs.com/drug-discovery/diagnostics/ivd-antibodies-for-sphingomyelin-marker.htm. Accessed July 11, 2022.
12. Liebisch G, Vizcaíno JA, Köfeler H, et al. Shorthand notation for lipid structures derived from mass spectrometry. *J Lipid Res*. 2013;54(6):1523-1530. doi:10.1194/JLR.M033506
13. Yin P, Xu G. Current state-of-the-art of nontargeted metabolomics based on liquid chromatography–mass spectrometry with special emphasis in clinical applications. *J Chromatogr A*. 2014;1374:1-13. doi:10.1016/J.CHROMA.2014.11.050
14. Contrepois K, Jiang L, Snyder M. Optimized analytical procedures for the untargeted metabolomic profiling of human urine and plasma by combining hydrophilic interaction (HILIC) and reverse-phase liquid chromatography (RPLC)-mass spectrometry. *Mol Cell Proteomics*. 2015;14(6):1684-1695. doi:10.1074/MCP.M114.046508/ATTACHMENT/F9FA5E8F-E110-4EFB-8D42-AD77B9D5C5A0/MMC1.ZIP
15. Contrepois K, Liang L, Snyder M. Can Metabolic Profiles Be Used as a Phenotypic Readout of the Genome to Enhance Precision Medicine? *Clin Chem*. 2016;62(5):676-678. doi:10.1373/CLINCHEM.2015.251181
16. Lee HC, Yokomizo T. Applications of mass spectrometry-based targeted and non-targeted lipidomics. *Biochem Biophys Res Commun*. 2018;504(3):576-581. doi:10.1016/J.BBRC.2018.03.081
17. Contrepois K, Mahmoudi S, Ubhi BK, et al. Cross-Platform Comparison of Untargeted and Targeted Lipidomics Approaches on Aging Mouse Plasma. *Sci Reports 2018 81*. 2018;8(1):1-9. doi:10.1038/s41598-018-35807-4
18. Cajka T, Fiehn O. Toward Merging Untargeted and Targeted Methods in Mass Spectrometry-Based Metabolomics and Lipidomics. *Anal Chem*. 2016;88(1):524-545. doi:10.1021/ACS.ANALCHEM.5B04491/ASSET/IMAGES/ACS.ANALCHEM.5B04491.SOCIAL.JPEG

_V03
19. Köfeler HC, Fauland A, Rechberger GN, Trötzmüller M. Mass Spectrometry Based Lipidomics: An Overview of Technological Platforms. *Metab 2012, Vol 2, Pages 19-38*. 2012;2(1):19-38. doi:10.3390/METABO2010019
20. Sud M, Fahy E, Cotter D, et al. LMSD: LIPID MAPS structure database. *Nucleic Acids Res*. 2007;35(suppl_1):D527-D532. doi:10.1093/NAR/GKL838
21. Fahy E, Subramaniam S, Brown HA, et al. A comprehensive classification system for lipids1. *J Lipid Res*. 2005;46(5):839-861. doi:10.1194/JLR.E400004-JLR200
22. Yang K, Han X. Lipidomics: Techniques, applications, and outcomes related to biomedical sciences. *Trends Biochem Sci*. 2016;41(11):954. doi:10.1016/J.TIBS.2016.08.010
23. Lydic TA, Goo Y-H. Lipidomics unveils the complexity of the lipidome in metabolic diseases. *Clin Transl Med 2018 71*. 2018;7(1):1-13. doi:10.1186/S40169-018-0182-9
24. Gossert AD, Hinniger A, Gutmann S, Jahnke W, Strauss A, Fernández C. A simple protocol for amino acid type selective isotope labeling in insect cells with improved yields and high reproducibility. *J Biomol NMR*. 2011;51(4):449-456. doi:10.1007/S10858-011-9570-9/FIGURES/6
25. BLIGH EG, DYER WJ. A RAPID METHOD OF TOTAL LIPID EXTRACTION AND PURIFICATION. *https://doi.org/101139/o59-099*. 2011;37(8):911-917. doi:10.1139/O59-099
26. Gil A, Zhang W, Wolters JC, et al. One- vs two-phase extraction: re-evaluation of sample preparation procedures for untargeted lipidomics in plasma samples. *Anal Bioanal Chem*. 2018;410(23):5859-5870. doi:10.1007/S00216-018-1200-X/FIGURES/6
27. Matyash V, Liebisch G, Kurzchalia T V., Shevchenko A, Schwudke D. Lipid extraction by methyl-terf-butyl ether for high-throughput lipidomics. *J Lipid Res*. 2008;49(5):1137-1146. doi:10.1194/JLR.D700041-JLR200/ATTACHMENT/128DF5F4-8BF9-4B83-B9E1-021DB9E24F57/MMC1.PDF
28. Löfgren L, Ståhlman M, Forsberg GB, Saarinen S, Nilsson R, Hansson GI. The BUME method: a novel automated chloroform-free 96-well total lipid extraction method for blood plasma [S]. *J Lipid Res*. 2012;53(8):1690-1700. doi:10.1194/JLR.D023036
29. Pellegrino RM, Di Veroli A, Valeri A, Goracci L, Cruciani G. LC/MS lipid profiling from human serum: A new method for global lipid extraction. *Anal Bioanal Chem*. 2014;406(30):7937-7948. doi:10.1007/S00216-014-8255-0/FIGURES/6
30. Reichl B, Eichelberg N, Freytag M, Gojo J, Peyrl A, Buchberger W. Evaluation and optimization of common lipid extraction methods in cerebrospinal fluid samples. *J Chromatogr B*. 2020;1153:122271. doi:10.1016/J.JCHROMB.2020.122271
31. Hummel J, Segu S, Li Y, Irgang S, Jueppner J, Giavalisco P. Ultra performance liquid chromatography and high resolution mass spectrometry for the analysis of plant lipids. *Front Plant Sci*. 2011;2(OCT):54. doi:10.3389/FPLS.2011.00054/BIBTEX
32. Loizides-Mangold U. On the future of mass-spectrometry-based lipidomics. *FEBS J*. 2013;280(12):2817-2829. doi:10.1111/febs.12202
33. HPLC Principles and parameters | KNAUER. https://www.knauer.net/en/Systems-Solutions/Analytical-HPLC-UHPLC/HPLC-Basics---principles-and-parameters. Accessed April 1, 2022.
34. Javier Arrebola-Lié banas F, Romero-Gonzá lez R, Garrido Frenich A. Chapter 1 – HRMS: Fundamentals and Basic Concepts. 2017. doi:10.1016/B978-0-12-809464-8.00001-4
35. Dass C. FUNDAMENTALS OF CONTEMPORARY MASS SPECTROMETRY.
36. Ekman R, Silberring J, Westman-Brinkmalm A, Kraj A. *Mass Spectrometry : Instrumentation, Interpretation, and Applications*. Hoboken N.J.: John Wiley & Sons; 2009. doi:10.1002/9780470395813
37. Allen DR, McWhinney BC. Quadrupole Time-of-Flight Mass Spectrometry: A Paradigm Shift in Toxicology Screening Applications. *Clin Biochem Rev*. 2019;40(3):135. doi:10.33176/AACB-19-00023
38. Gross JH. Mass Spectrometry.

39. Pitt JJ. Principles and Applications of Liquid Chromatography-Mass Spectrometry in Clinical Biochemistry. *Clin Biochem Rev*. 2009;30(1):19. /pmc/articles/PMC2643089/. Accessed July 11, 2022.
40. Similarities of Univariate & Multivariate Statistical Analysis. https://sciencing.com/similarities-of-univariate-multivariate-statistical-analysis-12549543.html. Accessed July 29, 2022.
41. Propionic Acidemia - NORD (National Organization for Rare Disorders). https://rarediseases.org/rare-diseases/propionic-acidemia/. Accessed April 1, 2022.
42. Propionic Acidemia - NORD (National Organization for Rare Disorders). https://rarediseases.org/rare-diseases/propionic-acidemia/. Accessed November 23, 2021.
43. Wongkittichote P, Ah Mew N, Chapman KA. Propionyl-CoA carboxylase – A review. *Mol Genet Metab*. 2017;122(4):145-152. doi:10.1016/J.YMGME.2017.10.002
44. Metabolic pathway for propionyl-CoA carboxylase (PCC). The pathways in... | Download Scientific Diagram. https://www.researchgate.net/figure/Metabolic-pathway-for-propionyl-CoA-carboxylase-PCC-The-pathways-in-a-normal-patient_fig1_23489438. Accessed April 1, 2022.
45. Mellon AF, Deshpande SA, Mathers JC, Bartlett K. Effect of oral antibiotics on intestinal production of propionic acid. *Arch Dis Child*. 2000;82(2):169-172. doi:10.1136/ADC.82.2.169
46. Arrigo T, Leonardi S, Cuppari C, et al. Role of the diet as a link between oxidative stress and liver diseases. *World J Gastroenterol*. 2015;21(2):384. doi:10.3748/WJG.V21.I2.384
47. Zheng W, Kollmeyer J, Symolon H, et al. Ceramides and other bioactive sphingolipid backbones in health and disease: Lipidomic analysis, metabolism and roles in membrane structure, dynamics, signaling and autophagy. *Biochim Biophys Acta - Biomembr*. 2006;1758(12):1864-1884. doi:10.1016/J.BBAMEM.2006.08.009
48. Hsu FF, Turk J, Zhang K, Beverley SM. Characterization of Inositol Phosphorylceramides from Leishmania major by Tandem Mass Spectrometry with Electrospray Ionization. *J Am Soc Mass Spectrom*. 2007;18(9):1591. doi:10.1016/J.JASMS.2007.05.017

7. Appendix

7.1 Lipid standards

Table 7. Lipid standards with their chemical names, abbreviations and their sources that were used to make the internal standard mix for the untargeted lipidomics experiment.

No.	Chemical name	Abbreviation	Source
1	1,2-diheptadecanoyl-*sn*-glycero-3-[Phospho-rac-(1-glycerol)]	PC(17:0/17:0)	Avanti Polar Lipids Inc.
2	1,2-Dimyristoyl-sn-Glycero-3-[Phospho-L-Serine]	PS(14:0/14:0)	Avanti Polar Lipids Inc.
3	1,1',2,2'-tetramyristoyl cardiolipin	CA(14:0)	Avanti Polar Lipids Inc.
4	1-Myristoyl-2-Hydroxy-sn-Glycero-3-Phosphocholine	LysoPC(14:0/14:0)	Avanti Polar Lipids Inc.
5	D-glucosyl-B-1,1'-N-palmitoyl-D-erythro-sphingosine	GlucCer(d18:1/16:0)	Avanti Polar Lipids Inc.
6	1,2-dipentadecanoyl-*sn*-glycero-3-phosphoethanolamine	PE(15:0/15:0)	Avanti Polar Lipids Inc.

Table 8. Sphingolipid standards with their chemical names, abbreviations and their sources that were used for the targeted lipidomics experiments.

No.	Chemical name	Abbreviation	Source
1	D-galactosyl-B1,1'-N-palmitoyl-D-erythro-sphingosine	Galactosyl Cer(d18:1/16:0)	Avanti Polar Lipids Inc.
2	D-galactosyl-B1-1'-D-erythro-sphingosine	Galactosyl Sph(d18:1)	Avanti Polar Lipids Inc.
3	D-glucosyl-B1-1' -D-erythro-sphingosine	Glucosyl Sph(d18:1)	Avanti Polar Lipids Inc.
4	D-lactosyl-B1-1'-D-erythro-sphingosine	Lactosyl Sph(d18:1)	Avanti Polar Lipids Inc.
5	D-erythro-sphingosine	Sph(d18:1)	Avanti Polar Lipids Inc.
6	D-lactosyl-B-1'1 N-palmitoyl-D-erythro-sphingosine	Lactosyl Cer(d18:1/16:0)	Avanti Polar Lipids Inc.
7	N-palmitoyl-D-erythro-sphingosine	Cer(d18:1/16:0)	Avanti Polar Lipids Inc.
8	D-glucosyl-B-1,1'-N-palmitoyl-D-erythro-sphingosine	Glucosyl Cer(d18:1/16:0)	Avanti Polar Lipids Inc.

7.2 Normalization of data

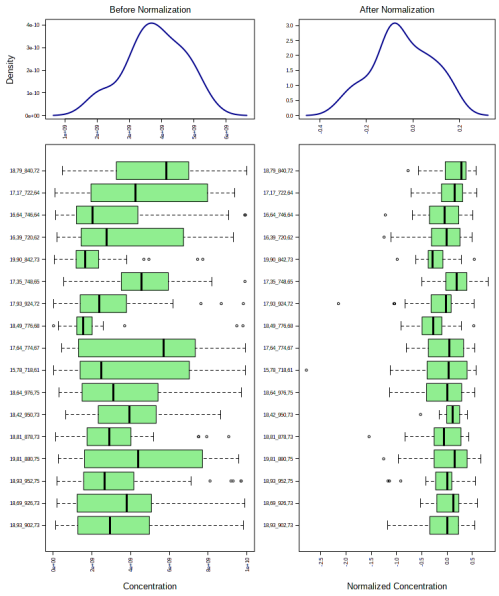

Figure 24. Before normalization of the data in Metaboanalyst.

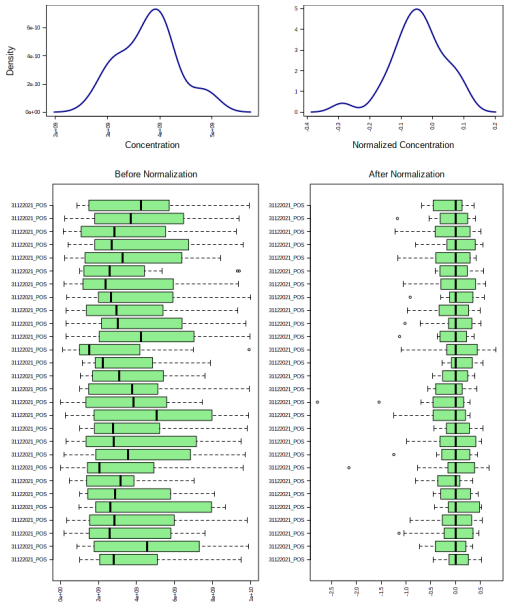

Figure 25. After normalization by median and log transformation of the data.

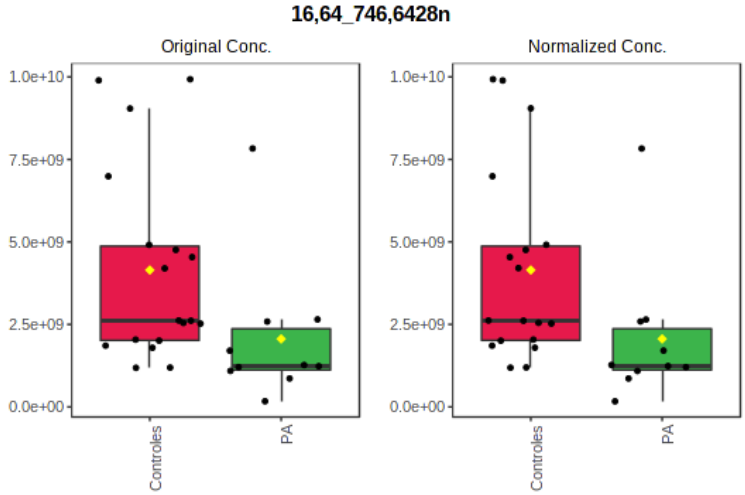

Figure 26. Original and normalized concentration of compound 16,64_746,6428n of PA patient and control samples.

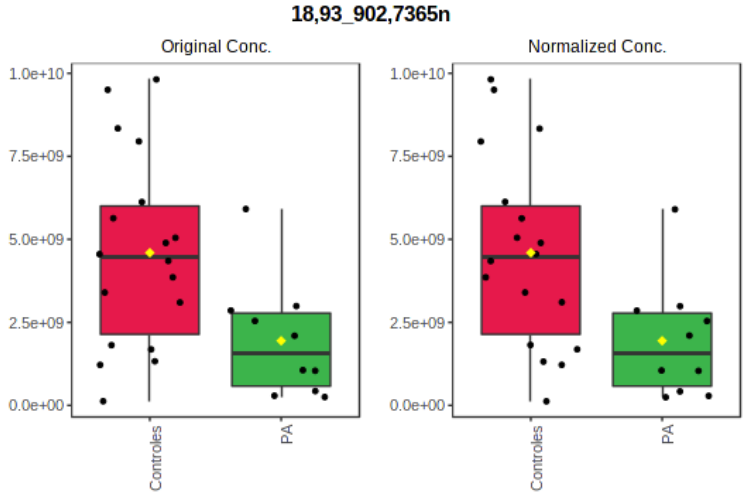

Figure 27. Original and normalized concentration of compound 18,93_902,7365n of PA patient and control samples.

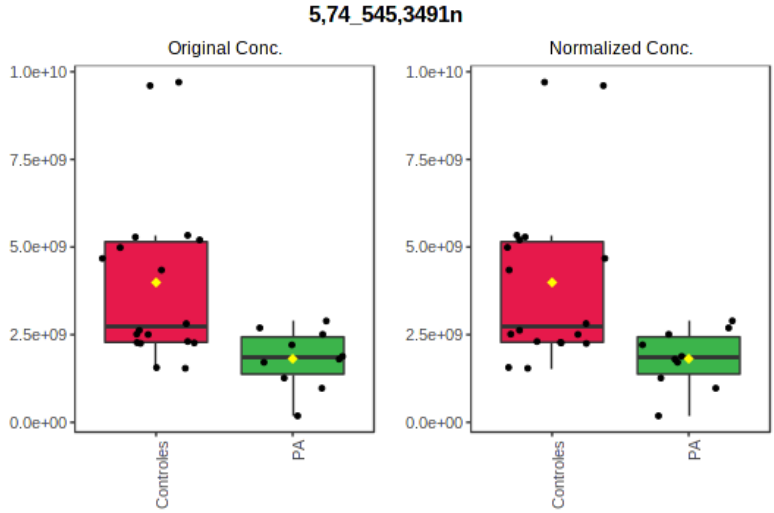

Figure 28. Original and normalized concentration of compound 5,74_545,3491n of PA patient and control samples.

7.3. Principal component analysis

TG

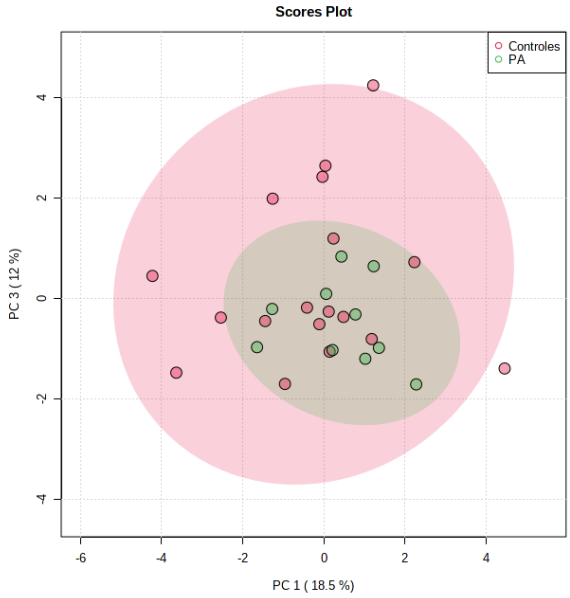

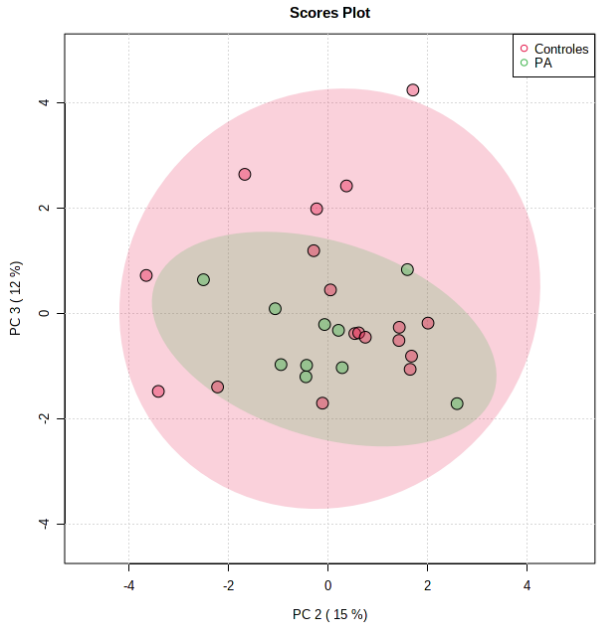

PC

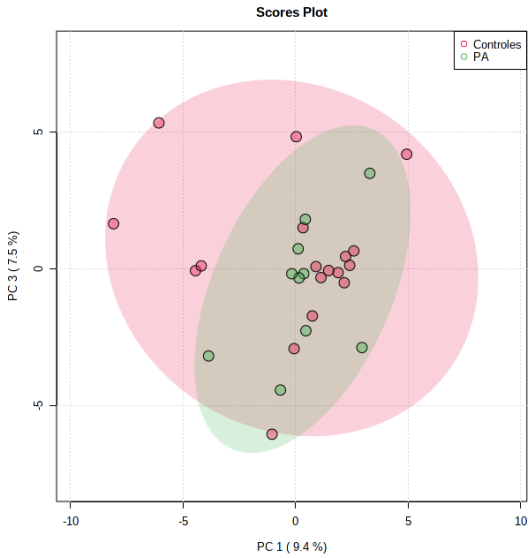
Scores Plot
Controles
PA
PC 3 (7.5 %)
PC 1 (9.4 %)
-10
-5
0
5
10
5
0
-5

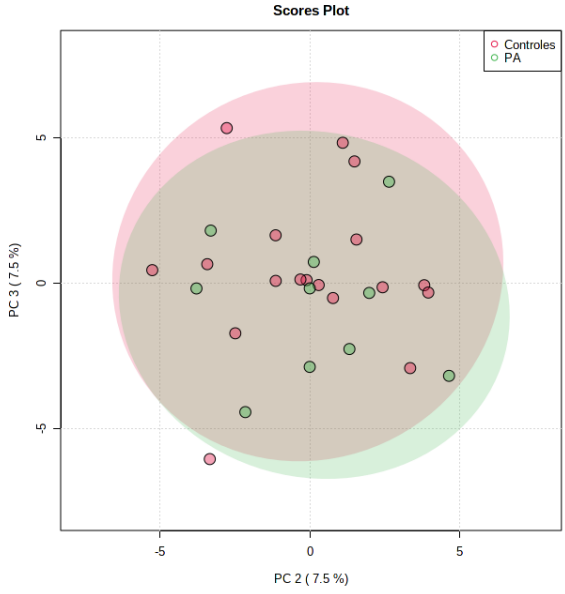
Scores Plot
Controles
PA
PC 3 (7.5 %)
PC 2 (7.5 %)
-5
0
5
5
0
-5

All annotated lipids

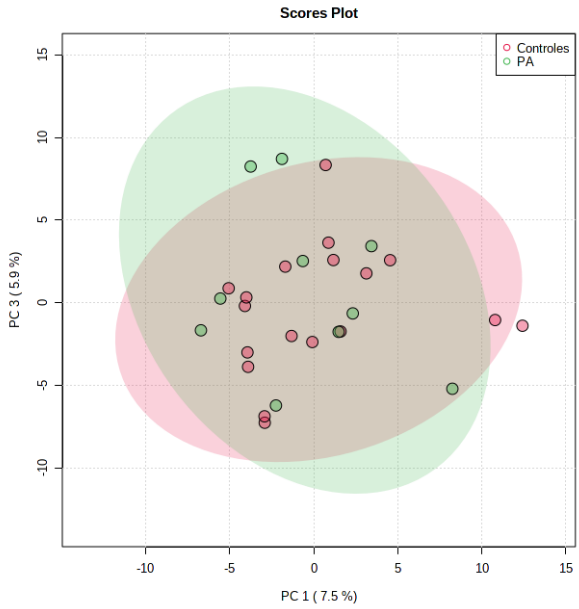

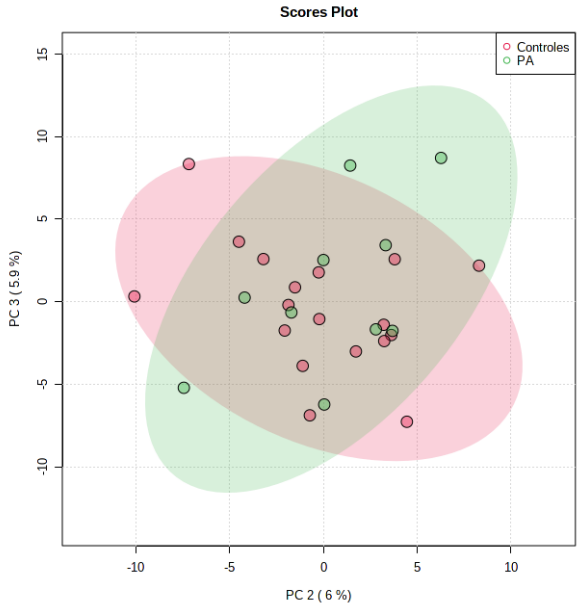

7.4 Univariate statistical analysis

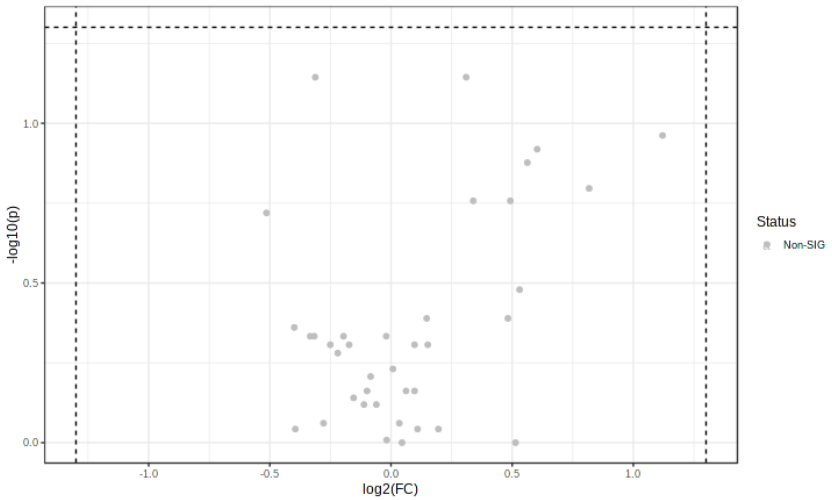

Figure 29. Volcano plot of the lipid subclass DG altered in proprionic aciduria patients vs controls. The Log_2 fold change (FC) was plotted against the $-log_{10}$ p-value. Statistical significance was evaluated by t-test (p-value <0.05) and the FC threshold was set to 2.0

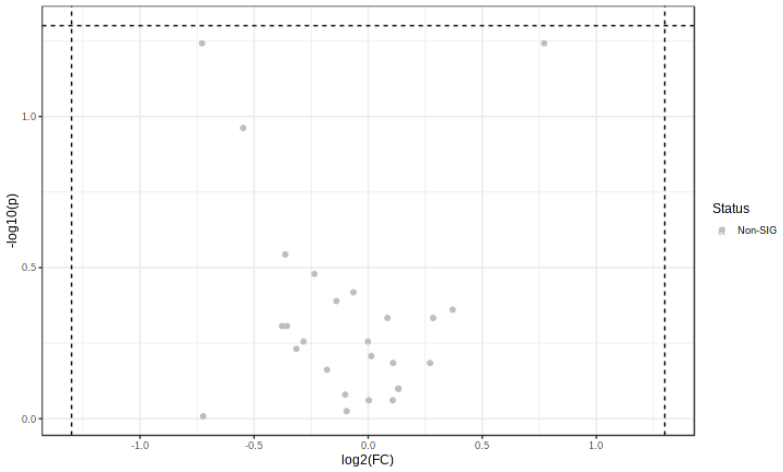

Figure 30. Volcano plot of the lipid subclass MG altered in proprionic aciduria patients vs controls. The Log_2 fold change (FC) was plotted against the $-log_{10}$ p-value. Statistical significance was evaluated by t-test (p-value <0.05) and the FC threshold was set to 2.0

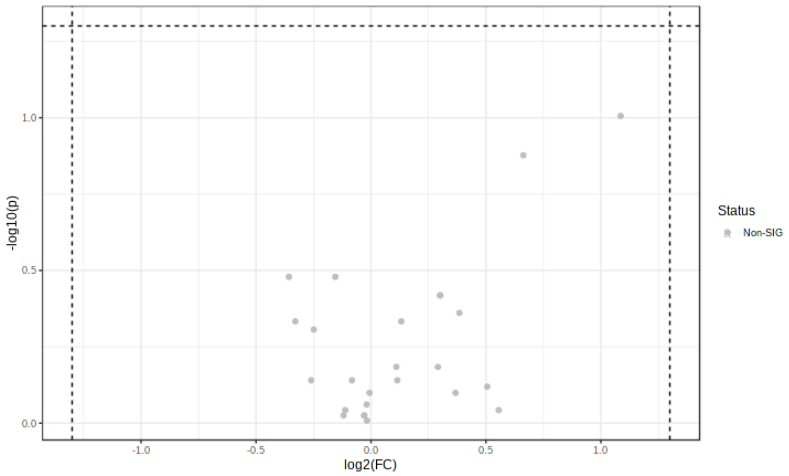

Figure 31. Volcano plot of the lipid subclass PE altered in proprionic aciduria patients vs controls. The Log_2 fold change (FC) was plotted against the $-log_{10}$ p-value. Statistical significance was evaluated by t-test (p-value <0.05) and the FC threshold was set to 2.0

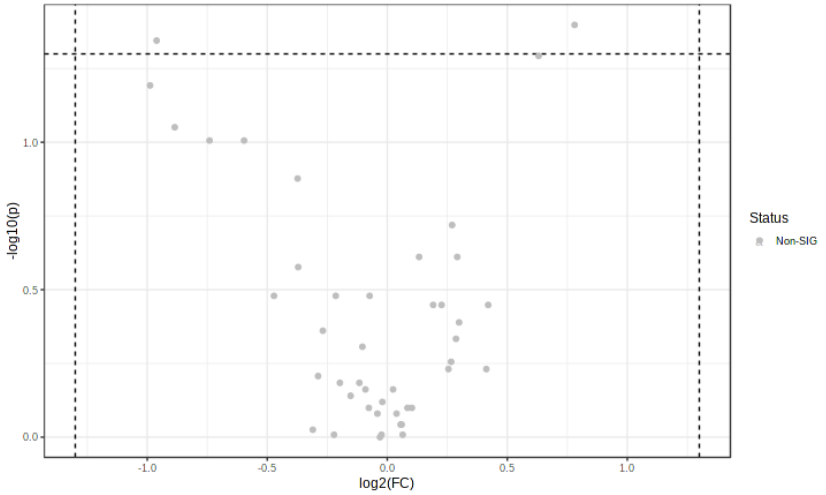

Figure 32. Volcano plot of the lipid subclass PA altered in proprionic aciduria patients vs controls. The Log_2 fold change (FC) was plotted against the $-log_{10}$ p-value. Statistical significance was evaluated by t-test (p-value <0.05) and the FC threshold was set to 2.0

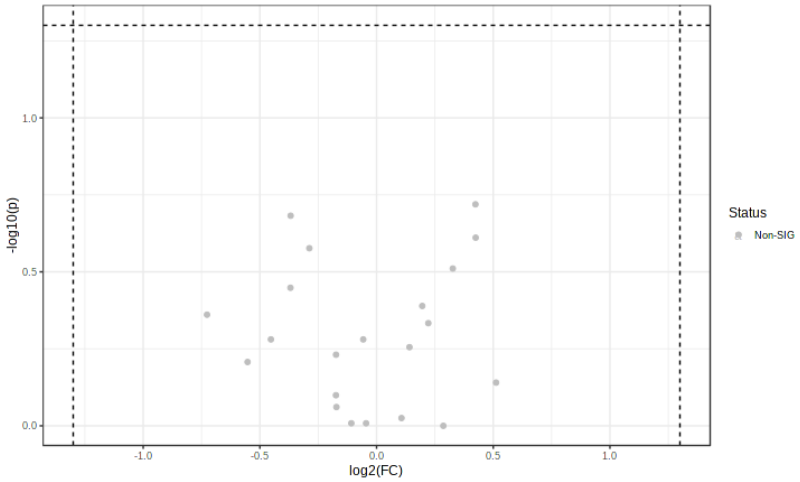

Figure 33. Volcano plot of the lipid subclass PS altered in proprionic aciduria patients vs controls. The Log_2 fold change (FC) was plotted against the $-log_{10}$ p-value. Statistical significance was evaluated by t-test (p-value <0.05) and the FC threshold was set to 2.0

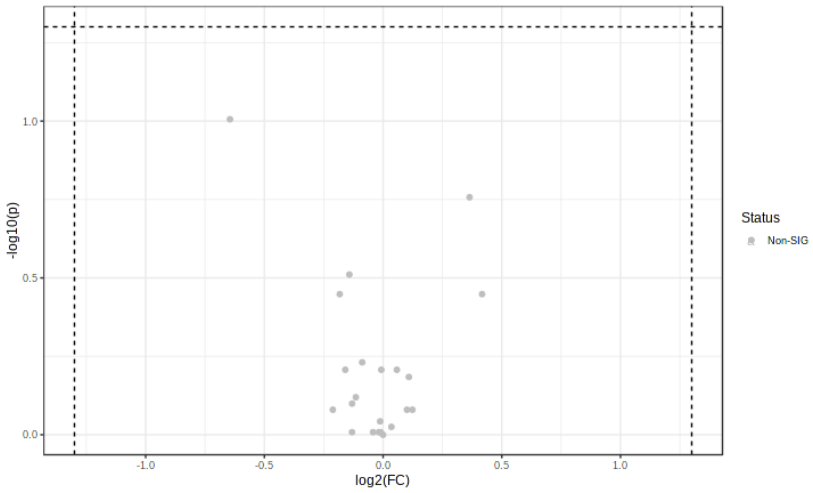

Figure 34. Volcano plot of the lipid subclass SM altered in proprionic aciduria patients vs controls. The Log_2 fold change (FC) was plotted against the $-log_{10}$ p-value. Statistical significance was evaluated by t-test (p-value <0.05) and the FC threshold was set to 2.0

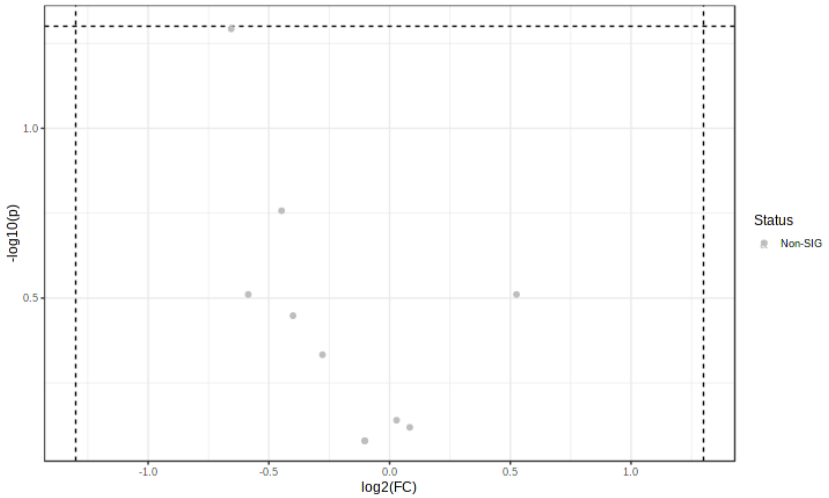

Figure 35. Volcano plot of the lipid subclass Cer altered in proprionic aciduria patients vs controls. The Log_2 fold change (FC) was plotted against the $-log_{10}$ p-value. Statistical significance was evaluated by t-test (p-value <0.05) and the FC threshold was set to 2.0

7.5 Confirmation of the identity of TG and PC

Table 9. Shorthand notation, m/z, retention time, number of carbon atoms and number of double bonds of identified lipids belonging to the TG subclass.

Compound (shorthand notation)	m/z	RT (min)	Carbon atoms	Double bonds
TG(42:0)	722,6424	17,17	42	0
TG(42:2)	718,6111	15,78	42	2
TG(44:1)	748,6581	17,35	44	1
TG(44:2)	746,6424	16,64	44	2
TG(46:1)	776,6894	18,49	46	1
TG(46:2)	774,6737	17,64	46	2
TG(51:3)	842,7363	19,90	51	3
TG(51:4)	840,7207	18,79	51	4
TG(54:5)	880,752	19,81	54	5
TG(54:6)	878,7363	18,81	54	6
TG(56:8)	902,7363	18,93	56	8
TG(58:10)	926,7363	18,69	58	10
TG(58:11)	924,7207	17,93	58	11
TG(60:11)	952,7520	18,93	60	11
TG(60:12)	950,7363	18,42	60	12
TG(62:13)	976,7520	18,64	62	13

Table 10. The m/z, retention time, number of carbon atoms and number of double bonds of identified lipids belonging to the PC subclass.

Compound	m/z	RT (min)	Carbon atoms	Double bonds
PC(14:0/0:0)	467,2995	3,96	14	0
PC(14:0/0:0)	467,3007	4,30	14	0
PC(15:0/0:0)	481,3178	5,01	15	0
PC(16:0/0:0)	495,3335	5,67	16	0
PC(17:0/0:0)	509,3491	6,28	17	0
PC(17:1/0:0)	507,3338	5,08	17	1
PC(17:1/0:0)	507,3338	5,34	17	1
PC(18:0/0:0)	523,3648	6,83	18	0
PC(18:1/0:0)	521,3491	5,72	18	1
PC(18:2/0:0)	519,3337	5,23	18	2
PC(18:2/0:0)	519,3334	4,95	18	2
PC(18:3/0:0)	517,3165	4,54	18	3
PC(18:3/0:0)	517,3144	11,23	18	3
PC(18:0/0:0)	523,3638	6,57	18	0
PC(19:0/0:0)	537,3797	7,34	19	0
PC(20:3/0:0)	545,3491	5,74	20	3
PC(20:3/0:0)	545,3491	5,49	20	3
PC(20:3/0:0)	546,353	12,86	20	3
PC(20:4/0:0)	543,3335	5,25	20	4
PC(20:4/0:0)	543,3338	5,01	20	4
PC(20:5/0:0)	541,3173	4,55	20	5
PC(22:0/0:0)	579,4266	8,60	22	0
PC(22:5/0:0)	569,3492	5,64	22	5
PC(22:6/0:0)	567,3337	5,25	22	6
PC(24:0/0:0)	607,4578	9,49	24	0
PC(26:0/0:0)	649,4683	9,95	26	0
PC(26:2/0:0)	645,4687	7,84	26	2

GPCho(24:1/3:0)	661,4683	7,60	27	1
GPCho(14:0/14:0)	677,5006	9,85	28	0
GPCho(14:0/16:0)	705,5318	10,78	30	0
GPCho(15:1/15:0)	703,5152	10,06	30	1
GPCho(14:0/16:0)	705,5318	10,78	30	0
GPCho(15:1/15:0)	703,5152	10,06	30	1
GPCho(14:0/16:0)	705,5318	10,78	30	0
GPCho(15:1/15:0)	703,5152	10,06	30	1
GPCho(15:0/18:1)	745,5622	11,46	33	1
GPCho(15:0/18:2)	743,5465	10,85	33	2
GPCho(10:0/24:0)	761,5935	12,66	34	0
GPCho(16:0/18:2)	757,5622	11,30	34	2
GPCho(17:2/17:2)	753,5309	10,32	34	4
GPCho(16:1/18:4)	751,5152	9,81	34	5
GPCho(18:1/17:0)	773,5935	11,59	35	1
GPCho(17:0/18:1)	773,5935	12,41	35	1
GPCho(17:1/18:1)	771,5778	12,83	35	2
GPCho(15:0/20:4)	767,5465	10,79	35	4
GPCho(18:4/17:1)	765,5309	10,27	35	5
GPCho(18:1/18:0)	787,6091	12,86	36	1
GPCho(18:3/18:3)	777,5309	10,25	36	6
GPCho(16:0/20:5)	779,5465	10,74	36	5
GPCho(18:2/18:2)	781,5622	10,90	36	4
GPCho(16:0/20:4)	781,5622	11,23	36	4
GPCho(18:3/18:2)	779,5465	11,35	36	5
GPCho(11:0/26:0)	803,6404	14,47	37	0
GPCho(18:0/20:3)	811,6091	12,57	38	3
GPCho(18:1/20:4)	807,5778	11,46	38	5
GPCho(18:0/20:4)	809,5935	12,18	38	4
GPCho(18:0/20:5)	807,5778	11,67	38	5
GPCho(18:0/20:2)	813,6248	13,10	38	2
GPCho(15:1/24:4)	821,5935	13,44	39	5
GPCho(17:0/22:6)	819,5778	10,18	39	6
GPCho(17:1/22:2)	825,6248	9,85	39	3
GPCho(18:1/22:6)	831,5778	11,37	40	7
GPCho(20:2/20:2)	837,6248	12,91	40	4
GPCho(20:3/20:3)	833,5935	11,83	40	6
GPCho(20:3/20:3)	833,5935	12,10	40	6
GPCho(20:2/20:3)	835,6091	12,39	40	5
GPCho(18:4/26:2)	889,6561	14,32	44	6
GPCho(22:2/22:2)	893,6874	14,79	44	4

7.6 Triple quadrupole mass spectrometry spectra

7.6.1. C16 galactosyl ceramide

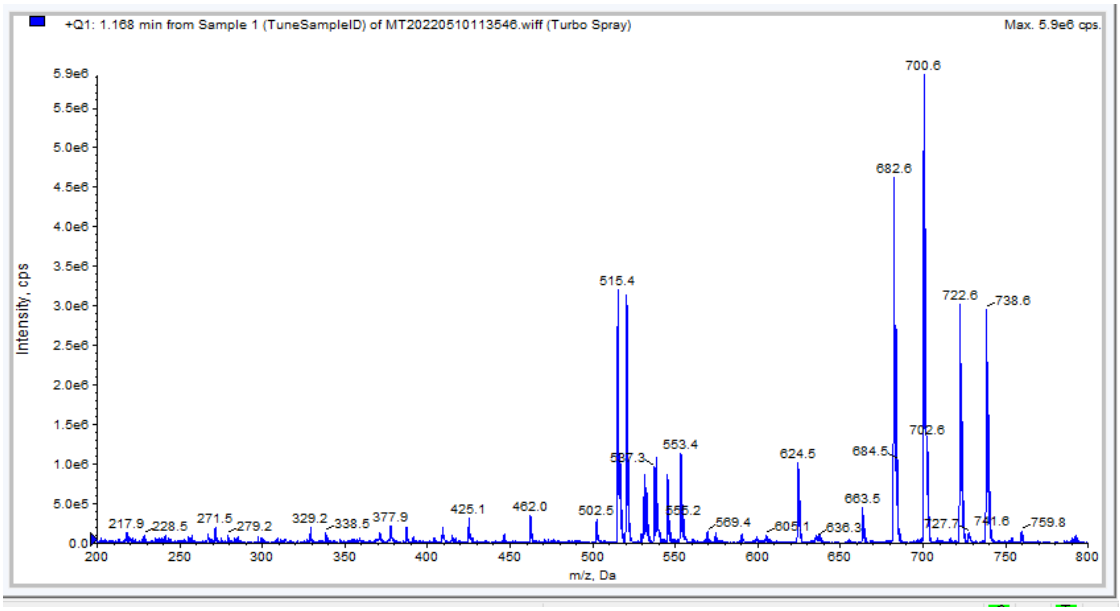

Figure 36. The m/z is plotted against the Intensity of the mass spectrum measuring in Q1 using SCIEX API 3200 LC-MS/MS of C16 galactosyl ceramide. The peak at m/z = 700.6 is determined to be the {M+H] adduct.

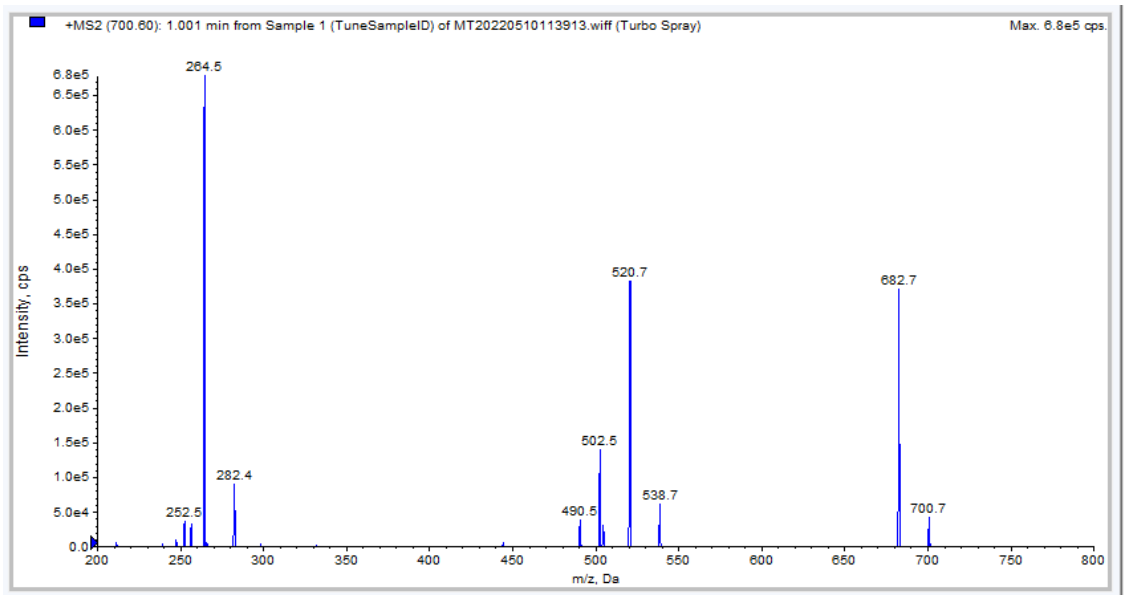

Figure 37. The m/z is plotted against the Intensity of the mass spectrum measuring in MS2 mode using SCIEX API 3200 LC-MS/MS of C16 galactosyl ceramide showing the product ions of the [M+H] adduct.

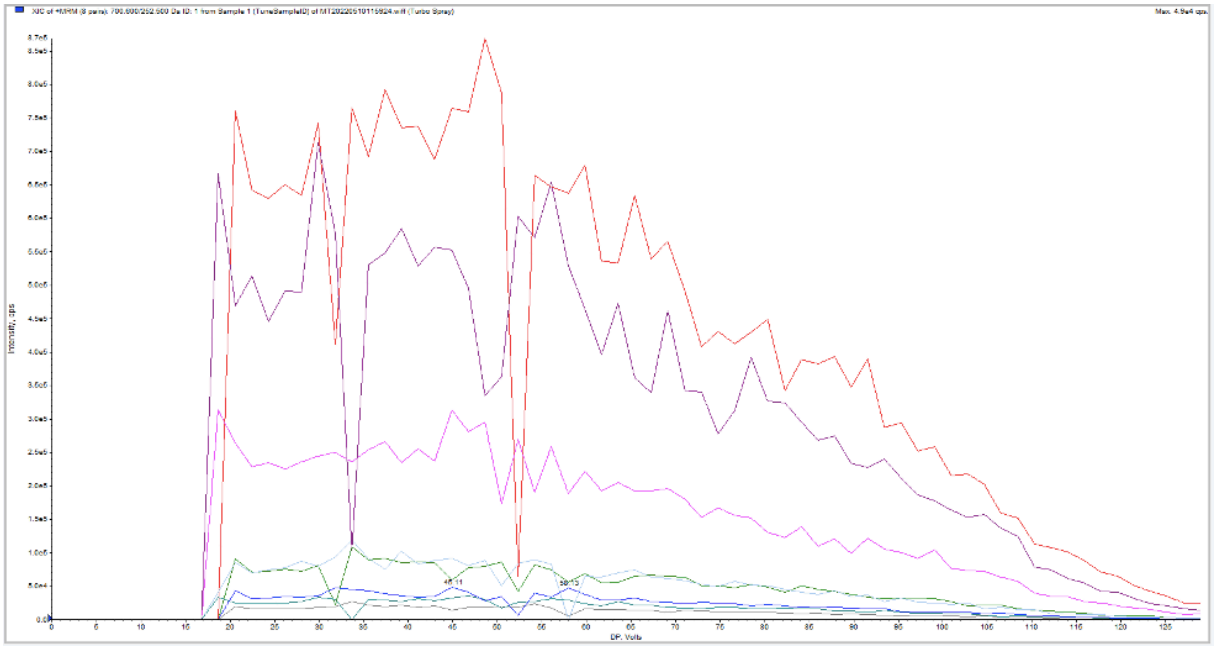

Figure 38. The declustering potential is plotted against the Intensity of the product ions of the [M+H] adduct of C16 galactosyl ceramide measured in MRM mode using SCIEX API 3200 LC-MS/MS of the product ions m/z: 252.5, 264.5, 282.4, 490.5, 502.5, 520.7, 538.7, 682.7 and 700.7.

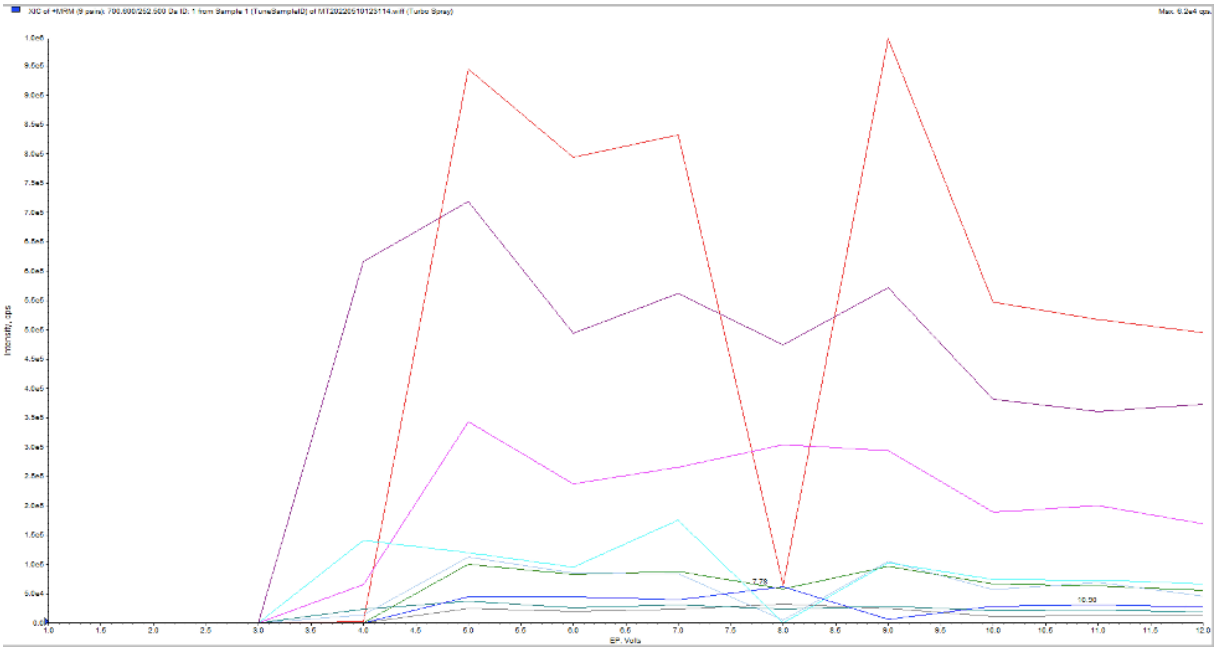

Figure 39. The entrance potential is plotted against the Intensity of the product ions of the [M+H] adduct of C16 galactosyl ceramide measured in MRM mode using SCIEX API 3200 LC-MS/MS of the product ions m/z: 252.5, 264.5, 282.4, 490.5, 502.5, 520.7, 538.7, 682.7 and 700.7.

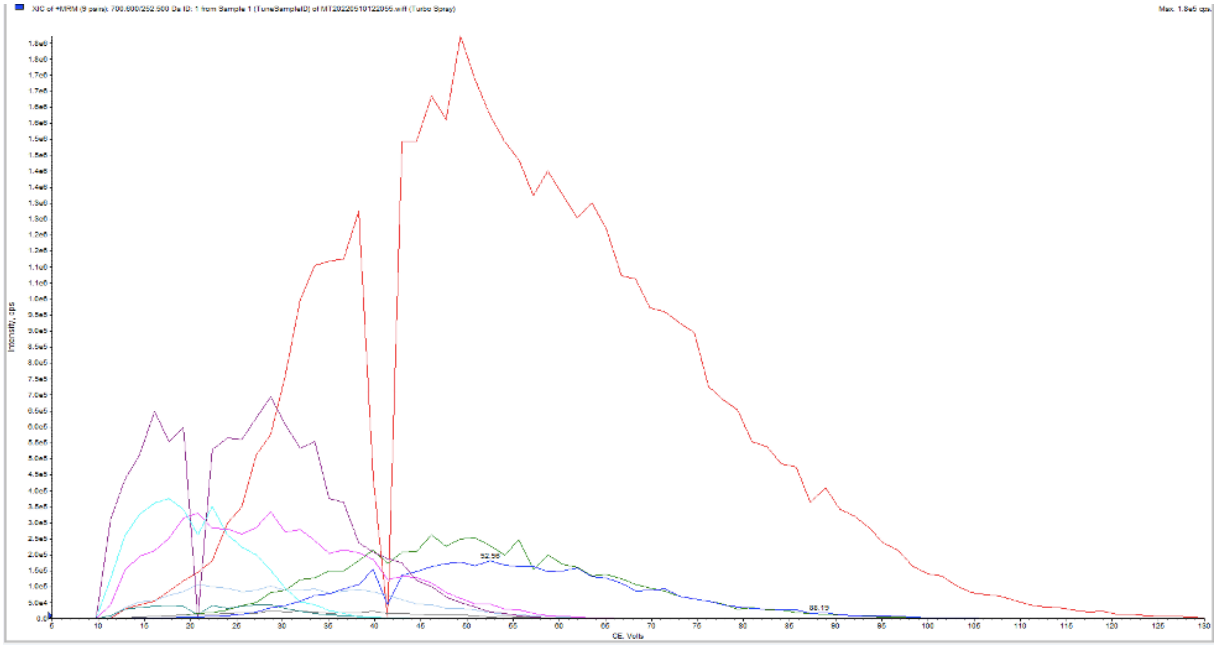

Figure 40. The collision energy is plotted against the Intensity of the product ions of the [M+H] adduct of galactosyl ceramide measured in MRM mode using SCIEX API 3200 LC-MS/MS of the product ions m/z: 252.5, 264.5, 282.4, 490.5, 502.5, 520.7, 538.7, 682.7 and 700.7.

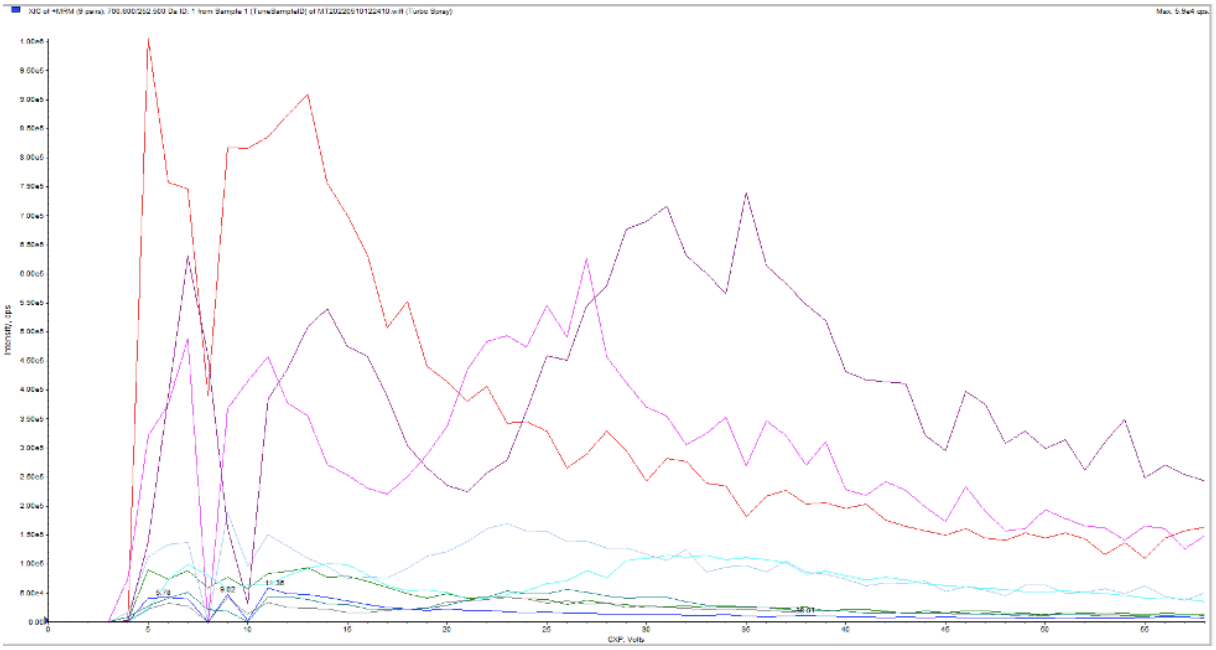

Figure 41. The collision cell exit potential is plotted against the Intensity of the product ions of the [M+H] adduct of galactosyl ceramide measured in MRM mode using SCIEX API 3200 LC-MS/MS of the product ions m/z: 252.5, 264.5, 282.4, 490.5, 502.5, 520.7, 538.7, 682.7 and 700.7.

7.6.2. Galactosyl sphingosine

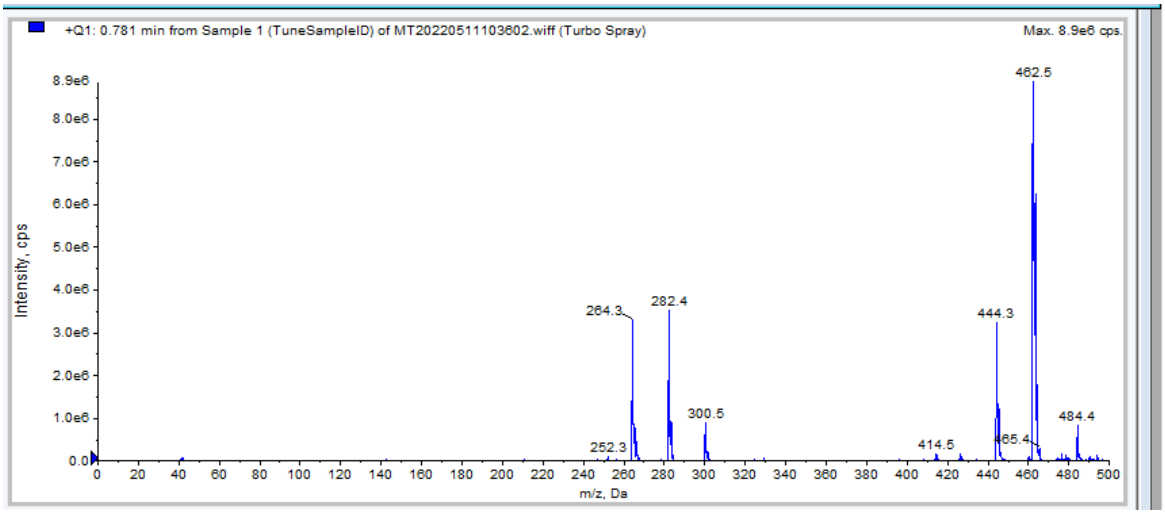

Figure 42. The m/z is plotted against the Intensity of the mass spectrum measuring in Q1 using SCIEX API 3200 LC-MS/MS of galactosyl sphingosine. The peak at m/z = 462.5 is determined to be the {M+H] adduct.

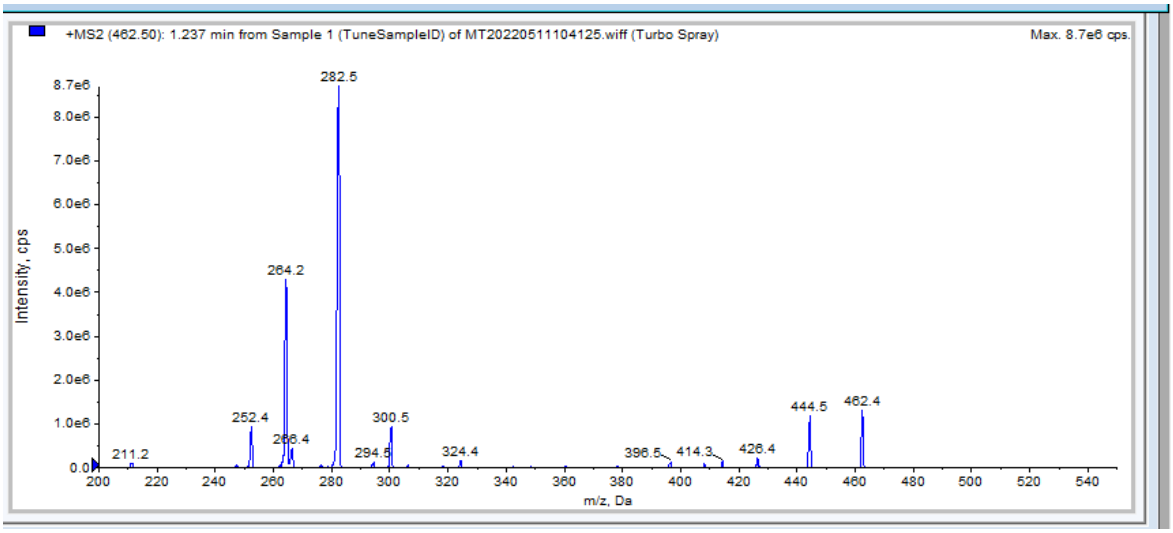

Figure 43. The m/z is plotted against the Intensity of the mass spectrum measuring in MS2 mode using SCIEX API 3200 LC-MS/MS of galactosyl sphingosine showing the product ions of the [M+H] adduct.

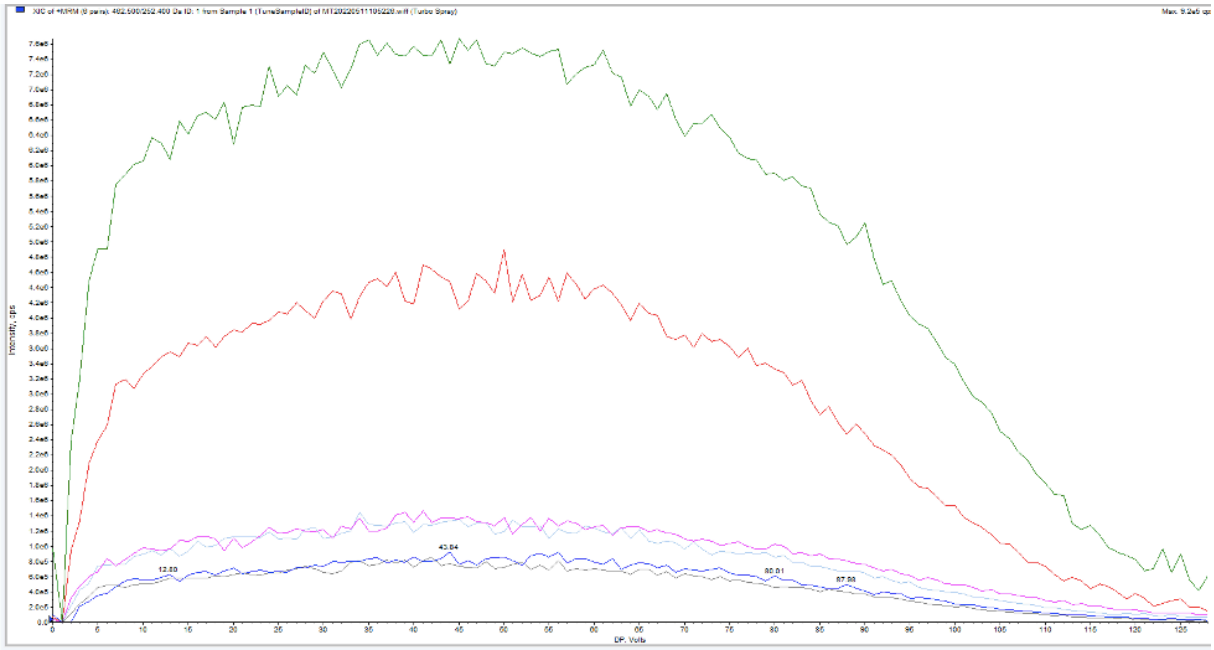

Figure 44. The declustering potential is plotted against the Intensity of the product ions of the [M+H] adduct of galactosyl sphingosine measured in MRM mode using SCIEX API 3200 LC-MS/MS of the product ions m/z: 252.4, 264.2, 282.5, 300.5, 444.5 and 462.4.

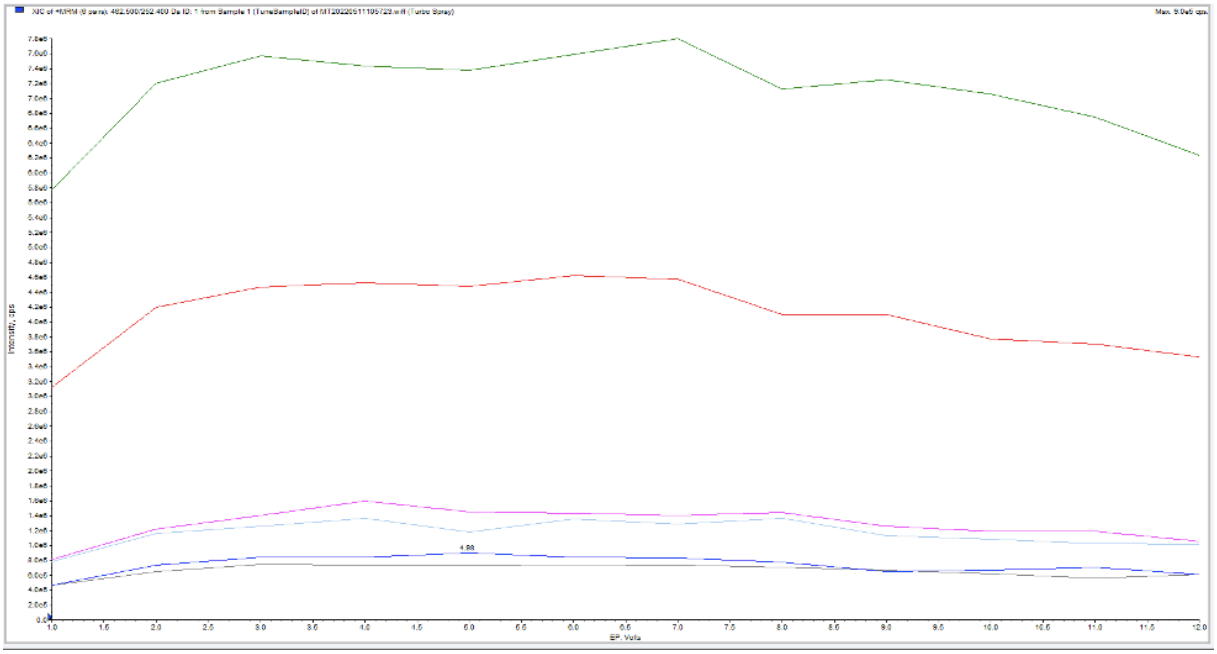

Figure 45. The entrance potential is plotted against the Intensity of the product ions of the [M+H] adduct of galactosyl sphingosine measured in MRM mode using SCIEX API 3200 LC-MS/MS of the product ions m/z: 252.4, 264.2, 282.5, 300.5, 444.5 and 462.4.

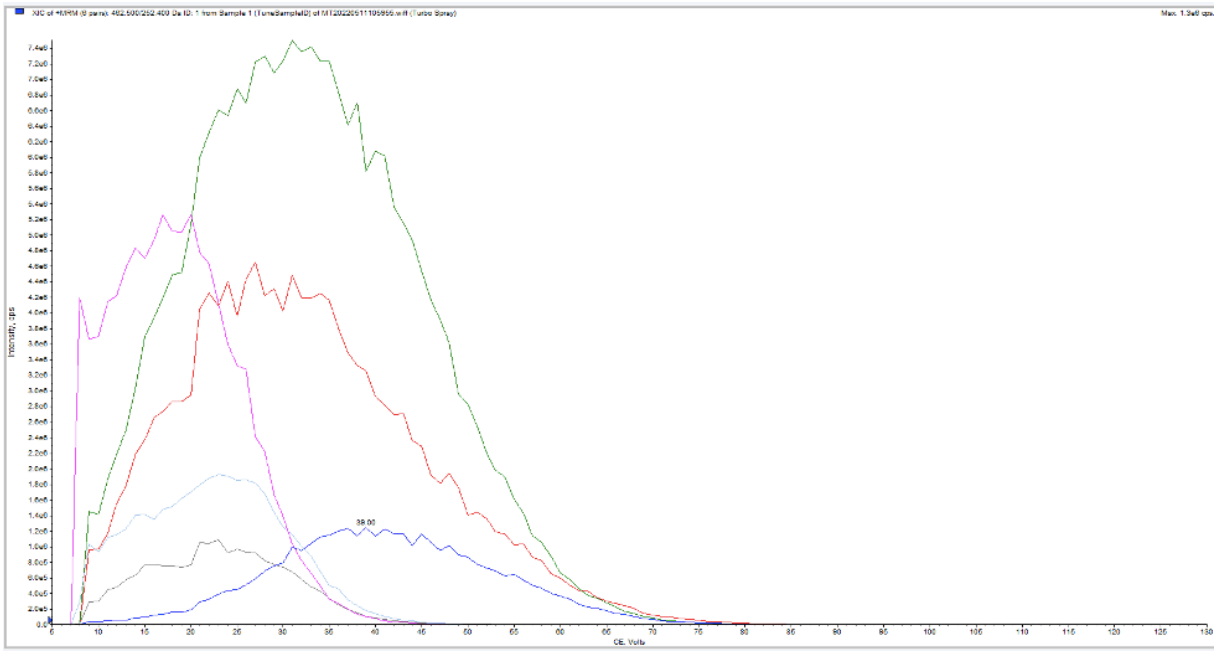

Figure 46. The collision energy is plotted against the Intensity of the product ions of the [M+H] adduct of galactosyl sphingosine measured in MRM mode using SCIEX API 3200 LC-MS/MS of the product ions m/z: 252.4, 264.2, 282.5, 300.5, 444.5 and 462.4.

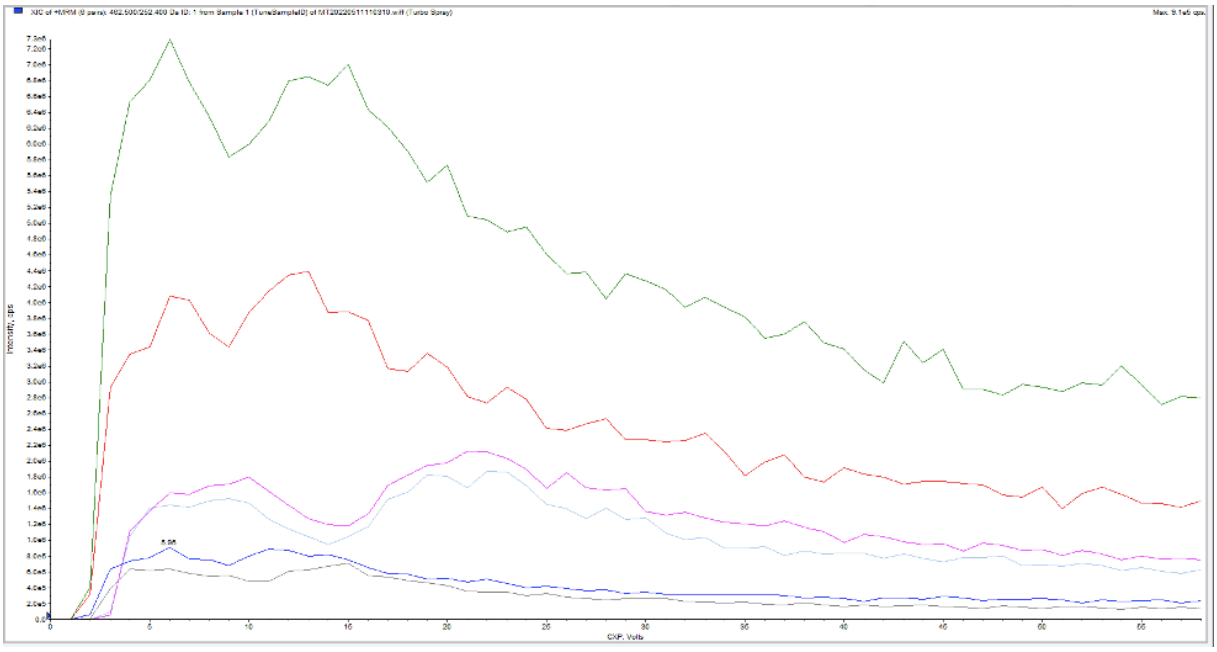

Figure 47. The collision cell exit potential is plotted against the Intensity of the product ions of the [M+H] adduct of galactosyl sphingosine measured in MRM mode using SCIEX API 3200 LC-MS/MS of the product ions m/z: 252.4, 264.2, 282.5, 300.5, 444.5 and 462.4.

7.6.3.Glucosyl sphingosine

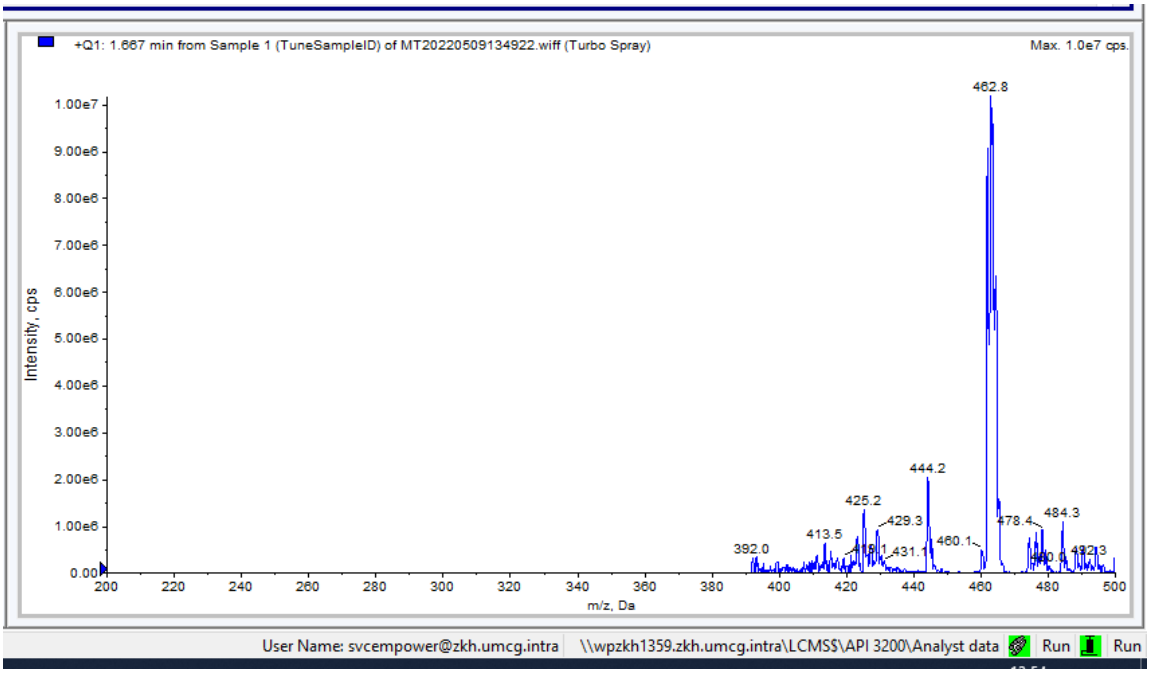

Figure 48. The m/z is plotted against the Intensity of the mass spectrum measuring in Q1 using SCIEX API 3200 LC-MS/MS of glucosyl sphingosine. The peak at m/z = 462.8 is determined to be the {M+H] adduct.

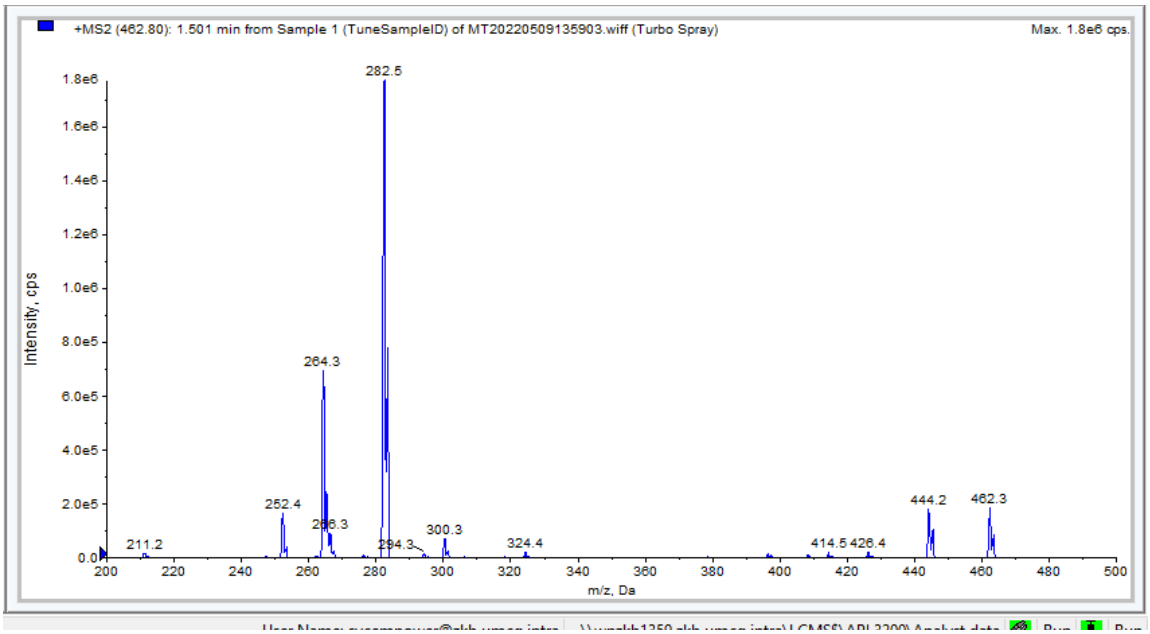

Figure 49. The m/z is plotted against the Intensity of the mass spectrum measuring in MS2 mode using SCIEX API 3200 LC-MS/MS of glucosyl sphingosine showing the product ions of the [M+H] adduct of glucosyl sphingosine.

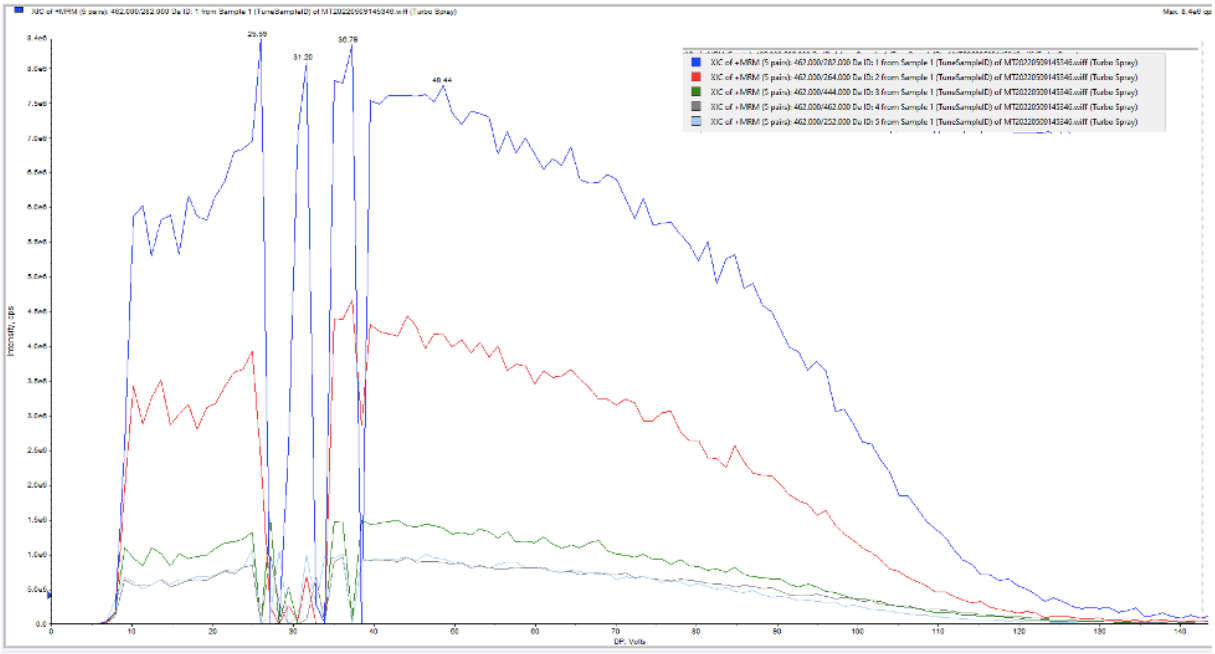

Figure 50. The declustering potential is plotted against the Intensity of the product ions of the [M+H] adduct of glucosyl sphingosine measured in MRM mode using SCIEX API 3200 LC-MS/MS. In the top right corner is the legend present showing the colors of the product ions m/z: 282.4, 264.2, 444.3, 462.4 and 252.4

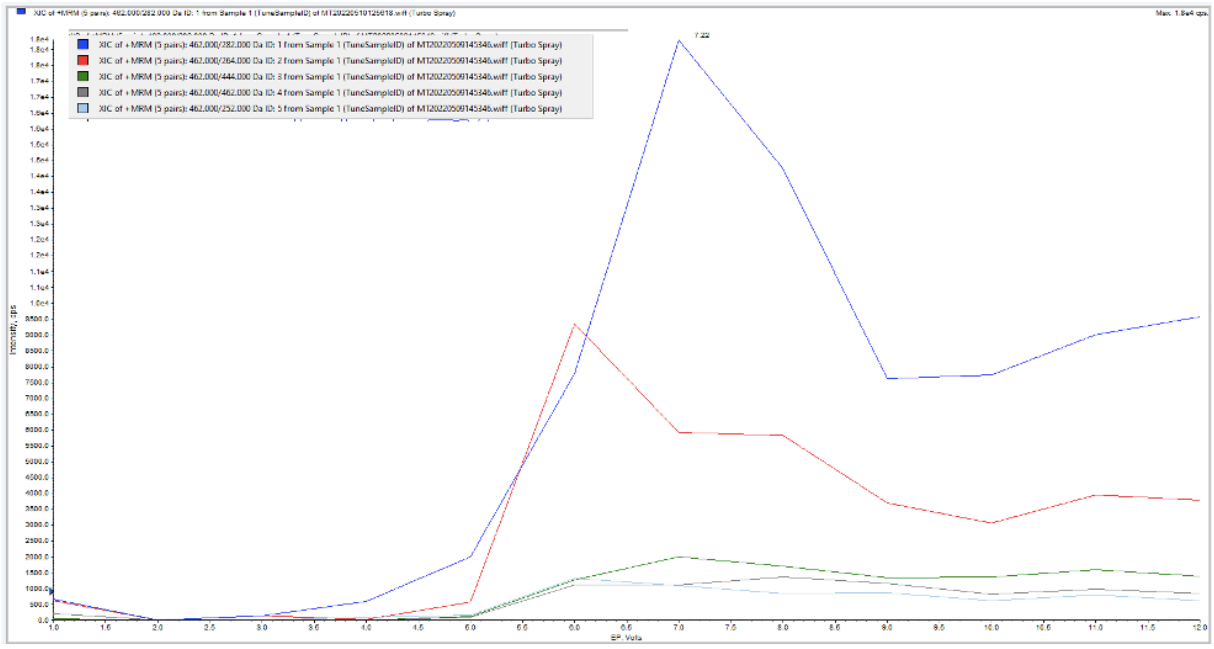

Figure 51. The entrance potential is plotted against the Intensity of the product ions of the [M+H] adduct of glucosyl sphingosine measured in MRM mode using SCIEX API 3200 LC-MS/MS. In the top left corner is the legend present showing the colors of the product ions m/z: 282.4, 264.2, 444.3, 462.4 and 252.4

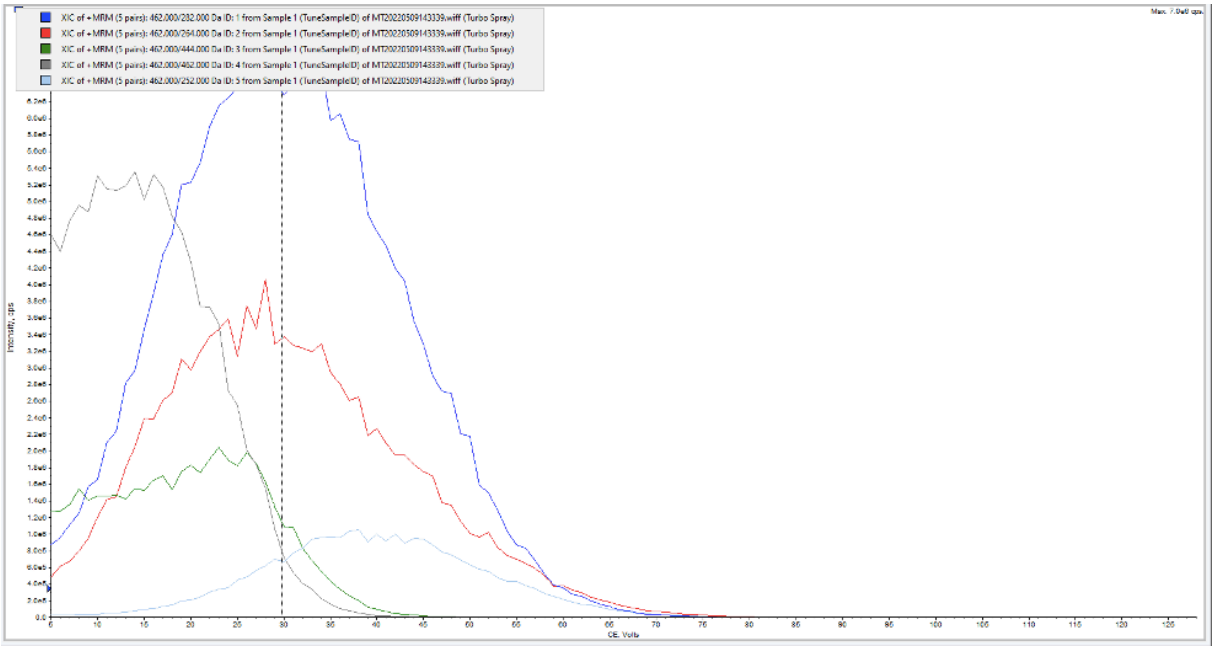

Figure 52. The collision energy is plotted against the Intensity of the product ions of the [M+H] adduct of glucosyl sphingosine measured in MRM mode using SCIEX API 3200 LC-MS/MS. In the top left corner is the legend present showing the colors of the product ions m/z: 282.4, 264.2, 444.3, 462.4 and 252.4

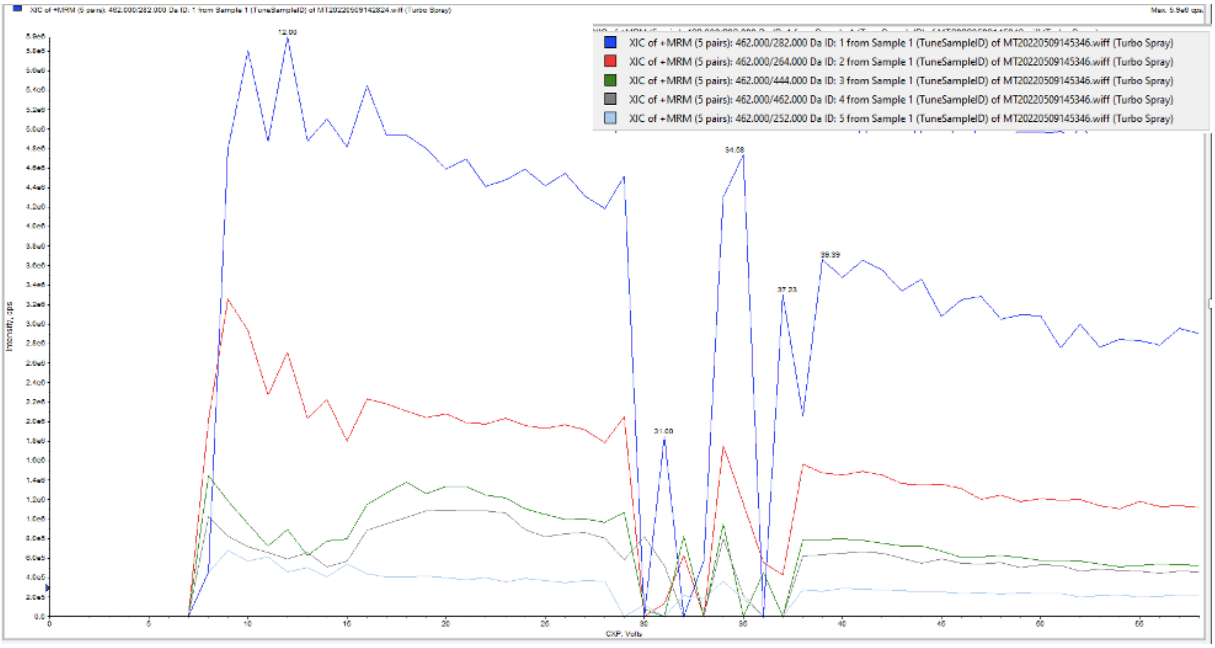

Figure 53. The collision cell exit potential is plotted against the Intensity of the product ions of the [M+H] adduct of glucosyl sphingosine measured in MRM mode using SCIEX API 3200 LC-MS/MS. In the top right corner is the legend present showing the colors of the product ions m/z: 282.4, 264.2, 444.3, 462.4 and 252.4

7.6.4. Lactosyl sphingosine

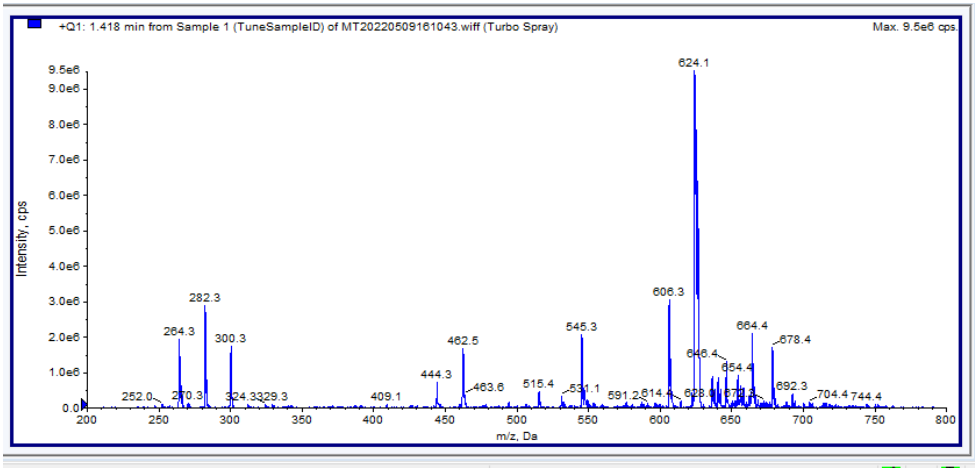

Figure 54. The m/z is plotted against the Intensity of the mass spectrum measuring in Q1 using SCIEX API 3200 LC-MS/MS of lactosyl sphingosine. The peak at m/z = 624.1 is determined to be the {M+H] adduct.

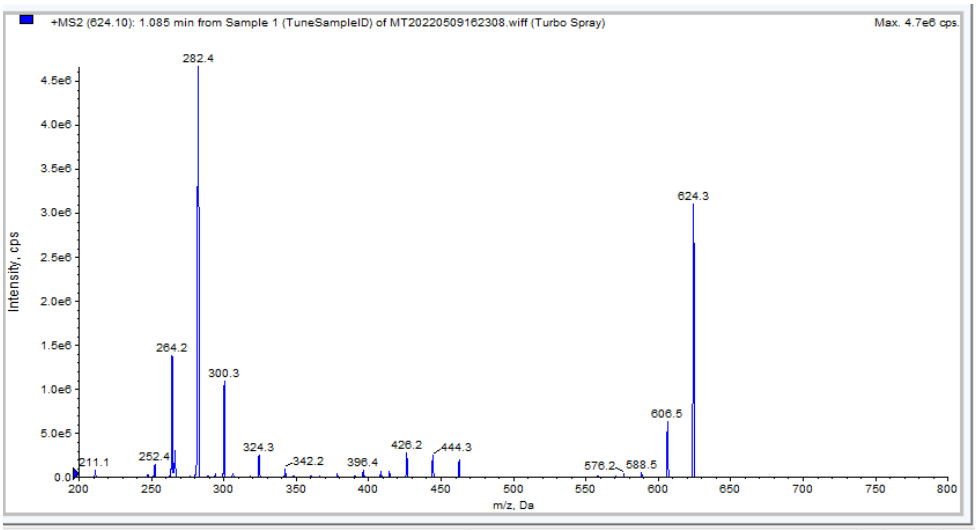

Figure 55. The m/z is plotted against the Intensity of the mass spectrum measuring in MS2 mode using SCIEX API 3200 LC-MS/MS of lactosyl sphingosine showing the product ions of the [M+H] adduct of lactosyl sphingosine.

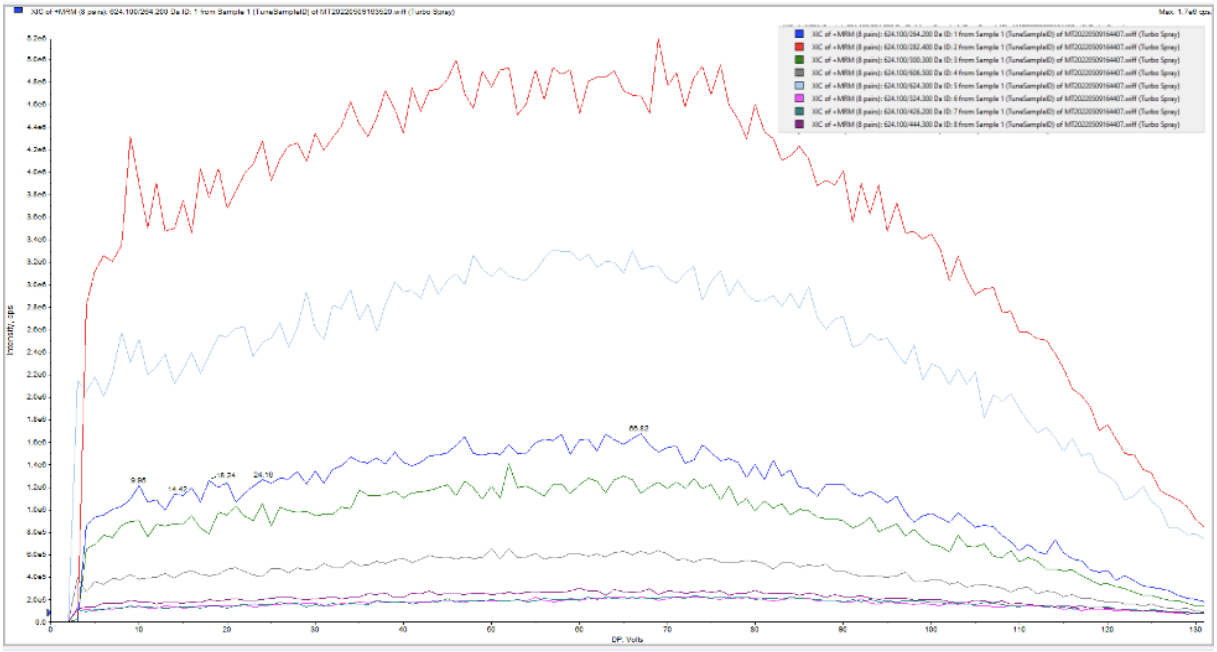

Figure 56. The declustering potential is plotted against the Intensity of the product ions of the [M+H] adduct of lactosyl sphingosine measured in MRM mode using SCIEX API 3200 LC-MS/MS. In the top right corner is the legend present showing the colors of the product ions m/z: 264.2, 282.4, 300.3, 606.5, 624.3, 324.3, 426.2 and 444.3.

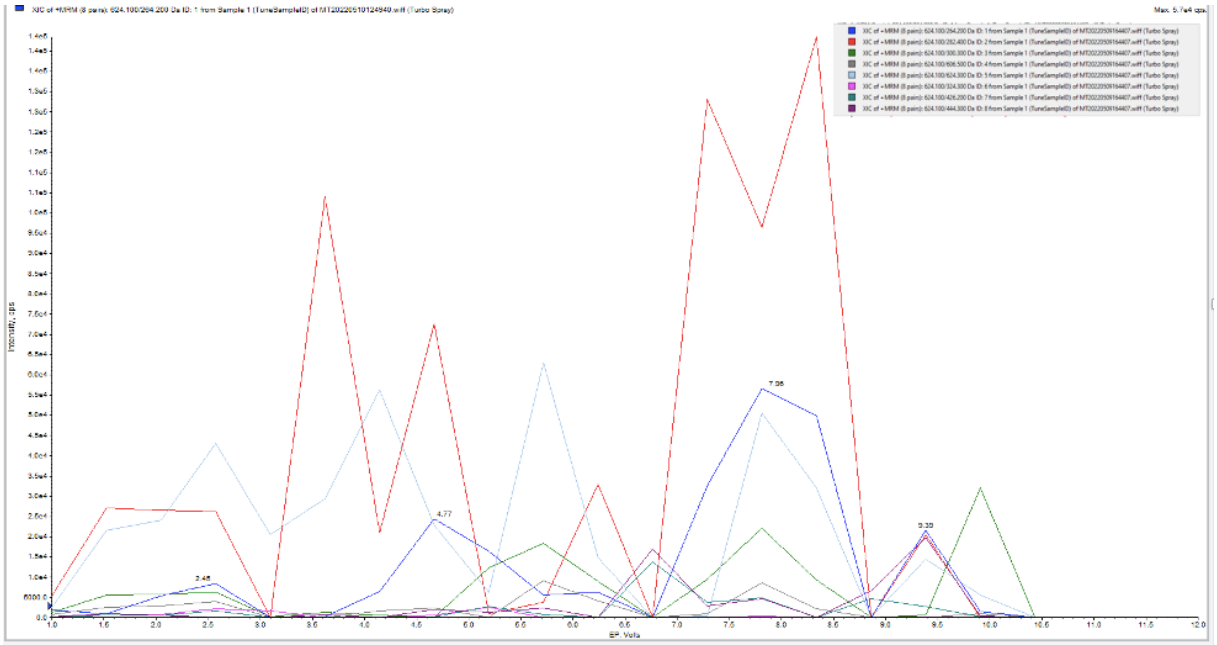

Figure 57. The entrance potential is plotted against the Intensity of the product ions of the [M+H] adduct of lactosyl sphingosine measured in MRM mode using SCIEX API 3200 LC-MS/MS. In the top right corner is the legend present showing the colors of the product ions m/z: 264.2, 282.4, 300.3, 606.5, 624.3, 324.3, 426.2 and 444.3.

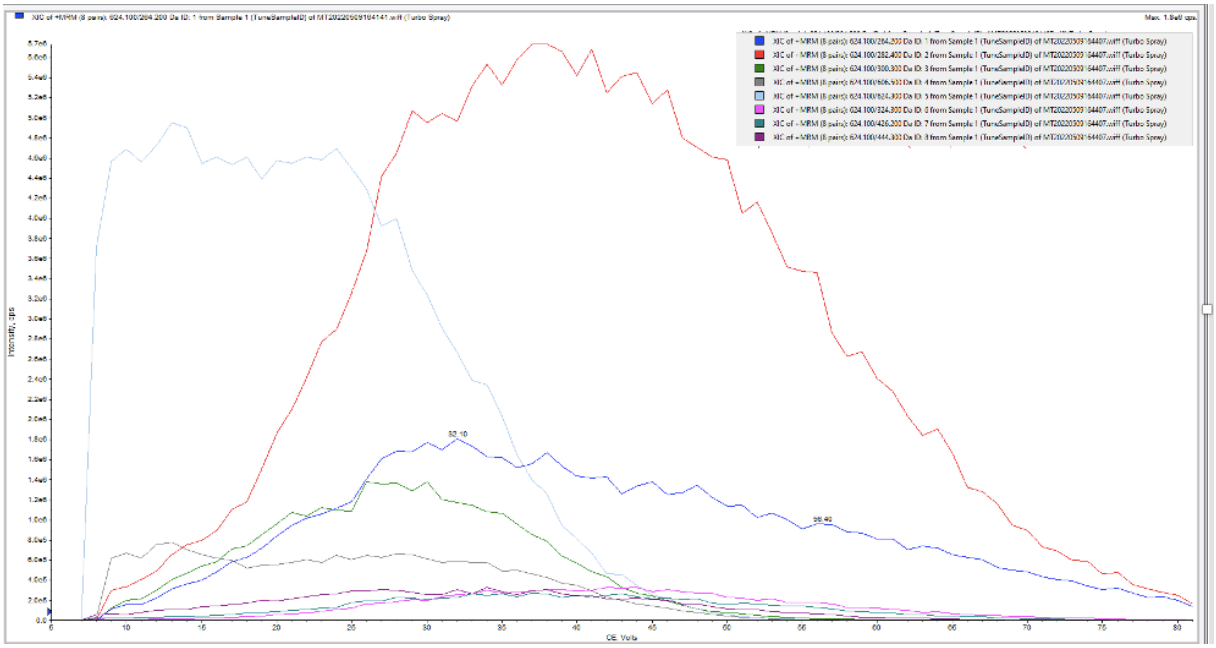

Figure 58. The collision energy is plotted against the Intensity of the product ions of the [M+H] adduct of lactosyl sphingosine measured in MRM mode using SCIEX API 3200 LC-MS/MS. In the top right corner is the legend present showing the colors of the product ions m/z: 264.2, 282.4, 300.3, 606.5, 624.3, 324.3, 426.2 and 444.3.

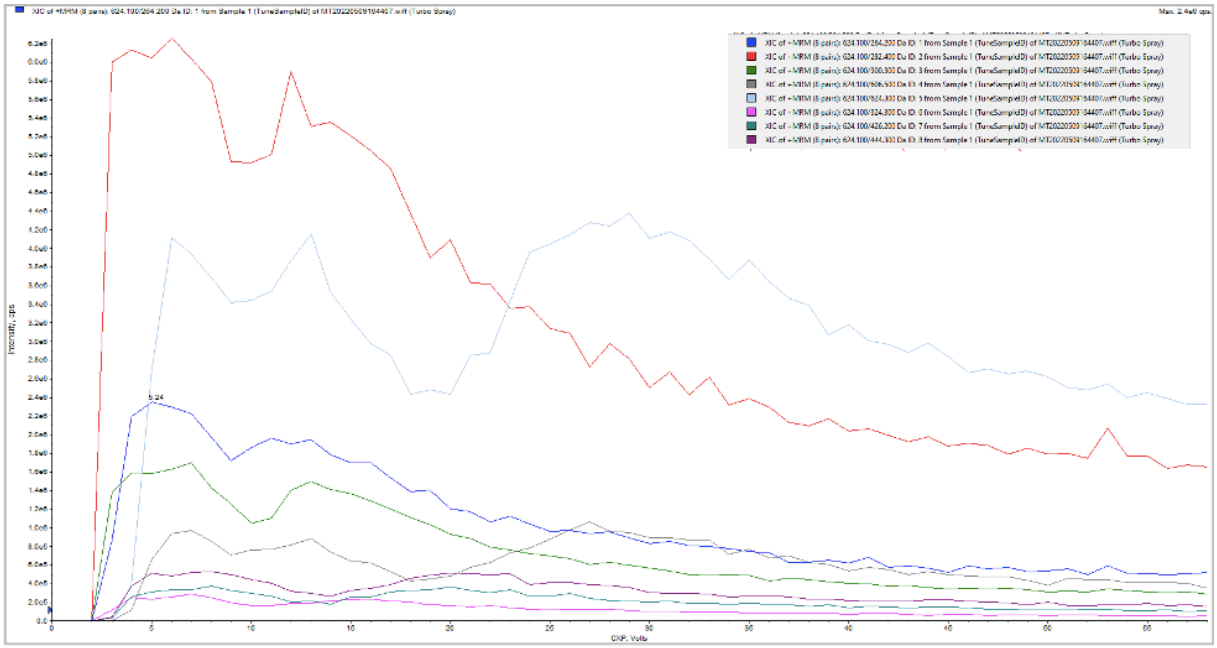

Figure 59. The collision cell exit potential is plotted against the Intensity of the product ions of the [M+H] adduct of lactosyl sphingosine measured in MRM mode using SCIEX API 3200 LC-MS/MS. In the top right corner is the legend present showing the colors of the product ions m/z: 264.2, 282.4, 300.3, 606.5, 624.3, 324.3, 426.2 and 444.3.

7.6.5. D-sphingosine

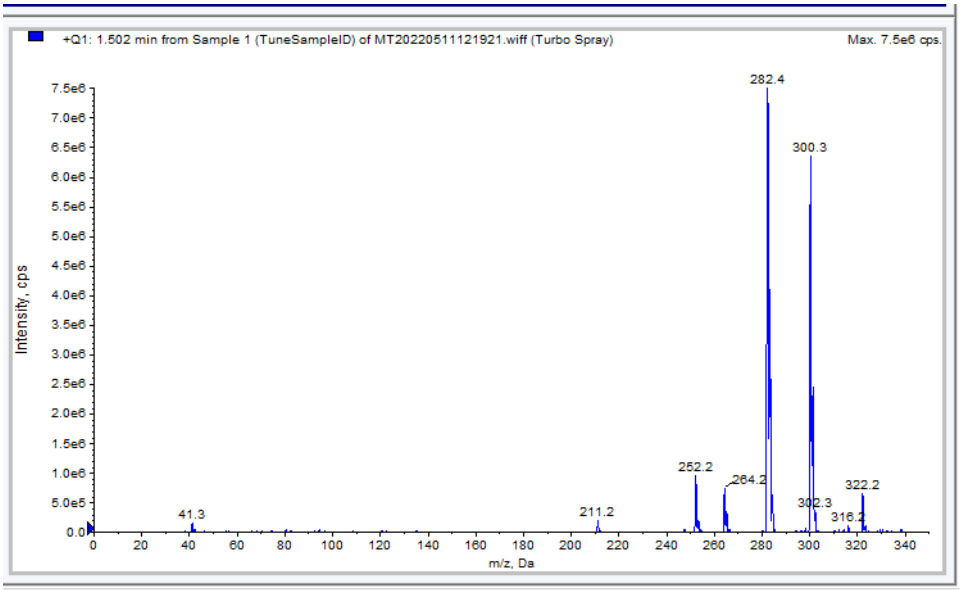

Figure 60. The m/z is plotted against the Intensity of the mass spectrum measuring in Q1 using SCIEX API 3200 LC-MS/MS of D-sphingosine. The peak at m/z = 300.3 is determined to be the {M+H] adduct.

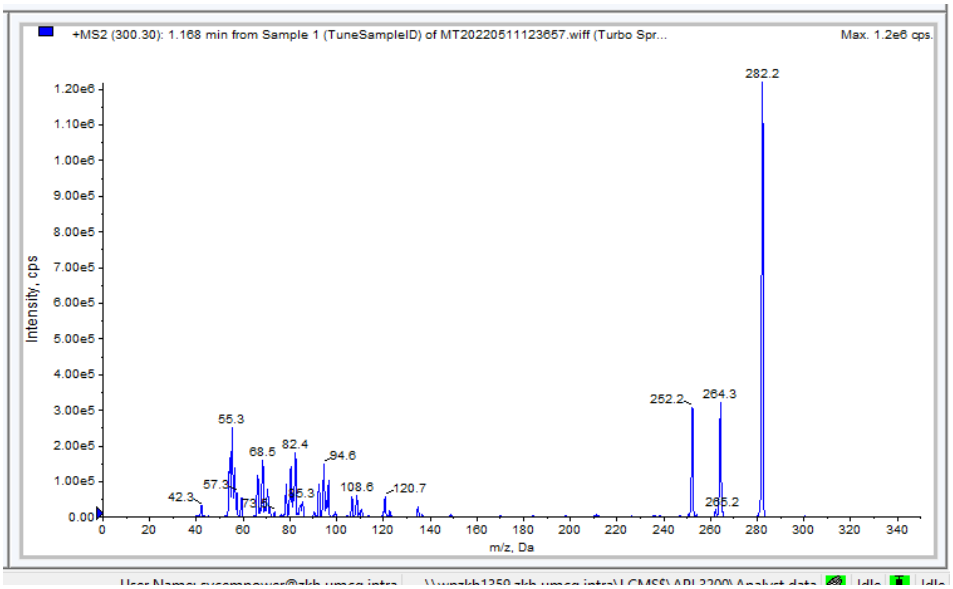

Figure 61. The m/z is plotted against the Intensity of the mass spectrum measuring in MS2 mode using SCIEX API 3200 LC-MS/MS of D-sphingosine showing the product ions of the [M+H] adduct.

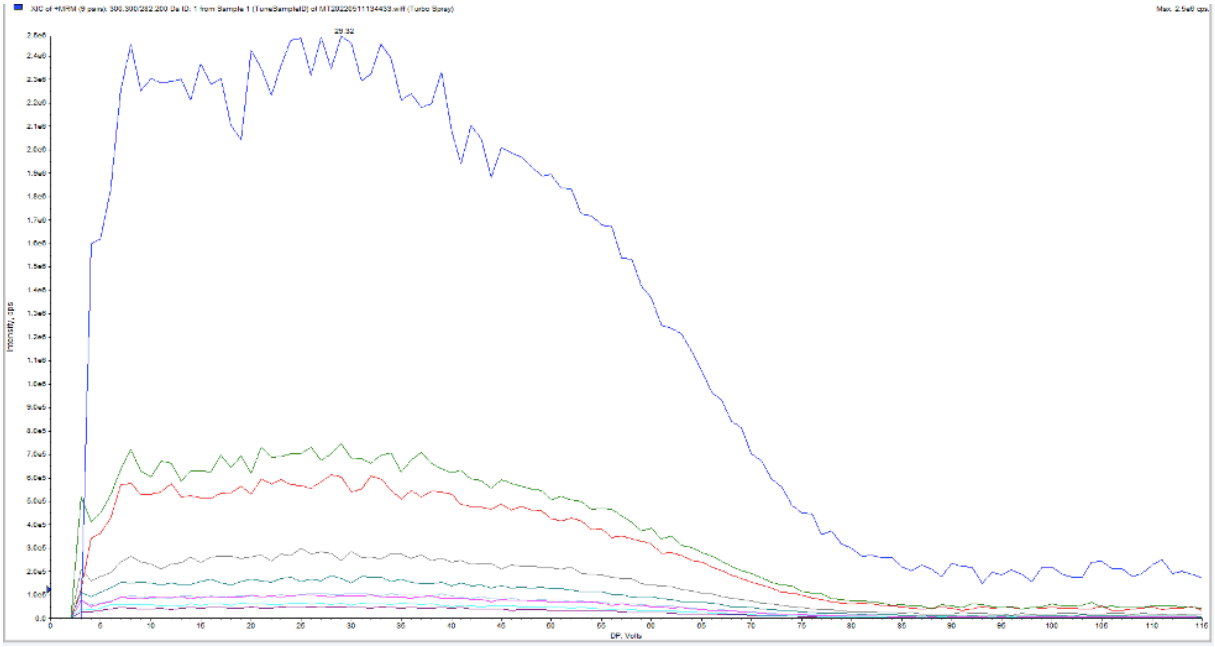

Figure 62. The declustering potential is plotted against the Intensity of the product ions of the [M+H] adduct of D-sphingosine measured in MRM mode using SCIEX API 3200 LC-MS/MS of the product ions m/z: 282.2, 264.3, 252.2, 55.3, 68.5, 82.4, 94.6, 108.6 and 120.7.

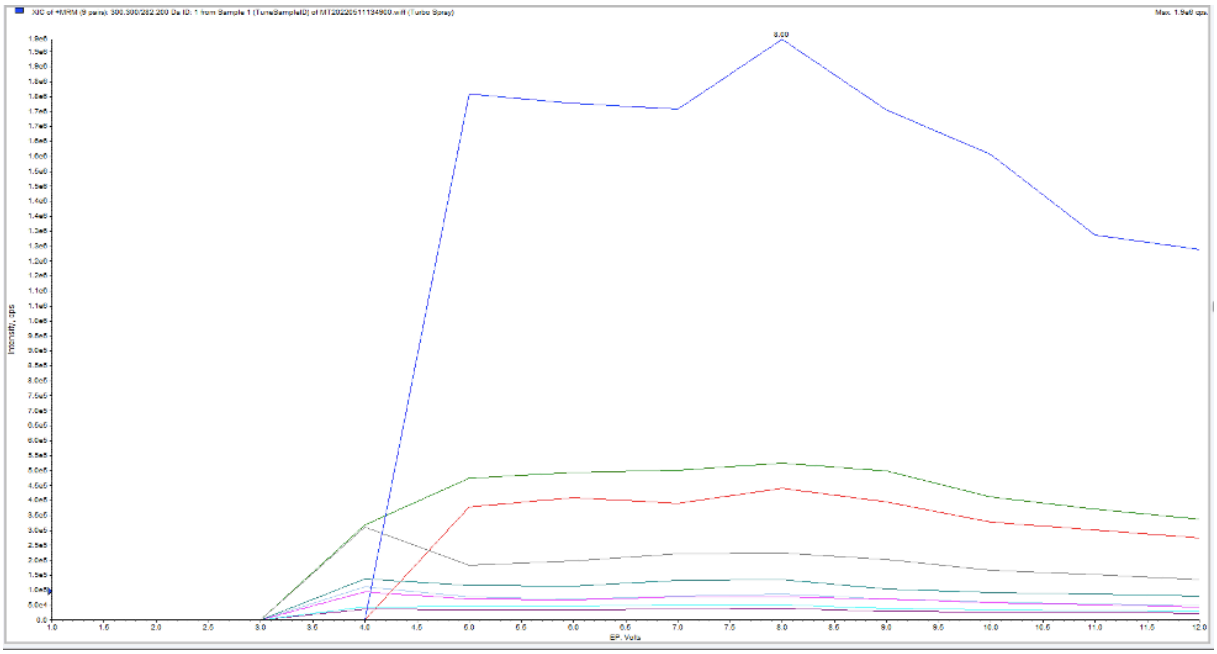

Figure 63. The entrance potential is plotted against the Intensity of the product ions of the [M+H] adduct of D-sphingosine measured in MRM mode using SCIEX API 3200 LC-MS/MS of the product ions m/z: 282.2, 264.3, 252.2, 55.3, 68.5, 82.4, 94.6, 108.6 and 120.7.

.

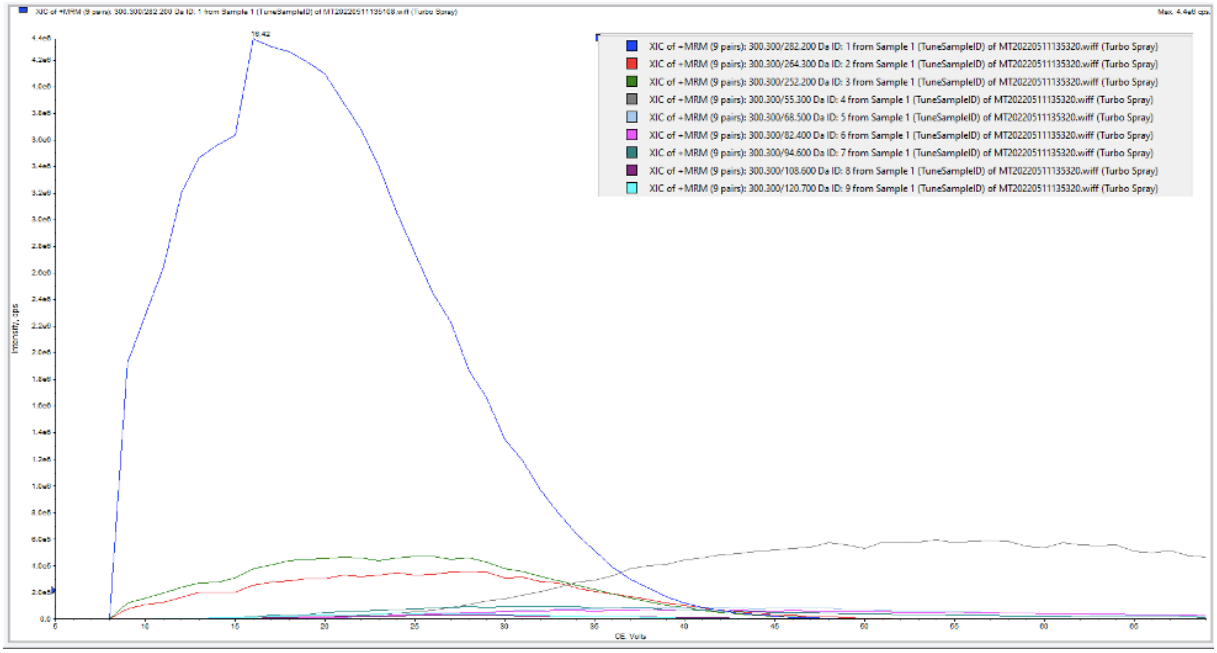

Figure 64. The collision energy is plotted against the Intensity of the product ions of the [M+H] adduct of D-sphingosine measured in MRM mode using SCIEX API 3200 LC-MS/MS. In the top right corner is the legend presented showing the colors of the product ions m/z: 282.2, 264.3, 252.2, 55.3, 68.5, 82.4, 94.6, 108.6 and 120.7.

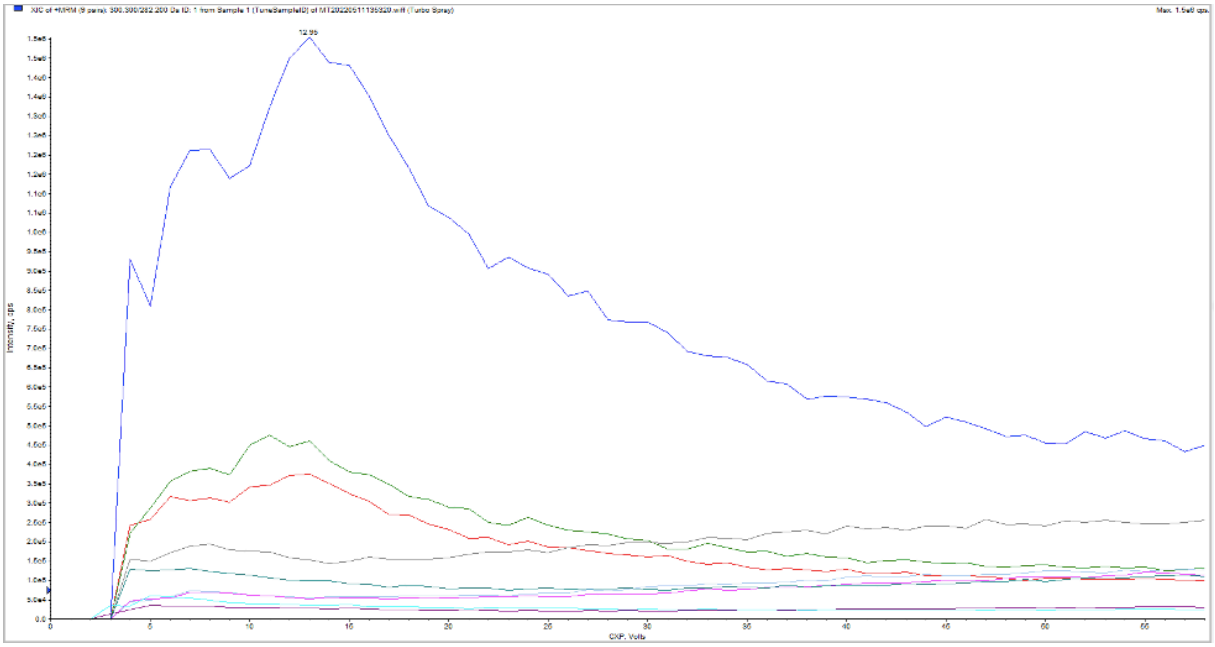

Figure 65. The collision cell exit potential is plotted against the Intensity of the product ions of the [M+H] adduct of D-sphingosine measured in MRM mode using SCIEX API 3200 LC-MS/MS of the product ions m/z: 282.2, 264.3, 252.2, 55.3, 68.5, 82.4, 94.6, 108.6 and 120.7.

7.6.6. Lactosyl ceramide

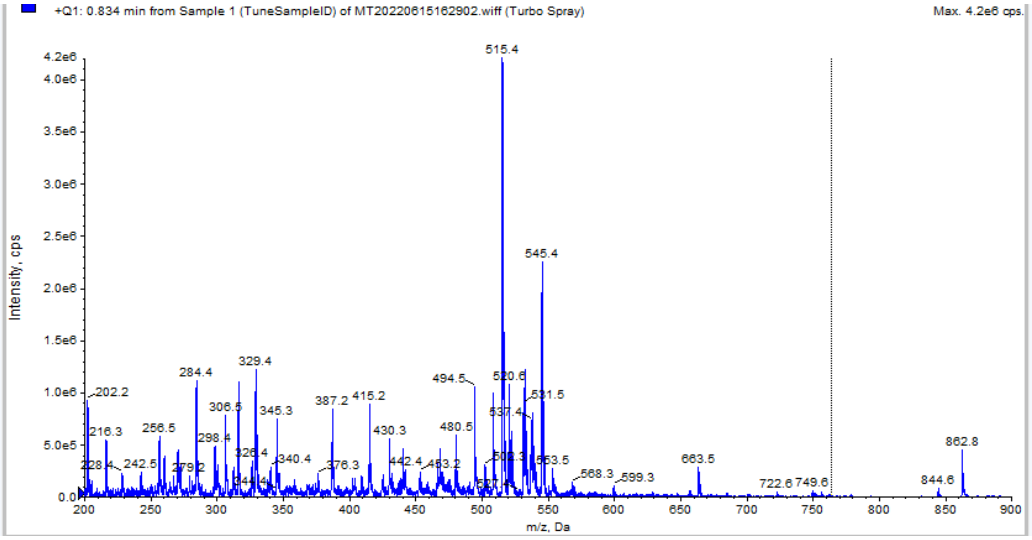

Figure 66. The m/z is plotted against the Intensity of the mass spectrum measuring in Q1 using SCIEX API 3200 LC-MS/MS of lactosyl ceramide. The peak at m/z = 862.8 is determined to be the {M+H] adduct.

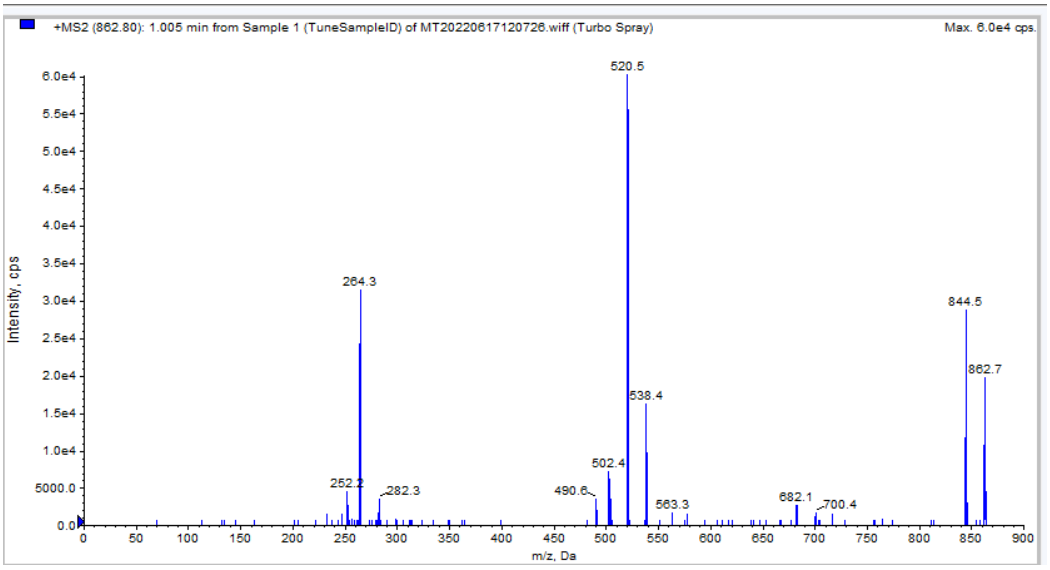

Figure 67. The m/z is plotted against the Intensity of the mass spectrum measuring in MS2 mode using SCIEX API 3200 LC-MS/MS of lactosyl ceramide showing the product ions of the [M+H] adduct.

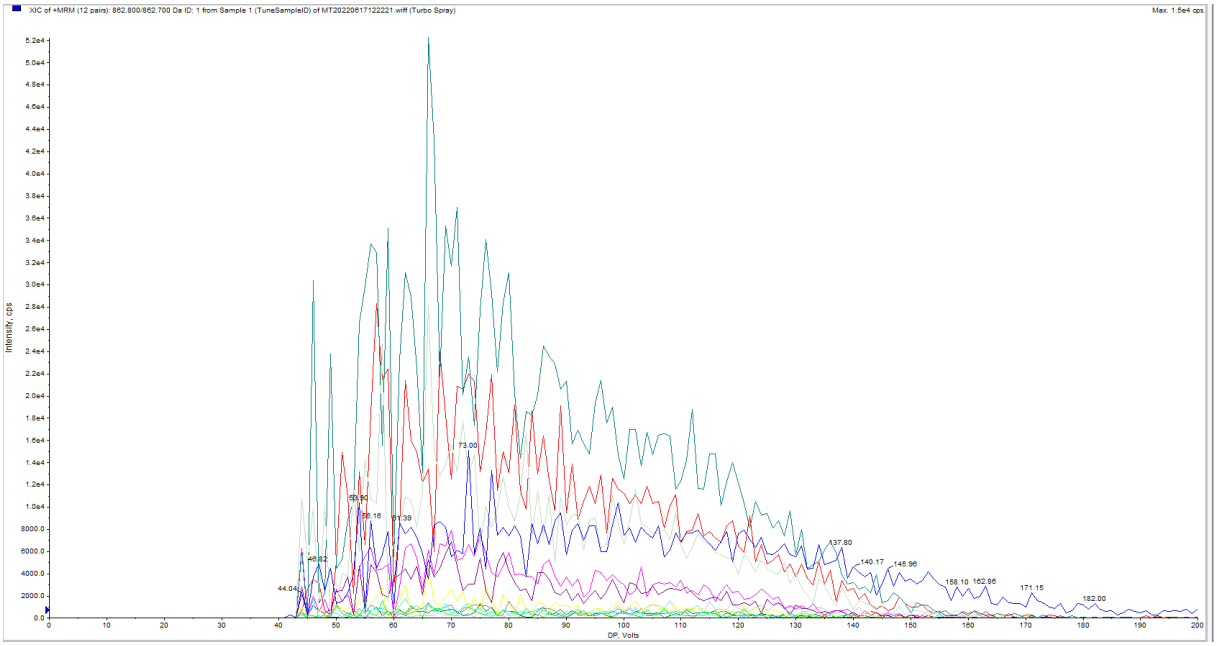

Figure 68. The declustering potential is plotted against the Intensity of the product ions of the [M+H] adduct of lactosyl ceramide measured in MRM mode using SCIEX API 3200 LC-MS/MS of the product ions m/z: 862.7, 844.5, 700.4, 682.1, 563.3, 538.4, 520.5, 502.4, 490.6, 282.3, 264.3 and 252.2.

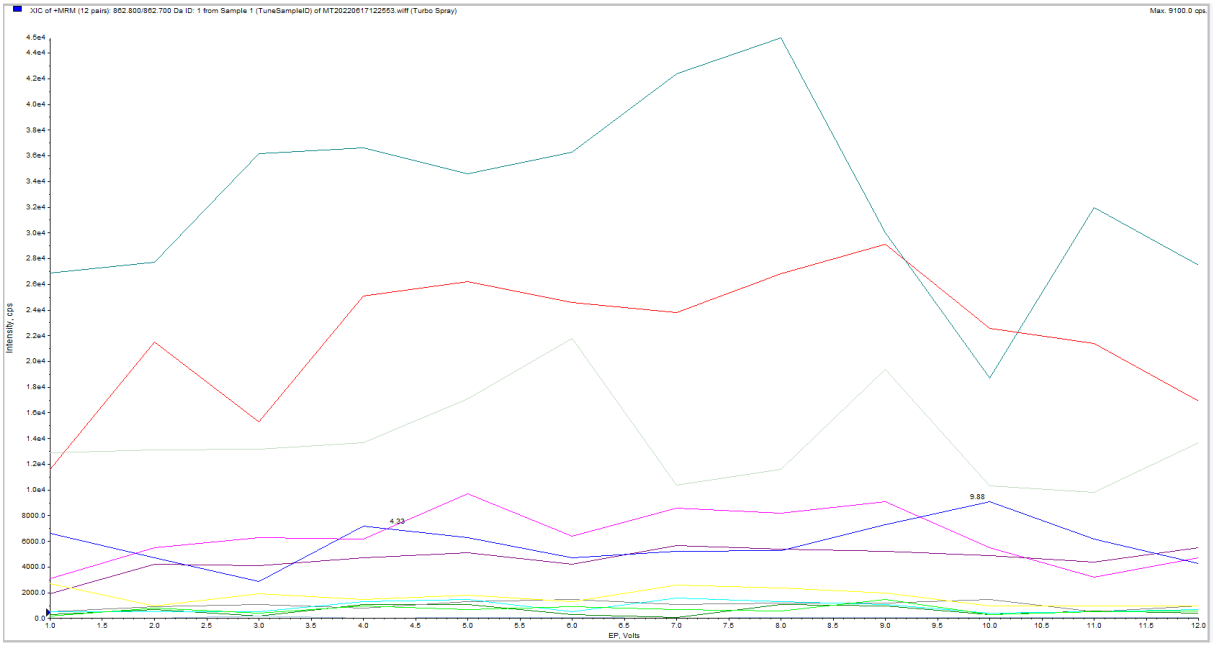

Figure 69. The entrance potential is plotted against the Intensity of the product ions of the [M+H] adduct of lactosyl ceramide measured in MRM mode using SCIEX API 3200 LC-MS/MS of the product ions m/z: 862.7, 844.5, 700.4, 682.1, 563.3, 538.4, 520.5, 502.4, 490.6, 282.3, 264.3 and 252.2.

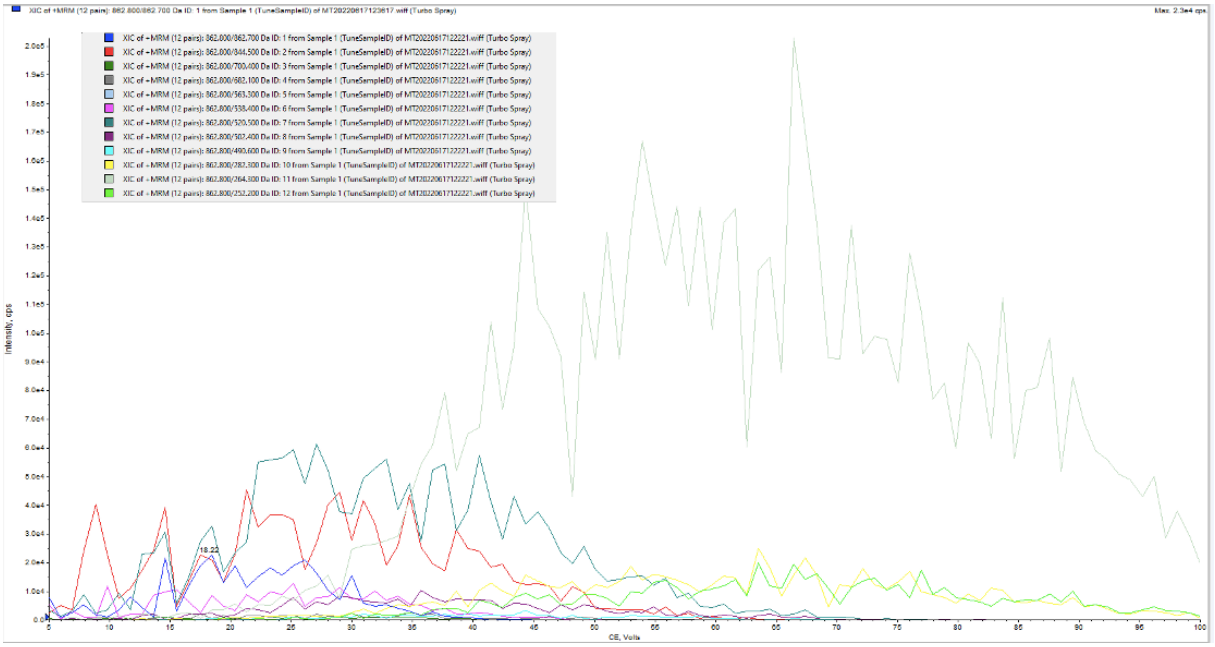

Figure 70. The collision energy is plotted against the Intensity of the product ions of the [M+H] adduct of lactosyl ceramide measured in MRM mode using SCIEX API 3200 LC-MS/MS. In the top left corner is the legend present showing the colors of the product ions m/z: 862.7, 844.5, 700.4, 682.1, 563.3, 538.4, 520.5, 502.4, 490.6, 282.3, 264.3 and 252.2.

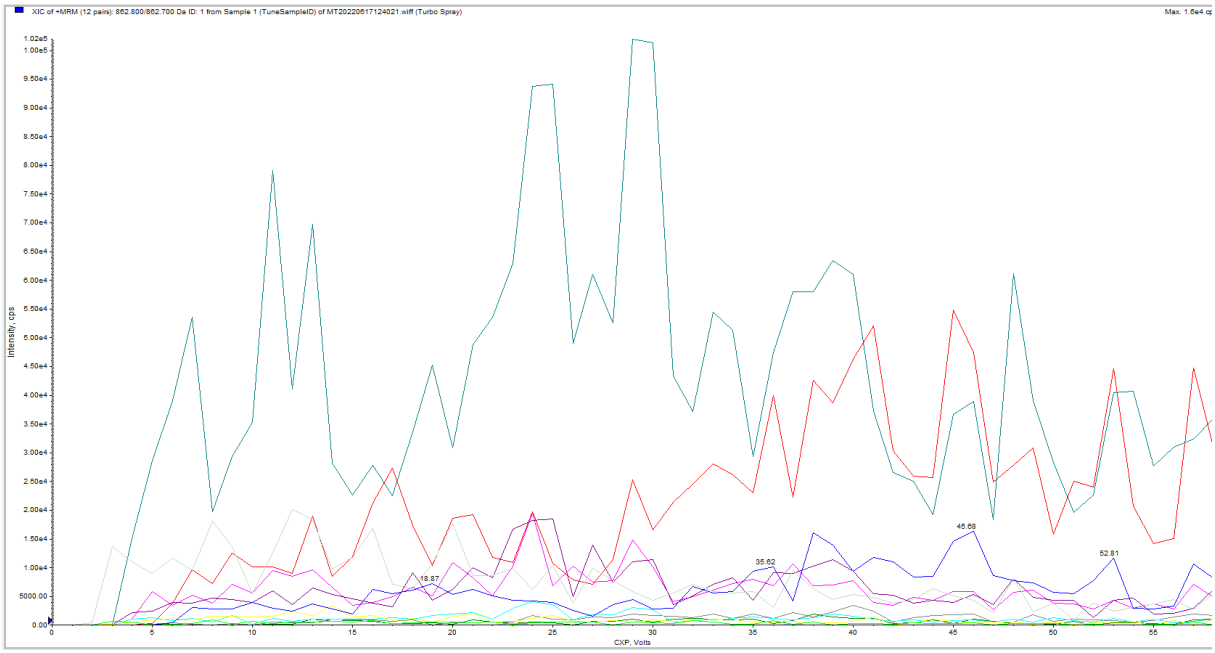

Figure 71. The collision cell exit potential is plotted against the Intensity of the product ions of the [M+H] adduct of lactosyl ceramide measured in MRM mode using SCIEX API 3200 LC-MS/MS of the product ions m/z: 862.7, 844.5, 700.4, 682.1, 563.3, 538.4, 520.5, 502.4, 490.6, 282.3, 264.3 and 252.2.

7.6.7. C16 ceramide

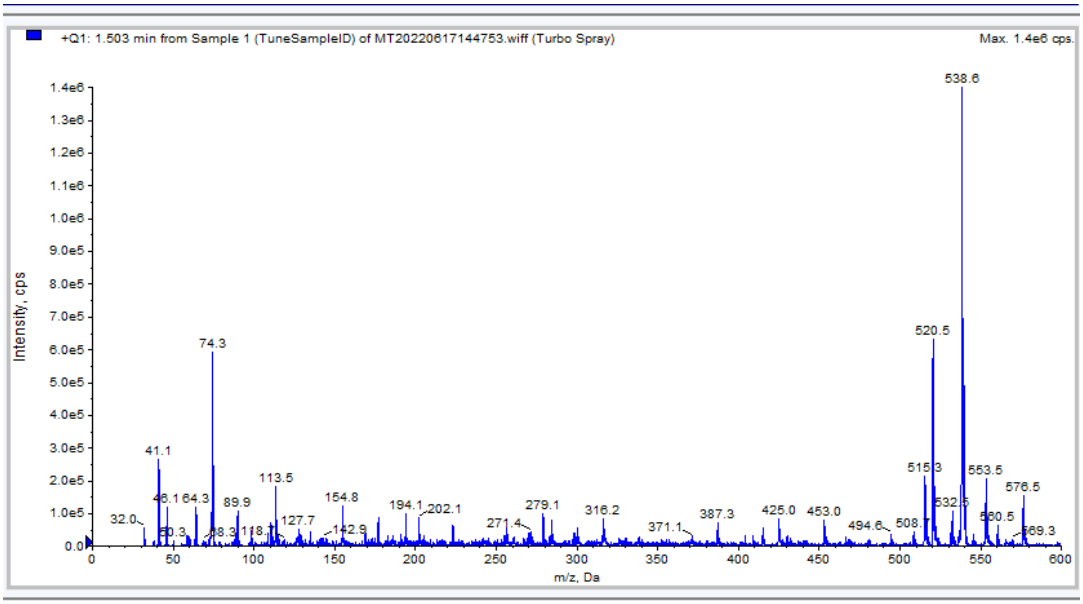

Figure 72. The m/z is plotted against the Intensity of the mass spectrum measuring in Q1 using SCIEX API 3200 LC-MS/MS of C16 ceramide. The peak at m/z = 538.6 is determined to be the {M+H] adduct.

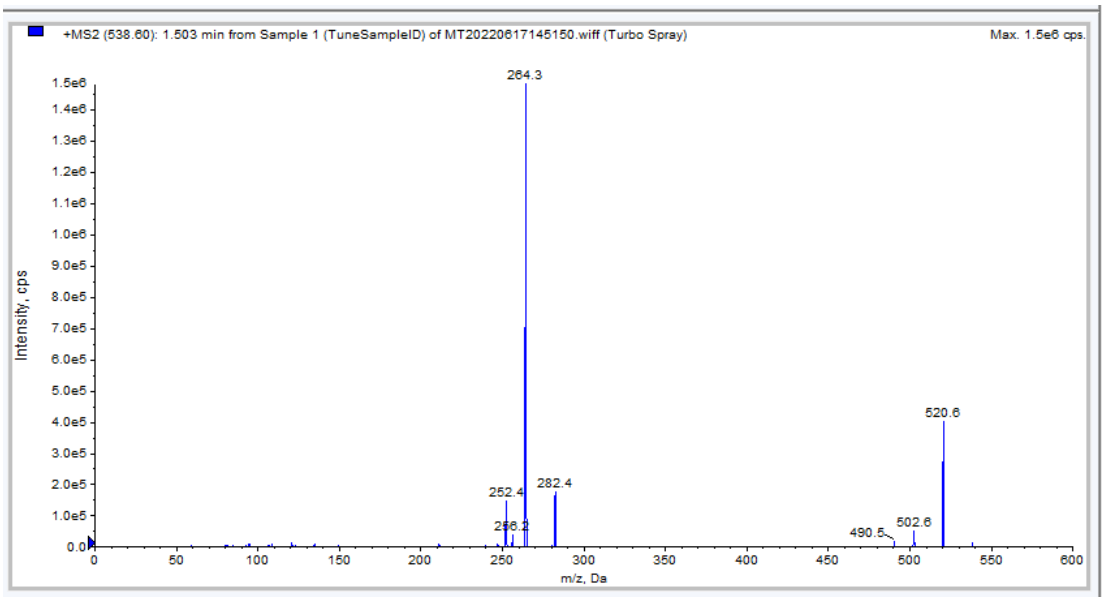

Figure 73. The m/z is plotted against the Intensity of the mass spectrum measuring in MS2 mode using SCIEX API 3200 LC-MS/MS of C16 ceramide showing the product ions of the [M+H] adduct.

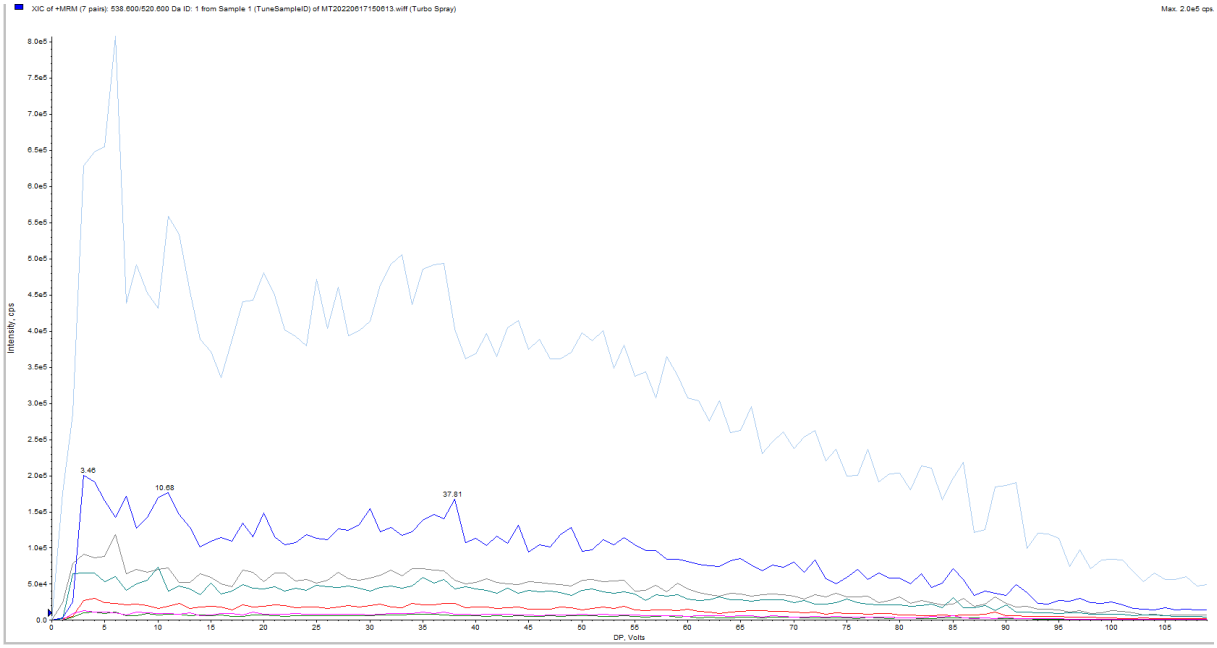

Figure 74. The declustering potential is plotted against the Intensity of the product ions of the [M+H] adduct of C16 ceramide measured in MRM mode using SCIEX API 3200 LC-MS/MS of the product ions m/z: 520.6, 502.6, 490.5, 282.4, 264.3, 256.2 and 252.4.

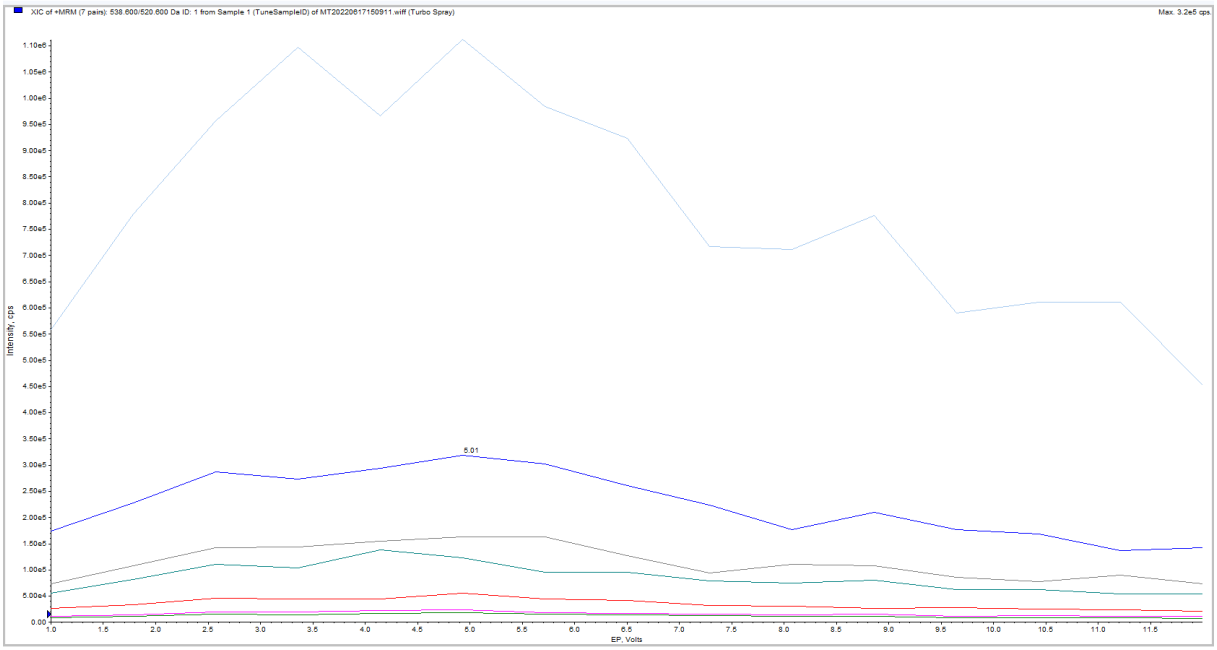

Figure 75. The entrance potential is plotted against the Intensity of the product ions of the [M+H] adduct of C16 ceramide measured in MRM mode using SCIEX API 3200 LC-MS/MS of the product ions m/z: 520.6, 502.6, 490.5, 282.4, 264.3, 256.2 and 252.4.

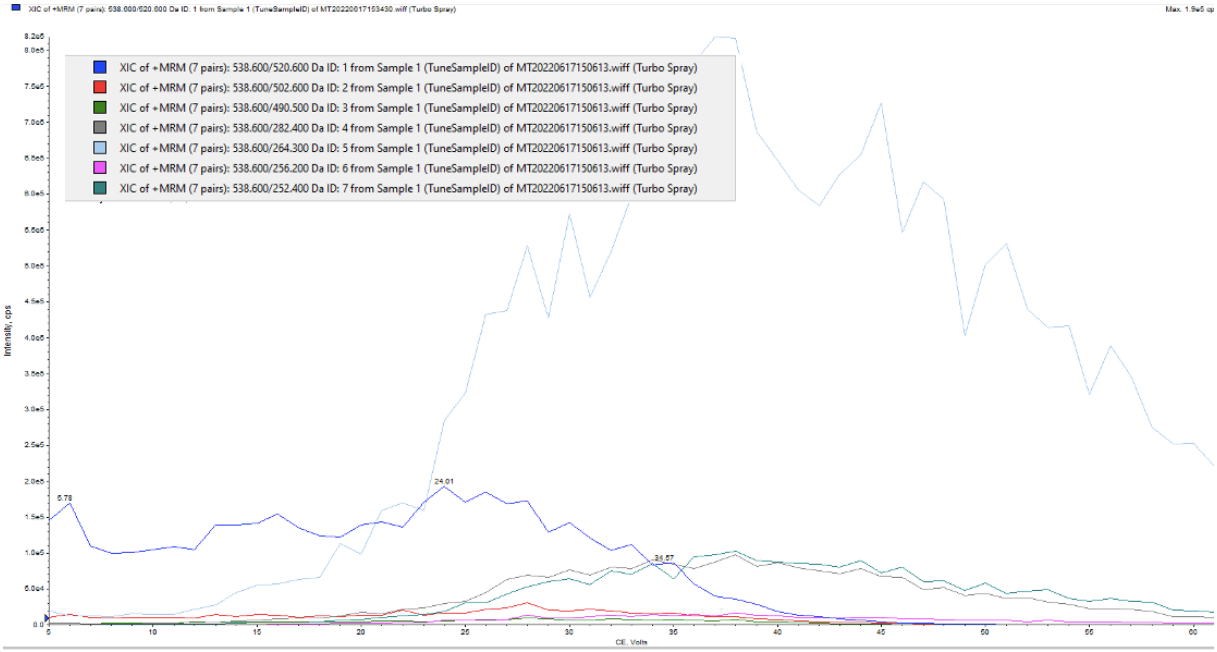

Figure 76. The collision energy is plotted against the Intensity of the product ions of the [M+H] adduct of C16 ceramide measured in MRM mode using SCIEX API 3200 LC-MS/MS. In the top left corner is the legend present showing the colors of the product ions m/z: 520.6, 502.6, 490.5, 282.4, 264.3, 256.2 and 252.4.

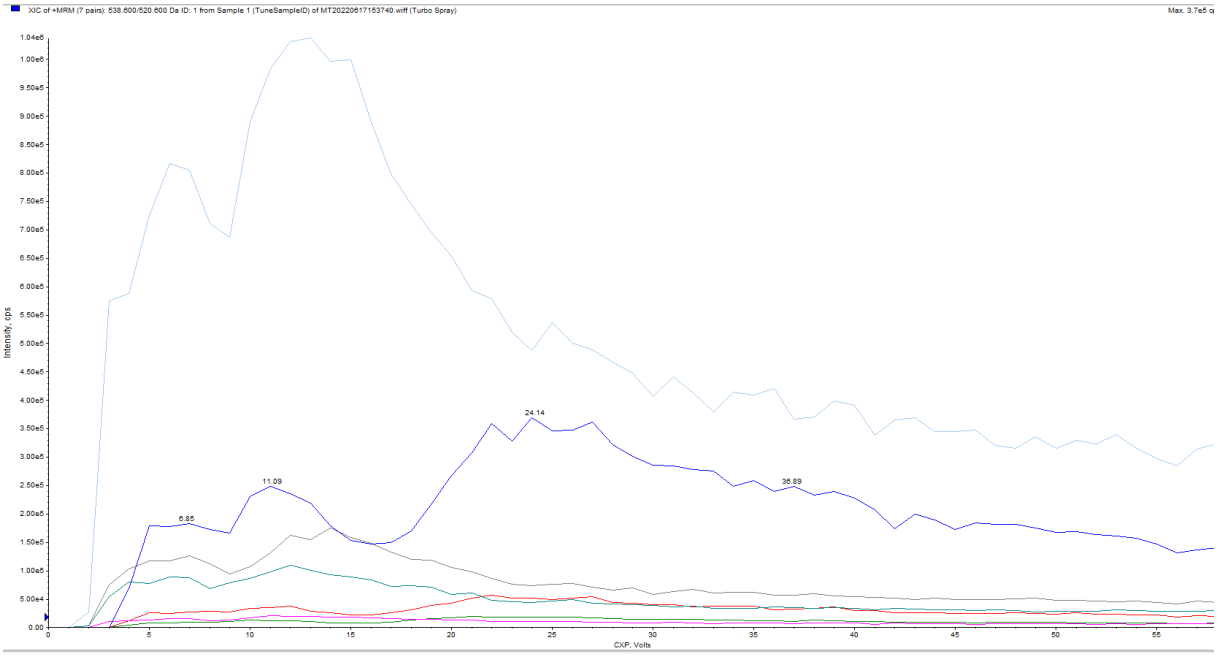

Figure 77. The collision cell exit potential is plotted against the Intensity of the product ions of the [M+H] adduct of C16 ceramide measured in MRM mode using SCIEX API 3200 LC-MS/MS of the product ions m/z: 520.6, 502.6, 490.5, 282.4, 264.3, 256.2 and 252.4.

7.6.8. Glucosyl ceramide

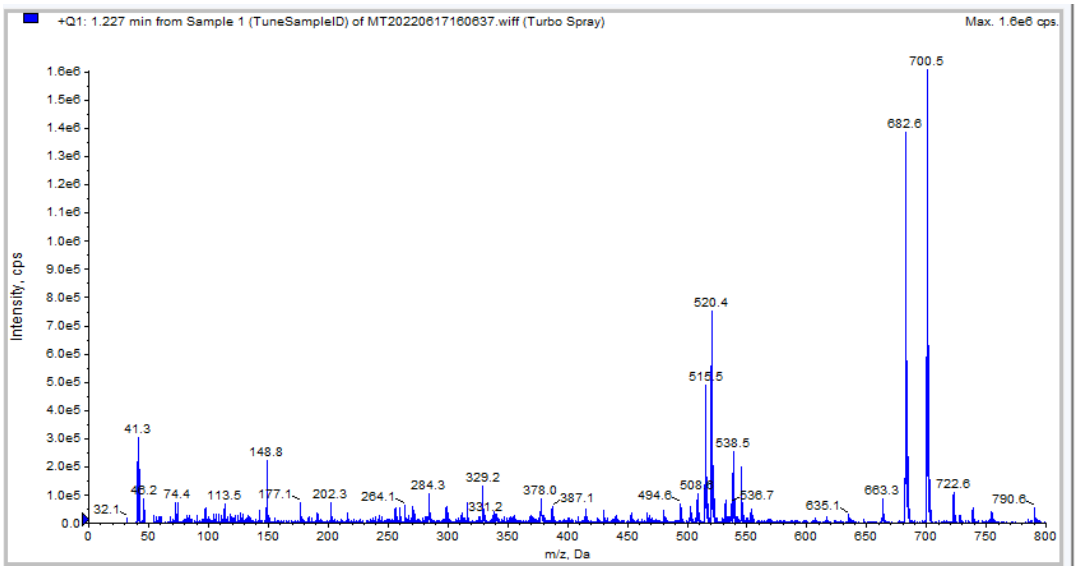

Figure 78. The m/z is plotted against the Intensity of the mass spectrum measuring in Q1 using SCIEX API 3200 LC-MS/MS of glucosyl ceramide. The peak at m/z = 700.5 is determined to be the {M+H] adduct.

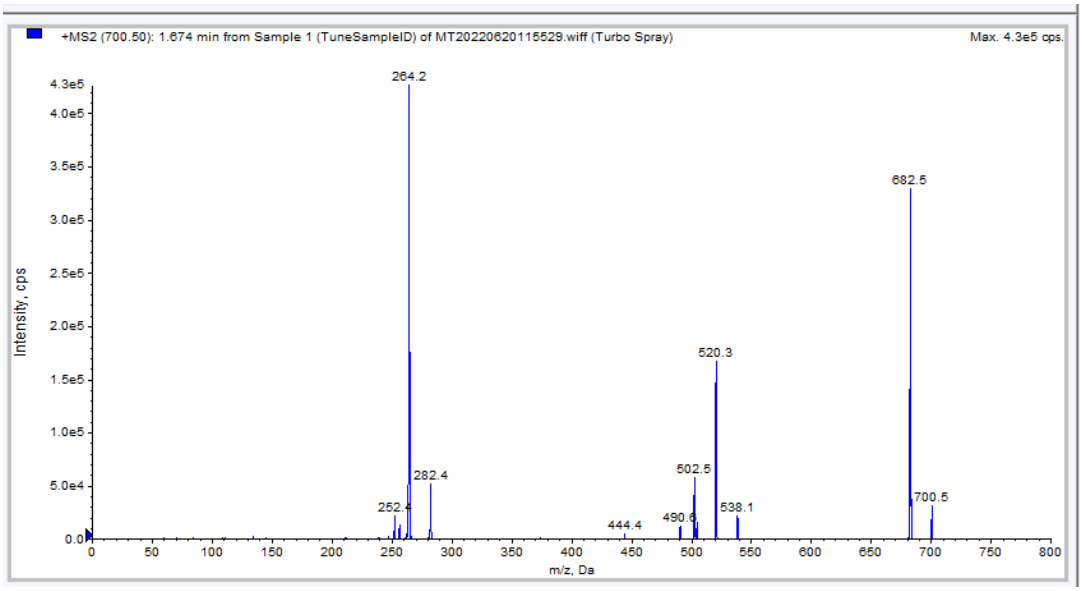

Figure 79. The m/z is plotted against the Intensity of the mass spectrum measuring in MS2 mode using SCIEX API 3200 LC-MS/MS of glucosyl ceramide showing the product ions of the [M+H] adduct.

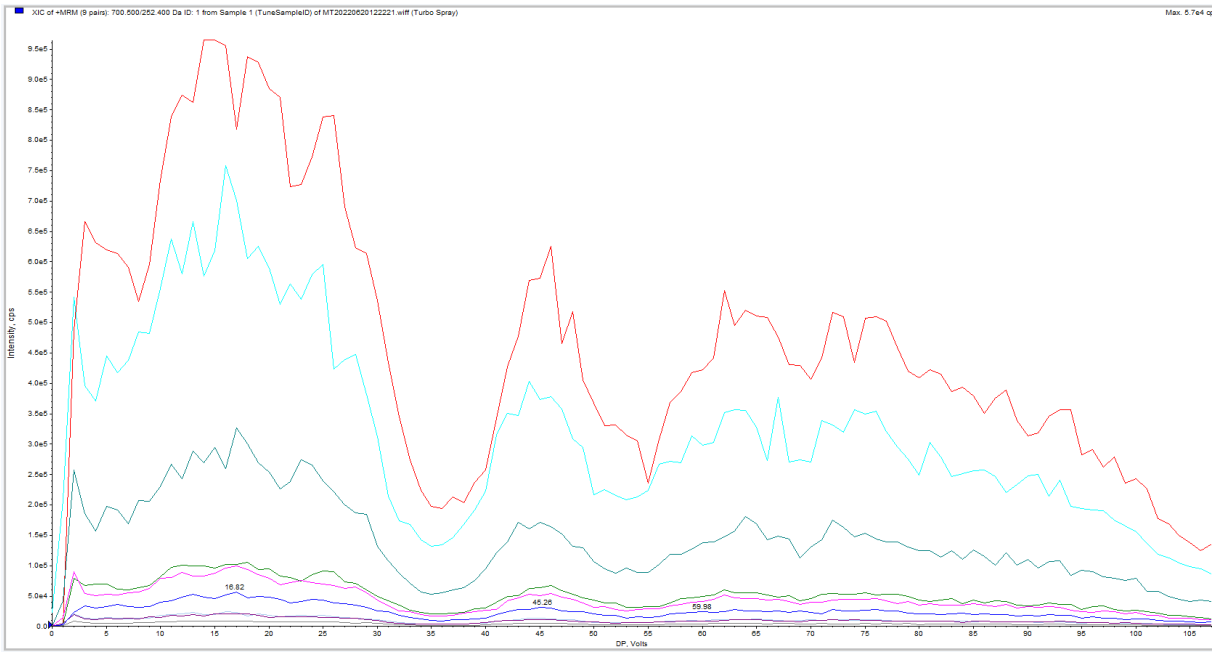

Figure 80. The declustering potential is plotted against the Intensity of the product ions of the [M+H] adduct of glucosyl ceramide measured in MRM mode using SCIEX API 3200 LC-MS/MS of the product ions m/z: 252.4, 264.2, 282.4, 444.4, 490.6, 502.5, 520.3, 538.1 and 682.5.

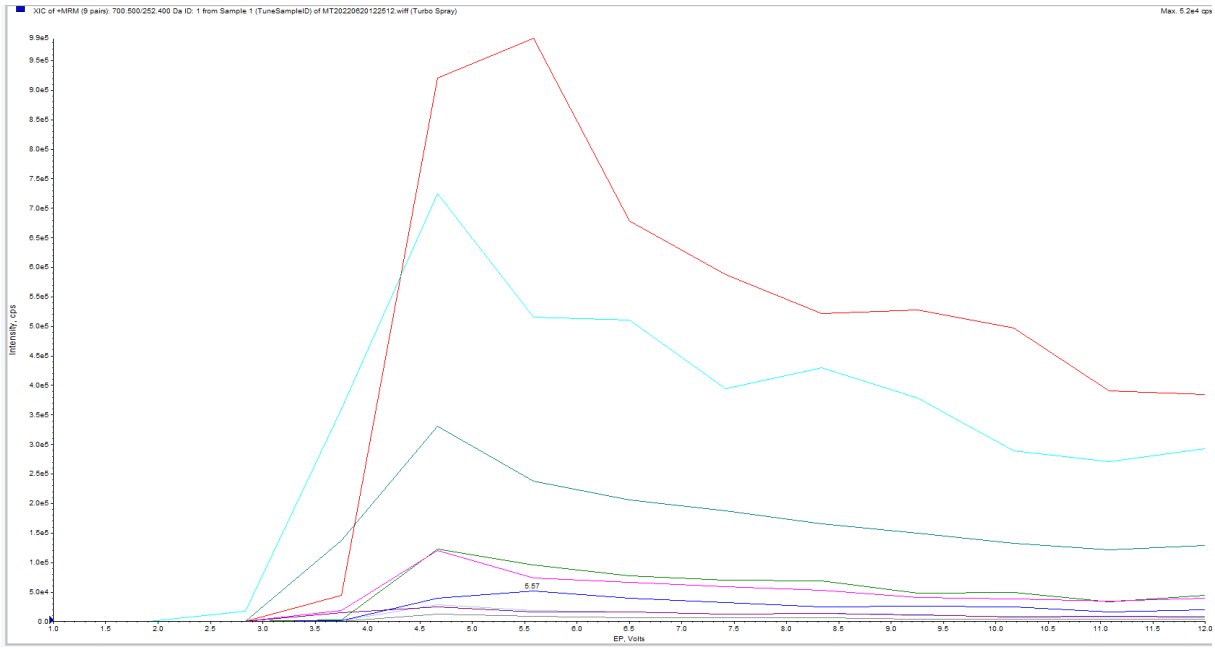

Figure 81. The entrance potential is plotted against the Intensity of the product ions of the [M+H] adduct of glucosyl ceramide measured in MRM mode using SCIEX API 3200 LC-MS/MS of the product ions m/z: 252.4, 264.2, 282.4, 444.4, 490.6, 502.5, 520.3, 538.1 and 682.5.

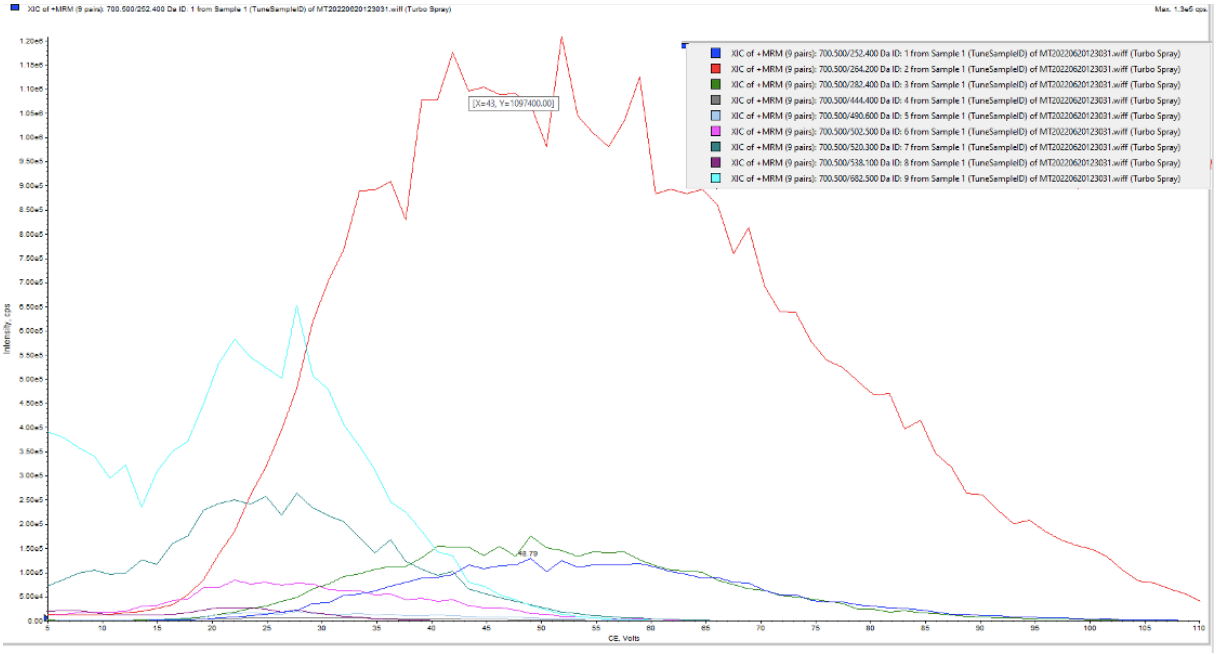

Figure 82. The collision energy is plotted against the Intensity of the product ions of the [M+H] adduct of glucosyl ceramide measured in MRM mode using SCIEX API 3200 LC-MS/MS. In the top right corner is the legend present showing the colors of the product ions m/z: 252.4, 264.2, 282.4, 444.4, 490.6, 502.5, 520.3, 538.1 and 682.5.

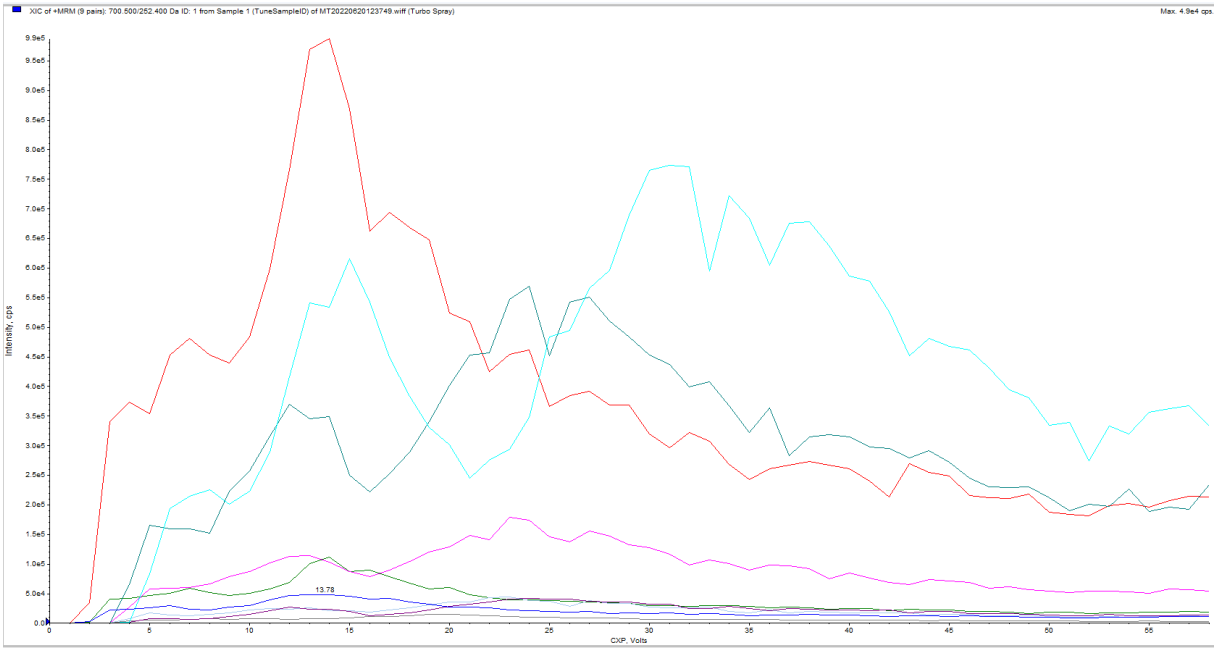

Figure 83. The collision cell exit potential is plotted against the Intensity of the product ions of the [M+H] adduct of glucosyl ceramide measured in MRM mode using SCIEX API 3200 LC-MS/MS of the product ions m/z: 252.4, 264.2, 282.4, 444.4, 490.6, 502.5, 520.3, 538.1 and 682.5.

7.7. LC method development and optimization of sphingolipid standards

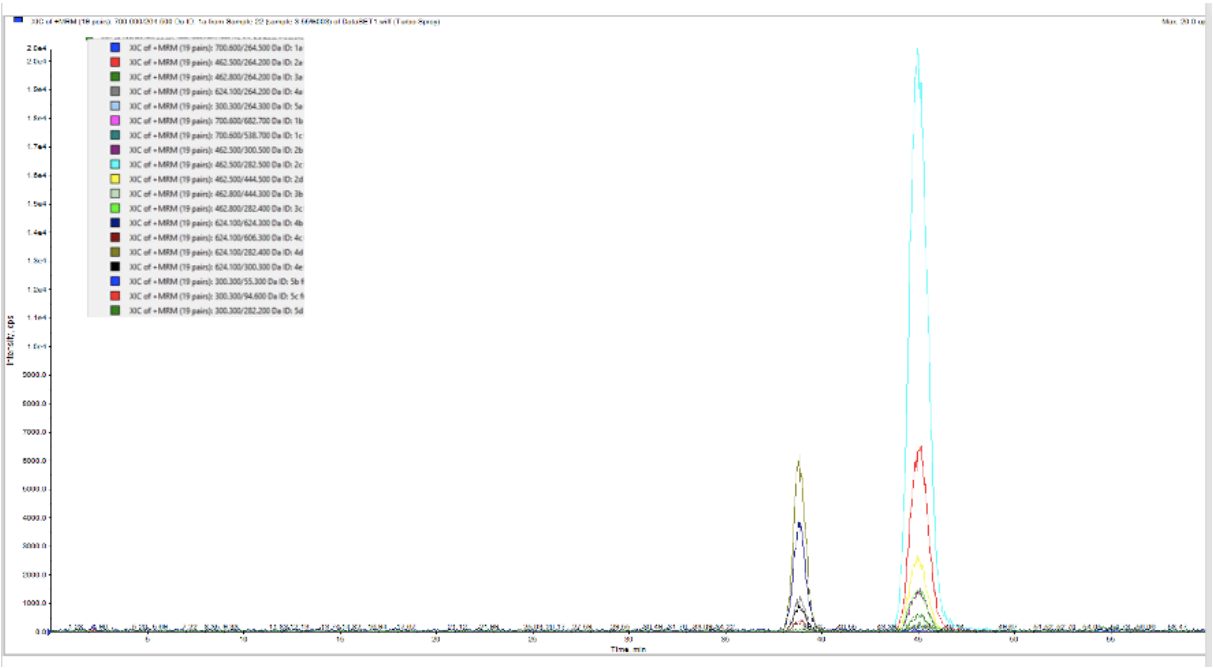

Figure 84. LC-MS/MS chromatogram using an isocratic elution of 55% mobile phase B showing the intensity (cps) plotted against the time (min) eluting the sphingolipid standards: lactosyl sphingosine, galactosyl sphingosine and glucosyl sphingosine. The legend at the top right shows the colors of the product ions of the sphingolipid standards.

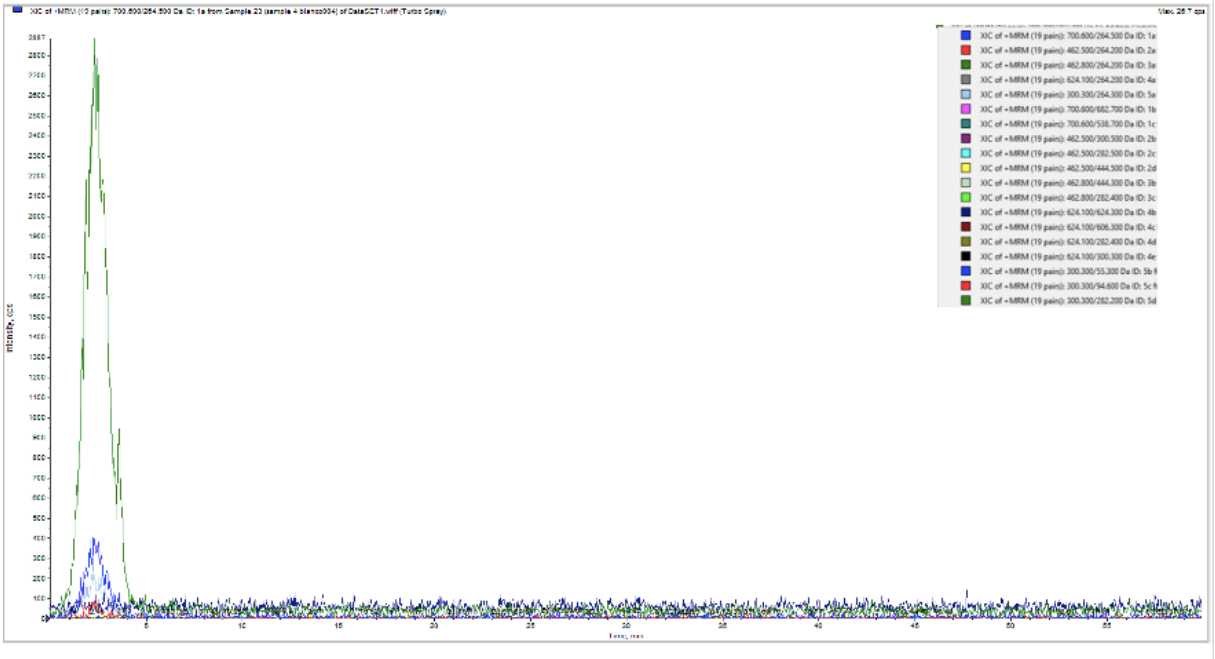

Figure 85. LC-MS/MS chromatogram blank measurement using an isocratic elution of 55% mobile phase B showing the intensity (cps) plotted against the time (min) eluting the sphingolipid standard D-sphingosine. The legend at the top right shows the colors of the product ions of the sphingolipid standards.

7.8 Column void time calculations

Column void volume

Column empty volume formula: $V= L*pi(D/2)^2$
V= empty volume (ml)
L= column length (cm)
D = Column diameter (cm)

$V = 10 * 3.14(0,21/2)^2 = 0.346$ ml

Column void volume formula: $V_0 = 0.66 * V = 0.229$ ml
V_0 = void volume (ml)
V= empty volume (ml)

Flow = 0,3 ml/min
Column void time = 0.229/0,3 = 0.76 min